Establishing Process Conditions for Optimal Wastewater Treatment Processes Using a Microfluidic Platform

Dissertation (monograph) approved by the Doctoral Degree Committee of

Hamburg University of Technology

in pursuit of the academic degree of

Doktor-Ingenieurin (Dr. -Ing.)

written by
Berivan Akgün

from
Istanbul, Türkiye

2026

Reviewers:	Prof. Dr. Johannes Gescher
	Prof. Dr. Andreas Liese
Chair of the Examination Committee:	Prof. Dr. Kerstin Kuchta
Date of the Oral Examination:	03.06.2026

DOI:	https://doi.org/10.15480/882.17304
Handle:	https://hdl.handle.net/11420/63471
ORCiD:	https://orcid.org/0009-0003-1811-7071

Abstract

Conventional wastewater treatment technologies are undergoing constant development to enhance sustainability, driven by the increasingly growing need to reduce energy consumption and stringent regulations. These systems must be robust, continuous, and scalable, yet elucidating the effect of operational parameters should at best rely on multiparallel, small-scale experiments for controlled investigation of biological activity. This thesis employed microfluidic biofilm cultivation systems to investigate the influence of process conditions for two wastewater treatment technologies.

In bioelectrochemical systems (BES), biofilm–electrode interaction is a key factor for electricity generation, and low electron transfer rates limit system efficiency. To address this, electrode surfaces in a microfluidic BES were functionalized with riboflavin and AQDS, and combined with rough surface materials to cultivate co-culture biofilms of *Geobacter sulfurreducens* and *Shewanella oneidensis*. Surface pre-treatment and increased roughness enhanced biofilm-electrode interaction compared to a naturally formed biofilm matrix, yielding over fivefold higher mean current densities and reducing initiation time by improving initial electroactive biofilm attachment, biocompatibility, and electron transfer.

Enhanced biological phosphorus removal (EBPR) is a widely applied biological phosphorus (P) removal strategy that mitigates eutrophication and supports regulatory compliance. P-removal is primarily performed by polyphosphate-accumulating organisms (PAOs), yet their responses to varying operational conditions remain poorly understood, underscoring a critical knowledge gap. A microfluidic model biofilm system (MMBS) was used to systematically analyze key process conditions, including carbon (C) source, COD/P ratio, pH and temperature, and their effect on the activity of PAOs and other species, as well as EBPR performance. Metagenomic analysis demonstrated that *Dechloromonas* and *Zoogloea* were prevalent under all the tested conditions. The C source exerted a stronger influence on system dynamics, with glucose and acetate/propionate supporting the highest P-removal, while ethanol, glycerol, and amino acids led to limited system performance. A low COD:P ratio enhanced phosphorus removal and biofilm formation, and PAO activity was maximal at pH≤7.5, whereas operation at 12 °C did not adversely affect process efficiency. These results guide optimizing design and operation parameters in full-scale wastewater treatment plants (WWTPs).

Zusammenfassung

Herkömmliche Abwasserbehandlungstechnologien werden kontinuierlich weiterentwickelt, um ihre Nachhaltigkeit zu verbessern, was durch den zunehmend wachsenden Bedarf an Energieeinsparungen und strengen Vorschriften vorangetrieben wird. Diese Systeme müssen robust, kontinuierlich und skalierbar sein, doch die Erforschung des Einflusses von Betriebsparametern stützt sich im besten Fall auf multiparallele, kleinräumige Experimente zur kontrollierten Untersuchung der biologischen Aktivität. In dieser Arbeit wurden mikrofluidische Biofilm-Kultivierungssysteme eingesetzt, um den Einfluss der Prozessbedingungen für zwei Abwasserbehandlungstechnologien zu untersuchen.

In bioelektrochemischen Systemen (BES) ist die Wechselwirkung zwischen Biofilm und Elektrode ein entscheidender Faktor für die Stromerzeugung, hierbei begrenzen niedrige Elektronentransferraten die Systemeffizienz. Um diesem Problem zu begegnen, wurden die Elektrodenoberflächen in einem mikrofluidischen BES mit Riboflavin und AQDS funktionalisiert und mit rauen Oberflächenmaterialien kombiniert, um Co-Kultur-Biofilme aus *Geobacter sulfurreducens* und *Shewanella oneidensis* zu kultivieren. Die Vorbehandlung der Oberfläche und die erhöhte Rauheit verbesserten die Wechselwirkung zwischen Biofilm und Elektrode im Vergleich zu einer natürlich gebildeten Biofilmmatrix, was zu einer mehr als fünffach höheren mittleren Stromdichte führte und die Anlaufzeit durch Verbesserung der anfänglichen elektroaktiven Biofilmhaftung, Biokompatibilität und Elektronentransfer verkürzte.

Die verbesserte biologische Phosphorentfernung (EBPR) ist eine weit verbreitete Strategie zur biologischen Entfernung von Phosphor (P), die die Eutrophierung mindert und die Einhaltung gesetzlicher Vorschriften unterstützt. Die P-Entfernung wird in erster Linie durch polyphosphatakkumulierende Organismen (PAOs) durchgeführt, doch ihre Reaktionen auf unterschiedliche Betriebsbedingungen sind nach wie vor kaum verstanden, was eine kritische Wissenslücke darstellt. Ein mikrofluidisches Modell-Biofilmsystem (MMBS) wurde verwendet, um wichtige Prozessbedingungen, darunter Kohlenstoffquelle (C), COD/P-Verhältnis, pH-Wert und Temperatur, sowie deren Auswirkungen auf die Aktivität von PAOs und anderen Spezies sowie die EBPR-Leistung systematisch zu analysieren. Die metagenomische Analyse zeigte, dass *Dechloromonas* und *Zoogloea* unter den getesteten Bedingungen vorherrschend waren. Die Kohlenstoffquelle hatte einen stärkeren Einfluss auf die Systemdynamik, wobei Glukose und Acetat/Propionat die höchste Phosphorentfernung

unterstützten, während Ethanol, Glycerin und Aminosäuren zu einer eingeschränkten Systemleistung führten. Ein niedriges COD:P-Verhältnis verbesserte die Phosphorentfernung und die Biofilmbildung, und die PAO-Aktivität war bei einem pH-Wert von ≤7,5 am höchsten, während der Betrieb bei 12 °C die Prozesseffizienz nicht beeinträchtigte. Diese Ergebnisse dienen als Leitfaden für die Optimierung der Auslegungs- und Betriebsparameter in vollwertigen Kläranlagen (WWTPs).

Acknowledgements

There are many people to whom I owe my professional and personal gratitude throughout the course of my Ph.D.

First and foremost, I would like to express my sincere gratitude to Prof. Johannes Gescher for giving me the opportunity to conduct my research under his supervision, and for his time and guidance during my doctoral studies.

I would also like to acknowledge the scholarship provided by the Ministry of National Education of the Republic of Türkiye, which supported my studies in Germany to pursue a Ph.D. in the field of "Wastewater Treatment and Circular Economy".

I am grateful to all members of AG Gescher-Lukas, Yitian, Sri, Melanie, Kerstin, Daniel, Chrissi, Laura, baby Karl, Carmen, Miri, Niko, Beshr, Varun, Suchet, Fernando,and Daniela- for creating such an amazing working environment. Petra, my dear, it is incredible how one person can be so many things: a wonderful colleague, a friend, and family. Your energy and presence have brought so much into my life, like sunshine. Sigi, thank you for your positive energy, professionalism, and strong work discipline. Nadja, I truly appreciate your thoughtfulness and the wonderful photos that capture so many beautiful moments. Janek, the king, it meant a lot to have you in the group. Your knowledge, perfectionism, and support were invaluable. A special thanks to Jonas, who significantly contributed to the direction of my research and provided valuable feedback throughout the process.

Leonie, thank you for your great tolerance as an office mate. Being able to distinguish you by the sound of your confident stride is part of office camaraderie. Benni, thank you for being such a great office mate and for always taking care of me.

Vivi and Melf, you have both brought great joy into my life. I am grateful for your warmth, emotional support, and for making me feel like part of your family.

René and Edina, my angels, your unwavering technical and emotional support are deeply appreciated. I am grateful for our strong connection throughout this journey. I would also like to thank the Klein family, especially Henni and Joey.

Marshid, thank you for always encouraging me and helping me remain objective in critical situations, as well as baby Raymon—what productive years those were. Ahmed, I literally thank you for your continuous support, your insightful comments on my work, and for teaching

me so much through your logical, well-structured, and organized approach. I strongly value your friendships, and deeply appreciate the shared moments and the great gatherings with your families.

I thank my friends Süheyla, Merve, Ayisha, and Izabela for their support. A special thanks to Aygül for her encouragement, great energy, and for always finding ways to make my life easier.

My sincere thanks go to Fatma Kazak for 20 years of friendship, as well as to my cousin Turgut and his wife Gülşah Akgün for believing in me. Without your support from the beginning, I could not have started my Ph.D. in Germany.

I am also deeply grateful to Bertuğ Uz, from the bottom of my heart, for being part of this long journey. Your excellent encouragement, friendship, and all the life hacks have meant more to me than anything.

Lastly, but most importantly, a massive thank you to my family. My mother, Fidan, and my father, Süleyman, have always provided me with unconditional love and support throughout my life. You are my greatest blessing in this life.

List of Contents

List of Figures

List of Tables

Abbreviations

ATP	adenosine triphosphate
Ag/AgCl	silver/silver chloride
BES	bioelectrochemical system
C	carbon
c-Cyts	*c*-type cytochromes
CO_2	carbon dioxide
COD:P	chemical oxygen demand to phosphorus ratio
Daime	Digital image analysis in microbial ecology
DET	direct electron transfer
DPAO	denitrifying polyphosphate-accumulating organisms
EAB	exoelectroactive bacteria
EBPR	enhanced biological phosphorus removal
EET	extracellular electron transfer
EMP	embden–meyerhof–parnas
EPS	extracellular polymeric substance
ETR	electron transfer resistance
FA	formamide
fGAO	fermentative glycogen-accumulating organisms
FISH	fluorescence in situ hybridization
FOV	frame of view
GAO	glycogen-accumulating organisms
HCl	hydrochloric acid
HRT	hydraulic retention time
HNAD	heterotrophic nitrification and oxic denitrification
H_2	hydrogen
LB	lysogeny broth
MEC	microbial electrolysis cell
MES	microbial electrochemical system
MET	mediated electron transfer
MFC	microbial fuel cell
MMBS	microfluidic model biofilm system

NADH	nicotinamide adenine dinucleotide
NO_2^-	nitrite
NO_3^-	nitrate
N_2	nitrogen
OD	optical density
OCT	optical coherence tomography
OGewV	the german surface water ordinance
OMCs	outer membrane cytochromes
O_2	oxygen
P	phosphorus
PAO	polyphosphate-accumulating organisms
PCA	principal component analysis
PDMS	polydimethylsiloxane
PHA	poly-β-hydroxyalkanoate
PHB	poly-β-hydroxybutyrate
PH2MV	poly-β-hydroxy-2-methylvalerate
PHV	poly-β-hydroxyvalerate
PMF	proton motive force
PO_4^{3-}	orthophosphate
poly-P	polyphosphate
ppk	phosphate kinase
ppx	phosphate hydrolase
Ra	arithmetic average surface roughness
SA	surface area
SA:V	surface area to volume ratio
SEM	scanning electron microscopy
SHE	standard hydrogen electrode
SRT	sludge retention time
TCA	tricarboxylic acid
TP	total phosphorus
VFA	volatile fatty acid
WWTP	wastewater treatment plant

1. Introduction

Wastewater management plays a crucial role in safeguarding water resources and significantly contributes to attaining and maintaining a high standard of water quality (Arle *et al.*, 2018). For this purpose, wastewater treatment plants (WWTPs) are systematically constructed to facilitate the remediation of municipal and industrial wastewaters, as well as the management and processing of sewage sludge, thereby ensuring compliance with environmental and public health standards (Kim *et al.*, 2025).

In recent years, the purification of wastewater has been extensively facilitated by the application of microorganisms (Weiler *et al.*, 2024). Within biological wastewater treatment systems, these microorganisms predominantly exist as microbial aggregates, including sludge flocs, biofilms, and granules, which play a central role in driving process performance and stability (Salama *et al.*, 2016). Compared to suspended biomass systems, biofilm processes are distinguished by lower sludge production, reduced carbon source requirements, and enhanced phosphorus accumulation efficiency. These advantages underscore the considerable potential of biofilm-based technologies for diverse wastewater treatment applications (Wang *et al.*, 2024). Of these, the targeted cultivation of biofilms offers great potential for both investigating processes within a system and studying organisms (Weiler, 2020). Insights into the dynamics of microbial communities within these systems are paramount for designing processes and optimizing treatment efficiency (McIlroy *et al.*, 2015). Such investigations could be facilitated by microfluidic platforms, as described by Hansen *et al.* (2019), which enable long-term biofilm cultivation under controlled conditions and allow parallel in situ analysis of biofilms.

Compared to traditional systems, these cultivation platforms use transparent polydimethylsiloxane (PDMS) microfluidics that enable simultaneous, non-destructive, real-time monitoring of biofilm growth, as well as their response to treatment using optical coherence tomography (OCT). This provides a detailed investigation of biofilm structure and microbial community dynamics at high spatial and temporal resolution, which is often challenging to achieve in larger laboratory set-ups or conventional full-scale WWTPs (Klein, 2018). In particular, PDMS-based microfluidic systems allow for precise control of flow regimes, nutrient gradients, shear forces, and feeding-starvation cycles. Additionally, the system can be operated under anoxic or oxic conditions, allowing the cultivation of both anoxic and aerobic organisms. This manipulation ability provides an accurate simulation of physiologically relevant environments, an alternative to conventional reactors (Abouhagger *et*

al., 2025). These attributes render microfluidic platforms highly resource-efficient, cost-effective and practical tools for developing model systems that closely mimic operational conditions in full-scale reactors. Furthermore, their design supports high-throughput screening of key operational parameters, thereby accelerating process optimization and technology development. This thesis investigated energy recovery and nutrient removal from wastewater using microfluidic systems, offering new insights for optimizing treatment processes.

1.1. Conventional wastewater treatment

Wastewater treatment originated in the late 1800s with the establishment of primary treatment methods. During the latter half of the twentieth century, process refinement intensified in response to increasingly rigorous environmental standards adopted by numerous countries. Thus, the 20th century marked a profound transformation in wastewater management (Sangamnere *et al.*, 2023). These advancements in treatment technology and regulatory drivers have progressively shifted focus from simple organic matter removal toward integrated nutrient management, in which biological nutrient removal now plays a central role within modern activated sludge-based wastewater treatment and water reclamation systems.

The presence of nutrients in treated wastewater effluents poses a high risk of algal blooms and eutrophication in aquatic ecosystems. Biological nutrient removal processes have a significant function in mitigating these risks by enabling effective control of nutrient discharges from municipal treatment and water reclamation facilities (Yuan *et al.*, 2025). The activated sludge process is the most extensively implemented and well-established biological approach for wastewater treatment, offering versatility for treating both municipal and industrial effluents (Gao *et al.*, 2025). It facilitates the enrichment of diverse bacterial populations responsible for the biological removal of organic substances, nutrients and a variety of pollutants. Enhanced biological phosphorus removal (EBPR) is a modification of the conventional activated sludge process, wherein the aeration tanks are partitioned into sequential anoxic and oxic zones. This arrangement fosters the enrichment of microorganisms capable of polyphosphate accumulation, resulting in the assimilation of inorganic phosphate and organic carbon from wastewater (Barr *et al.*, 2016; Wu *et al.*, 2006; Yuan *et al.*, 2025). In WWTPs, conventional wastewater treatment facilities operate generally through a sequential process comprising mechanical, biological, and chemical treatment stages, thereby ensuring comprehensive removal of contaminants, as demonstrated in Figure 1.

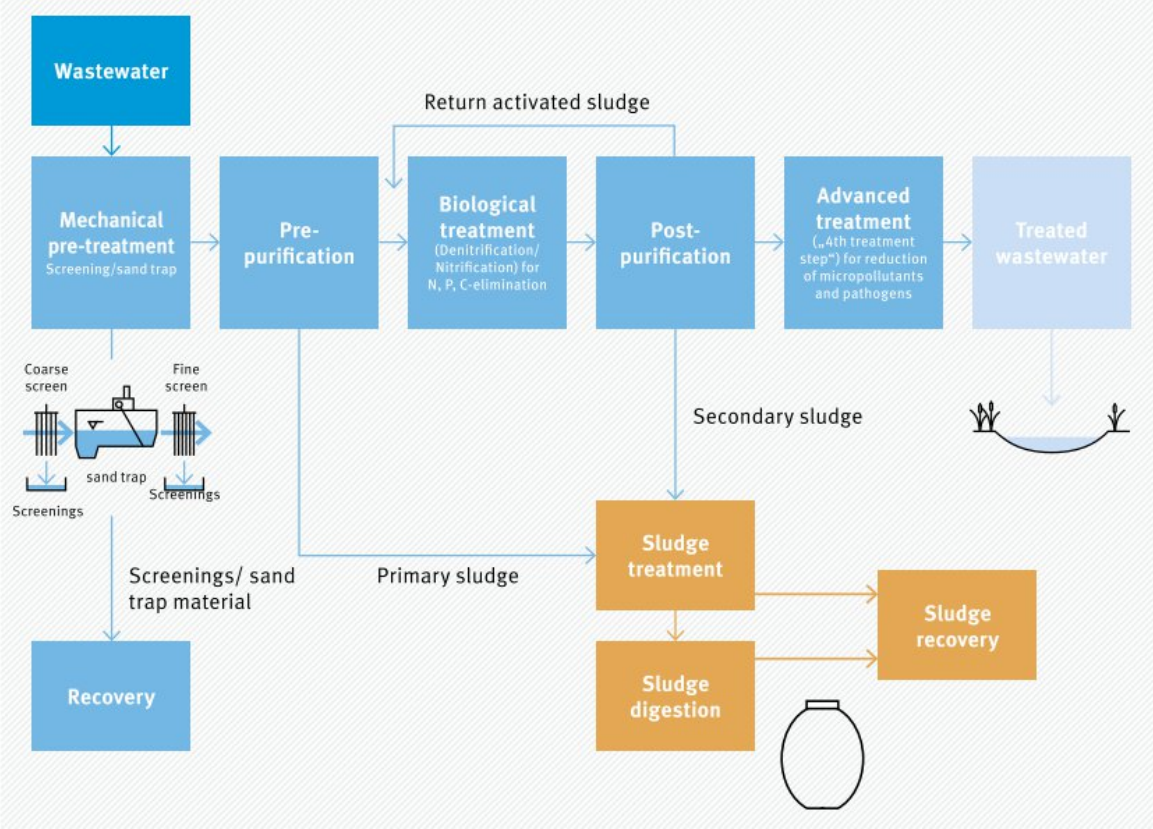

Figure 1. Schematic representation of wastewater treatment process (Arle et al., 2018).

In the mechanical pre-treatment, coarse impurities are removed by a coarse screen as well as a sand and grease trap, after which the wastewater enters a primary clarifier for pre-purification. In this tank, further solids are deposited due to a reduced flow velocity and can be removed as primary sludge. Biological treatment processes facilitate nitrification, denitrification, and biological phosphorus removal within wastewater treatment systems. Nitrogen (N), phosphorus (P), and carbon (C) compounds are eliminated from wastewater through biological treatment. Since microorganisms use the organic material removed from the wastewater for their growth, the total amount of sludge increases, and sludge flocs are separated from the treated wastewater by sedimentation in the post-purification steps. This biomass is removed from the system as so-called secondary sludge and treated in a digestion tower for sludge recovery, while some parts of the activated sludge must be returned to have sufficient organisms present in the biological treatment stage. Moreover, advanced chemical methods employ specific reagents for precipitation, flocculation, or neutralization. Following these treatment steps, the treated effluent is subsequently discharged into a receiving water body.

Although wastewater treatment technologies have been successfully applied worldwide for more than a century, these facilities are characterized by substantial electricity demand, categorized as high consumers. Specifically, the global increase in population, coupled with rapid urbanization, has led to higher wastewater production and, consequently, greater energy demand for wastewater treatment processes. Accounting for approximately 20% of total electricity use within the public sector, treatment plants and pumping stations exhibit significantly higher energy consumption compared to schools, hospitals, administrative offices, and other municipal facilities (Arle *et al.*, 2018). Accordingly, there is an urgent need to develop advanced technologies that can address rising energy demands while supporting sustainable electricity generation. In addition to established renewable sources such as wind, hydro, and solar power, biotechnology offers further potential for sustainable energy recovery. Bioelectrochemical systems (BES) exemplify such innovations by enabling the conversion of chemical energy into electrical energy, thereby turning previously unused biological waste streams into valuable energy resources for electricity production (Knoll, 2023).

1.2. Carbon elimination and energy recovery with exoelectrogens in BES

Microbial electrochemical systems (MESs) exhibit a remarkably broad spectrum of potential applications (Klein *et al.*, 2023). Specifically, anodic BESs serve as versatile platforms for converting chemical energy into electrical energy through microbially catalyzed oxidation reactions at the anode and reduction processes at the cathode (Engel *et al.*, 2019; Knoll, 2023). These systems have attracted extensive research interest due to their potential for sustainable energy recovery, wastewater treatment and broader environmental remediation. A prominent example is their use in wastewater treatment, where exoelectrogenic biofilms oxidize organic carbon to generate energy, thereby achieving carbon removal and, in some cases, facilitating resource recovery (Carmona, 2012; Martinez and Alvarez, 2018). Besides, the synthesis of value-added products from organic and inorganic wastes offers a sustainable approach to mitigating global challenges related to energy scarcity and environmental deterioration (Zou *et al.*, 2019). However, achieving industrial application of this potential necessitates a concentrated effort on optimizing biofilm development to ensure sustained and controllable performance over extended operational periods (Klein *et al.*, 2024b). The key requirement for this is a thorough understanding and improvement of the electron transfer mechanism.

1.2.1. Basic mechanisms of extracellular electron transfer in BES

Based on the direction of electron flux, MESs are generally categorized into anodic and cathodic configurations. In anodic MESs, exoelectrogenic microorganisms, growing as biofilms on the electrode surface, oxidize organic and/or inorganic substrates serving as electron donors and transfer the electrons to the anode, which functions as an external electron acceptor. At the same time, protons produced through oxidation reactions in the anode chamber diffuse toward the cathode to preserve charge balance within the system (Knoll, 2023). MESs are further classified according to their mode of operation (Figure 2). Microbial fuel cells (MFCs) employ exoelectrogenic microorganisms to oxidize substrates at the anode and transfer electrons to the cathode, thereby generating an electric current without external energy input. Typically, oxygen (O_2) serves as the terminal electron acceptor at the cathode. Owing to their ability to degrade organic pollutants simultaneously and produce electricity, MFCs present a promising and cost-effective strategy for wastewater treatment and environmental monitoring (Arinda *et al*., 2019; Gemünde *et al*., 2022; Logan *et al.*, 2019; L. Zhang *et al.*, 2024). In contrast, microbial electrolysis cells (MECs) operate with an externally applied potential that provides the additional energy required to drive the reduction of protons to hydrogen gas (H_2) at the cathode (Klein *et al.*, 2023).

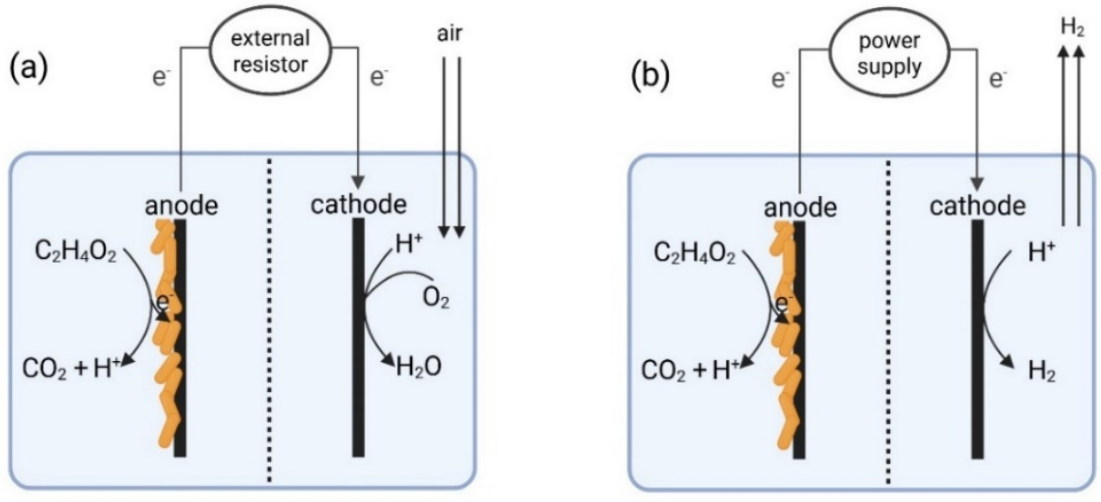

Figure 2. Schematic representation of microbial electrochemical system. In both systems, microorganisms typically develop as biofilms on the anode surface, facilitating electron transfer to the electrode. In MFCs (a), an external resistor connects the anode and cathode to enable electricity generation, whereas MECs (b) require additionally applied power to drive H_2 production at the cathode.

In BES, extracellular electron transfer (EET) by exoelectroactive bacteria (EAB) represents a fundamental process through which microorganisms generate energy to support cellular growth and maintenance (Carmona, 2012). Electrons can be transferred from microbial cells to extracellular anodes either directly, through long-range transfer via conductive cell appendages, including pili and/or nanowire filaments or short-range electron transfer by membrane-bound redox-active molecules (*c*-type cytochromes), known as direct electron transfer (DET), as demonstrated in Figure 3. Moreover, electrons can be transferred through soluble redox mediators, which act as an electron shuttle referred to as mediated electron transfer (MET) (Engel *et al.*, 2019). The mediator molecules can be self-produced mediators, such as flavin, phenazine, and quinones, or artificial exogenous mediators (Arinda *et al.*, 2019).

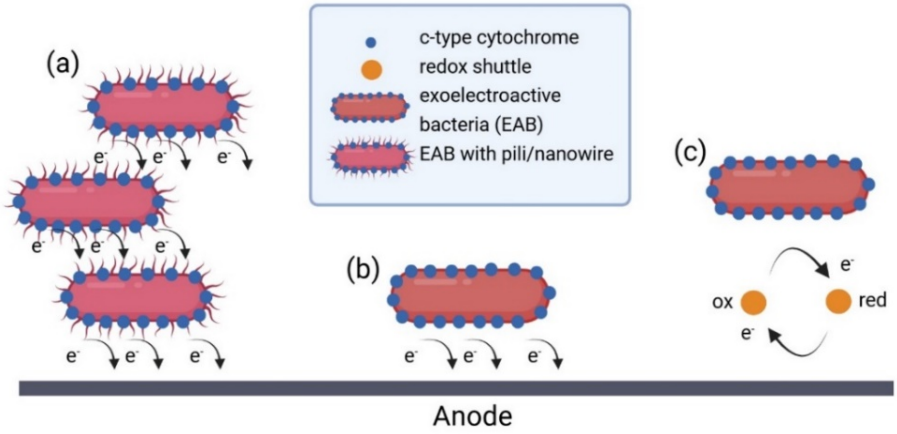

Figure 3. Mechanisms of extracellular electron transfer (EET) by exoelectroactive bacteria (EAB). Direct electron transfer (DET) may occur either through conductive cellular structures, including pili and nanowires, which enable long-range DET (a) or through redox-active outer membrane proteins, such as *c*-type cytochromes, which support short-range DET (b). In addition, in the mediated electron transfer (MET), soluble redox mediators can shuttle electrons, being reduced by the organisms and subsequently regenerated at the anode (c) (modified from Knoll, 2023).

While most microorganisms rely on soluble electron donors and acceptors for respiratory energy generation, EAB are uniquely capable of using solid-phase electrodes as electron donors or acceptors in BESs, serving as biocatalysts for the conversion between chemical and electrical energy (Engel *et al.*, 2019; Martinez and Alvarez, 2018; Zou *et al.*, 2019). The diverse composition of microbial communities enables the coexistence of multiple EET mechanisms, which collectively enhance the electroactivity of bacterial consortia (Pinck *et al.*, 2020). Moreover, mixed microbial consortia have generally been shown to generate higher electricity than pure cultures of electrochemically active microorganisms from municipal

wastewater, suggesting that utilizing them offers a distinct performance advantage (Heydorn et al., 2020).

The most extensively studied EABs in BESs are *Shewanella oneidensis* MR-1 and *Geobacter sulfurreducens* PCA due to their well-characterized metabolic pathways and abilities to interact with electrodes (Carmona, 2012; Heydorn *et al*., 2020). According to Engel *et al.* (2019), co-cultures of *G. sulfurreducens* and *S. oneidensis* mutually enhanced each other's activity, yielding a 38% increase in current density and a 35% thicker biofilm dominated by *G. sulfurreducens* compared with their respective pure cultures.

1.2.2. EET mechanisms in *G. sulfurreducens* and *S. oneidensis*

G. sulfurreducens is distinguished in bioelectrochemical research for its high enrichment within anodic biofilms sourced from municipal wastewater in MFCs and MECs, reflecting its superior capacity for EET compared to other bacterial species (Engel *et al.*, 2019), which supports the generation of considerable current densities (Logan *et al.*, 2019). *G. sulfurreducens* has an electron transfer mechanism from the cytoplasmic membrane through the periplasm and the outer membrane (Klein *et al*., 2024a). The outer-surface *c*-type cytochrome OmcZ plays a critical role in enabling maximal current generation. During growth as a biofilm on a graphite anode that functioned as the sole electron acceptor, *G. sulfurreducens* exhibited a strong enrichment of OmcZ at the biofilm–electrode interface (Inoue *et al.*, 2011). Further, *G. sulfurreducens* generates self-synthesized electrically conductive nanowires that interconnect individual cells and facilitate electron transfer to the anode (Li and Cheng, 2019). These nanowires attach to the membrane-bound cytochromes of the cells and increase direct EET by facilitating the growth of dense electroactive biofilms (Angelaalincy *et al.*, 2018; Heydorn *et al.*, 2020). In contrast, many other microorganisms lack this capability due to their limited production of conductive pili, which are necessary for long-distance electron transfer within biofilms.

Besides*, S. oneidensis* is a facultative anoxic γ-proteobacterium renowned as a key model organism for EET, particularly due to its capability to respire insoluble electron acceptors such as metals and electrodes (Klein *et al.*, 2024b; Knoll, 2023). Unlike *G. sulfurreducens*, the cells of *S. oneidensis* commonly form thin biofilms on electrode surfaces, enabling EET that occurs through both direct and indirect electron transfer processes (Zhao *et al.*, 2023).

In *S. oneidensis*, the metal-reducing (Mtr) pathway functions as a central electron transport route facilitating the initial stage of EET (Yi *et al.*, 2021). *S. oneidensis* on the anode surface transfers electrons to the electrode surface from the cytoplasmic membrane (CymA), through the periplasm (STC and FccA) and across the outer membrane (OmcA-MtrABC), enabling electron transmission from the quinone pool to external electron acceptors (Yi *et al.*, 2021; Zhao *et al.*, 2023). Contact-based direct electron transfer occurs through outer membrane proteins (e.g., *c*-type cytochromes) (Li and Cheng, 2019). Further, indirect electron transfer occurs via soluble redox mediators to mediate transfer processes (Inoue *et al.*, 2011).

Although nearly all identified *Shewanella* strains are capable of secreting flavins as electron mediators during EET, their endogenous flavin concentrations are too low for efficient interfacial transfer. However, in *S. oneidensis*, electron transfer nonetheless predominantly relies on riboflavin despite limited mediator secretion and the presence of only a small number of outer membrane proteins that directly interact with the electrode (Yi *et al.*, 2021; Zou *et al.*, 2019). In addition to self-produced electron shuttles, they can also be artificially added to the system to improve EET efficiency (Salim *et al.*, 2025; You *et al.*, 2025). However, mediated electron transfer is constrained by the ongoing requirement to replenish electron shuttles, particularly under conditions that cause washout of these molecules (Engel *et al.*, 2019; Heydorn *et al.*, 2020). Frequent washout of soluble mediators in flow-through systems further constrains power generation by *S. oneidensis* with MET, resulting in reduced current generation and lower bacterial conductivity compared to *G. sulfurreducens* in BES applications (Klein *et al*., 2024b; Knoll *et al*., 2022; Logan *et al*., 2019). In addition to the EET mechanisms, the attachment and colonization of EAB on the electrode surface also play a crucial role in the system performance.

1.2.3. Biofilm formation of exoelectrogenic model organisms

Biofilms are microbial communities in which cells adhere to surfaces and form microcolonies embedded within an extracellular polymeric substance (EPS) matrix, facilitating robust attachment within microchannels (Blanco-Cabra *et al.*, 2021; Lakshminarasimman *et al.*, 2025). This EPS matrix not only anchors the biofilm but also provides a protective environment that enhances microbial activity and confers structural stability (Saini *et al.*, 2023; Waqas *et al.*, 2023). Although biofilms exhibit considerable variability, certain developmental processes and mechanisms are consistently observed across diverse microbial species

(Perchikov *et al.*, 2024). Biofilm developments undergo a life cycle characterized by five sequential steps: (i) reversible attachment, (ii) irreversible attachment, (iii) maturation I, (iv) maturation II, and (v) dispersion (Sauer *et al*., 2022).

The initial attachment phase (i), which lasts generally between 4 and 48 hours, is a key determinant in the establishment of biofilm structures (Chen and Ding, 2023). During this phase, bacteria loosely associate with the electrode surface through weak and reversible interactions, which is accompanied by reduced electron transfer efficiency and a risk of detachment-related instability (You *et al.*, 2025). In this step, cells adhere to the surface via van der Waals forces, electrostatic and acid–base interactions. Moreover, most bacteria possess extracellular appendages with distinct structures and functions, among which flagella and pili are central to the initial stages of cell–surface interaction, contributing to the transition from reversible to irreversible attachment and strengthening adhesion (Perchikov *et al.*, 2024). In parallel, surface functional groups regulate both the formation and structure of biofilms by influencing bacterial attachment. Furthermore, once bacteria have initially adhered, this early colonization substantially improves the surface microenvironment, thereby facilitating subsequent stages of biofilm development. Irreversible attachment (ii) is maintained through a combination of physicochemical forces, including long-range van der Waals forces, intermediate-range electrostatic forces, and short-range polar and hydrophobic interactions, which act together at the cell–surface interface. Besides, surface functional groups play a pivotal role in governing biofilm development and growth, as these groups directly participate in these interfacial interactions (Li and Cheng, 2019).

During the stage of irreversible attachment and microcolony formation (iii), microorganisms become firmly interconnected through the secretion of EPS, and in addition to effective direct electron transfer, indirect electron transfer is promoted via the production of redox-active mediators. As microcolonies develop, the initially attached monolayer of cells progressively transitions into a stratified, multilayered structure. To establish a three-dimensional architecture, bacteria must engage in diverse chemical interactions with one another. Following microcolony formation, cell aggregation intensifies, along with the production of EPS, until an optimal cell density is reached, which is controlled by microbial interactions. As the biofilm matures (iv), both the rate of electron transfer and the structural stability reach their maximum, leading to the establishment of a complex, multi-layered biofilm architecture. During the dispersion phase (v) following biofilm maturation, partial structural breakdown

occurs through processes such as detachment and dispersion, which may be triggered by mechanical damage, host immune attack, or cell death within the biofilm. This loss of biomass compromises biofilm integrity and leads to diminished BES performance, as reflected by reduced electron utilization and lower pollutant removal efficiency (Perchikov *et al.*, 2024; You *et al.*, 2025). As evident from the stages of biofilm development, the initial attachment constitutes a pivotal step in the transition from reversible attachment to irreversible attachment and in establishing stable electroactive biofilms, which are essential in BESs for enhancing electron transfer rates.

1.2.4. Optimization of microbe-electrode interaction

A major bottleneck arises from the difficulty of the inherently low electron transfer rates from microbial cell membranes to the electrode surface, which are critical for effective energy conversion and the overall system performance (Martinez and Alvarez, 2018; Zou *et al.*, 2019). To facilitate electron transfer processes, both biological and physicochemical approaches, such as source of electroactive microorganisms (pure culture, consortia), electrode material properties (its topography, potential, the nature of the material), bulk system characteristics (pH, temperature, nutrient concentration), and employing artificial redox mediators can be used to improve the biofilm growth and produced current density as well as optimize operating conditions in BES (Pinck et al., 2020; L. Zhang et al., 2024). Beyond these strategies, increasing attention is now directed toward the miniaturization of BESs for fundamental research, while extensive research has focused on scaling up MECs and MFCs for large-scale or industrial implementation. The development of microfluidic, microliter-scale BESs offers unique opportunities for detailed investigation of electroactive biofilms, microenvironmental dynamics, and other microscale processes, thereby broadening their research applications to improve wastewater treatment efficiency (Angelaalincy *et al.*, 2018; Li *et al.*, 2012).

Specifically, efficient direct electron transfer depends on maximizing the number of cells in contact with the electrode while reducing diffusion limitations for both substrates and products (Knoll *et al.*, 2022). These limitations can be addressed by modifying the electrode surface to enhance microbial cell adhesion and promote the development of thick, highly conductive biofilms (Martinez and Alvarez, 2018). These modifications, including electrode surface functionalization and the use of rough electrode materials as anodes, enhance the interaction

between microbial cells and the electrode by maximizing cell–electrode contact, thereby improving overall current production and supporting the development of cost-effective technologies for wastewater treatment.

1.2.5. Effect of surface functionalization on the efficiency of BES

Ensuring intimate contact between the biofilm and the electrode surface is essential because the initial biofilm formation layer directly adjacent to the electrode is typically the most electroactive region (Perchikov *et al.*, 2024). Microbe–electrode interactions and bacterial adhesion in BES can be effectively enhanced by modifying the electrode surface (Klein *et al.*, 2023). Physical or chemical surface modification techniques can alter key anode surface properties, including roughness, hydrophobicity, biocompatibility, chemical bonding characteristics, and the electrochemically active surface area. These treatments enable modification of the material's surface chemistry, thereby influencing microbial–electrode interactions mediated by hydrogen bonding, electrostatic forces, or van der Waals interactions (Mier *et al.*, 2021). Surface modification through physicochemical treatments, together with functionalization using various redox-active molecules, collectively promotes exoelectrogenic bacterial attachment, biofilm development, and improved electrochemical performance, leading to enhanced current density and improved carbon removal efficiency in wastewater treatment systems (Angelaalincy *et al.*, 2018; Li and Cheng, 2019; Zou *et al.*, 2019).

Electrode functionalization with suitable mediators emerges as a promising strategy to boost electrochemical activity at the interface and enhance microbial electrocatalysis (Mier *et al*., 2021; Zou *et al.*, 2019). Continuous dosing of redox mediators in BESs is not cost-effective and may also result in the constant release of compounds that are recalcitrant to biological degradation (Heydorn *et al.*, 2020; Martinez and Alvarez, 2018). In this context, surface functionalization by adsorbing diverse redox-active mediators onto electrode surfaces offers a simple and achievable strategy. Immobilizing electroactive organic molecules on the electrode relies on the physical adsorption (physisorption). These molecules facilitate redox reactions through interactions with cellular components mediated by non-covalent forces, such as π–π stacking and hydrogen bonding interactions (Andrés *et al.*, 2021; Kotal *et al.*, 2024; Răsădean *et al.*, 2021).

To improve interactions, an optimal exogenous redox mediator for immobilization should possess several important properties, including efficient transmembrane permeability, the ability to accept electrons from microbial electron carriers, and high electron transfer rates with electrodes. Additional criteria include chemical stability, non-toxicity to microorganisms, economic viability, adequate solubility and sufficient biocompatibility to support efficient microbial-electrode interactions while maintaining system safety and cost-effectiveness (Martinez and Alvarez, 2018; L. Zhang *et al.*, 2024).

Given that certain forms of flavins and quinones naturally participate in the electron transfer chain of *S. oneidensis*, these mediators are expected to be biocompatible and to preserve redox activity within the bacterial medium (L. Zhang *et al.*, 2024). Besides, according to Erben *et al.* (2021a), redox mediators, including flavins and quinones, have been shown to enhance current generation in *S. oneidensis*. In this thesis, considering the functional properties of redox-active molecules, flavin- and quinone-based compounds such as riboflavin 5'-monophosphate sodium (FMN-Na) and anthraquinone-2,6-disulfonic acid disodium (AQDS) have been employed as surface pretreatments in BES to enhance electron transfer processes. These mediators were chosen due to their proven efficacy in facilitating mediated EET, either dissolved in the anode chamber or immobilized on the electrode surface, thereby supporting higher electrocatalytic activity within BES (Heydorn *et al.*, 2020).

1.2.6. Effect of surface roughness on the efficiency of BES

A second surface modification strategy to enhance electron transfer between organisms and the electrode in BES is to improve surface roughness using an appropriate electrode material, since overall system performance is strongly influenced by this material. The selection of suitable electrode materials requires balancing high electron transfer capacity with chemical stability, mechanical robustness, and economic feasibility. Moreover, as efficient current generation depends on the establishment of biofilms on the electrode surface, biocompatibility and the ability to promote microbial adhesion are key design considerations (Heydorn *et al.*, 2020; Martinez and Alvarez, 2018).

Several studies have investigated the selection of optimal electrode materials for bioelectrochemical systems, generally distinguishing between metal-based electrodes, such as copper or steel and carbon-based electrodes, such as graphite derivatives, each offering distinct

advantages (Klein *et al.*, 2023; Knoll, 2023). Metal-based electrodes have been considered as potential low-cost anode alternatives; however, despite their superior electrical conductivity and mechanical strength, their limited biocompatibility, exhibiting corrosion sensitivity under specific conditions and relatively high overall costs restrict their broader application in bioelectrochemical systems (Ratheesh *et al.*, 2024). Conversely, carbon-based materials, particularly graphite, are the most commonly employed electrodes in BESs due to their favorable combination of biocompatibility, chemical stability, corrosion resistance, high conductivity, and relatively low cost (Carmona, 2012; Heydorn *et al*., 2020; Martinez and Alvarez, 2018). Furthermore, the graphite electrode offers a hydrophobic surface well-suited for the adsorption of various organic redox couples and is easily functionalized, thereby facilitating the investigation of electrochemical charge transfer processes (Malinauskas, 2008; Sang *et al.*, 2025).

Besides the selection of electrodes, the surface characteristics of the anode strongly influence microbial attachment and electron transfer efficiency. Rough electrode surfaces are generally more favorable than smooth ones, as they enhance the contact surface area between electroactive biofilms and the electrode, thereby promoting microbial colonization and improving system performance (Heydorn *et al.*, 2020; Martinez and Alvarez, 2018). Even though increased surface roughness can improve colonization, excessive roughness may introduce mass transfer limitations. Therefore, optimizing electrode texture is critical for facilitating stable biofilm development and effective electron exchange, particularly when designing materials for bioelectrochemical applications (Klein *et al*., 2024b).

Such integrated modifications, including the use of a defined mixed culture together with immobilized redox mediators on the rough electrode surface, can substantially improve biofilm formation by providing more attachment sites. In addition, this combination can enhance electron transfer throughout the biofilm by increasing conductivity and reducing the electrical resistance between the biofilm and the electrode. These approaches also aim to strengthen biocompatibility, ultimately yielding more effective microbe–electrode interactions. Altogether, these advancements have the potential to significantly improve the operational efficiency and broaden the applicability of BES, thereby supporting their integration into sustainable and resource-recovery-oriented wastewater treatment processes.

Given their potential to markedly decrease the high-energy demands associated with aeration in conventional wastewater treatment, BESs are considered a cost-effective alternative to

traditional treatment technologies. However, the limited electron transfer capacity in BESs, together with several drawbacks of conventional wastewater treatment systems, including substantial energy demand, excessive sludge generation, dependence on chemical additives for coagulation and flocculation, and the limited exploitation of the energy potential of wastewater, highlights the limitations of these technologies. Together with increasing energy demand and escalating environmental concerns, there is an urgent need for more efficient and sustainable wastewater treatment approaches (Salim *et al.*, 2025; Sang *et al.*, 2025). To this end, using microfluidic systems as research tools on a microliter scale provides opportunities for detailed investigation of treatment system optimization (Li *et al.*, 2012). This enables valuable insights into system parameters, particularly in complex treatment processes such as biological phosphorus removal from wastewater, as excessive phosphate in water bodies poses serious environmental problems.

1.3. Phosphate elimination and resource recovery with PAOs

As wastewater treatment technologies progress from conventional plants to advanced systems with integrated nutrient removal and ultimately toward resource recovery facilities, a nuanced understanding of the microbial consortia responsible for nutrient removal and recovery becomes increasingly indispensable (Dueholm *et al.*, 2022). Further, given the presence of phosphate in wastewater and increasingly stringent discharge criteria, systematically evaluating the mechanisms of phosphorus removal is essential for optimizing wastewater treatment performance and mitigating environmental impacts.

1.3.1. The environmental effects of phosphorus

The environmental impact of phosphorus is profound, as its excessive presence in aquatic ecosystems, primarily driven by anthropogenic activities such as rapid urbanization, agriculture, and industrial processes, adversely affects aquatic life and water quality (Huber *et al.*, 2020). Controlling phosphorus emissions from WWTPs is a key factor in preventing eutrophication of surface waters. Many WWTPs are required to meet total phosphorus (TP) limits in their effluents, and an increasing number of countries are also introducing obligations or targets for phosphorus recovery from sludge to support more sustainable treatment and resource recovery (Zhang *et al.*, 2024).

Achieving low concentrations of effluent generally requires enhanced biological phosphorus removal and chemical phosphorus removal processes based on precipitation. TP discharge limits vary depending on the country, population, national and local regulations, the receiving water bodies (e.g., rivers, lakes), and their classification status (e.g., Class I, II, III, IV, or V). In recent years, both the European Union (EU) and the United States Environmental Protection Agency (US EPA) have revised and strengthened the discharge standards for WWTPs. The 2022 draft revision of the Urban Wastewater Treatment Directive mandates reducing the phosphorus concentration in effluent to 0.5 mg P L^{-1} (or achieving at least 90% phosphorus removal efficiency), which is stricter than the previous limit of 1–2 mg P L^{-1} (Zhang *et al.*, 2024).

TP concentration in the influent of municipal wastewater generally ranges from 5 to 20 mg P_{total} L^{-1}. The German Surface Water Ordinance (OGewV) sets orientation values for phosphorus concentrations in surface waters to protect water quality and prevent eutrophication. According to the OGewV, the orientation value for "good ecological status" for TP is set at 0.10 mg P_{total} L^{-1}. Exceeding this value can indicate a risk of eutrophication (Huber *et al.*, 2020). Besides, the German Sewage Sludge Ordinance (AbfKlärV) sets a threshold phosphorus concentration of 20 g P/kg of dry matter in sewage sludge. This is equivalent to 2% phosphorus by weight in dry solids. Phosphorus recovery is obligatory for sewage sludges with more than this from 2029 in Germany. Recovered phosphorus has the potential to substitute up to 43% of the commercial fertilizer demand (Sichler *et al.*, 2022). Phosphorus is a finite, non-renewable resource on our planet, and the urgency to recover it from waste streams is steadily increasing. Consequently, WWTPs offer an efficient and practical route for phosphorus recovery, supporting both resource conservation and sustainable wastewater management.

1.3.2. Phosphorus removal from wastewater

Phosphorus removal from wastewater is achieved through chemical phosphorus precipitation, enhanced biological phosphorus removal, or a combination of chemical and biological methods. In chemical phosphorus precipitation, metal salts are dosed into the wastewater to react with soluble phosphate, forming insoluble metal–phosphate precipitates. These precipitates are then removed from the water through subsequent physical sludge separation processes, such as sedimentation and/or filtration (Huber *et al.*, 2020). Chemical P-removal

consumes large amounts of chemicals and generates hard-to-treat excess sludge. The stable binding of phosphorus within chemically precipitated sediments substantially hinders its release during the sludge treatment process, potentially leading to the permanent loss of phosphorus resources. In contrast, biological P-removal is considered more economical and sustainable than chemical methods, as it produces phosphorus-rich sludge that facilitates resource recovery. Consequently, the integration of biological phosphorus removal and recovery is regarded as a key trend for future wastewater treatment systems (Zhang *et al.*, 2024; Zhao *et al.*, 2022). In Figure 4, a typical EBPR reactor scheme is shown. The process relies on cycles of anoxic and oxic stages to support P-release and uptake by polyphosphate-accumulating organisms (PAOs) within the treatment system.

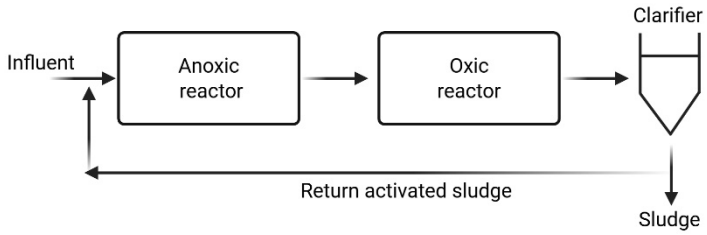

Figure 4. A schematic representation of the EBPR. The process operates through a sequence of an anoxic stage, during which phosphate is released, followed by an oxic stage, in which phosphate is taken up and removed from the liquid phase. Following phosphorus uptake, P-rich biomass (sludge) is separated via sedimentation and subsequently removed from the system.

In the EBPR process, PAOs are extensively used due to their ability to store polyphosphate (poly-P) within microbial cells (Petriglieri *et al.*, 2021; Y. Zhang *et al.*, 2024). PAOs enhance phosphorus incorporation into sludge by storing and hydrolyzing intracellular poly-P beyond their growth demands, thereby increasing the total phosphorus content retained in the biomass and facilitating efficient phosphorus removal during sludge wasting (Ziliani *et al.*, 2023).

1.3.3. Metabolism of PAOs and GAOs

PAOs are enriched for efficient EBPR by treating activated sludge with alternating anoxic feeding and oxic starvation conditions (Klein *et al.*, 2022; Petriglieri *et al.*, 2021). A stressful situation is induced for the microorganisms in the anoxic phase. PAOs take readily biodegradable organics, mainly volatile fatty acids (VFAs), to convert and store them as energy-containing poly-β-hydroxyalkanoates (PHAs) (Figure 5). The energy required for this conversion is supplied via adenosine triphosphate (ATP), while reducing equivalents are

provided by nicotinamide adenine dinucleotide (NADH), both of which are generated by the hydrolysis of intracellular poly-P and the glycolysis of internally stored glycogen reserves, respectively. The resulting PHAs serve as carbon stores to cope with a possibly prolonged absence of oxygen (Klein, 2018; Tarayre *et al.*, 2016; Zhang *et al.*, 2007). The hydrolysis of poly-P leads to the release of orthophosphate (PO_4^{3-}) into the bulk liquid, which is reflected by an increase in PO_4^{3-} concentration during the anoxic stage. In the subsequent oxic phase, external carbon substrates are absent. The internally stored PHA from the anoxic phase is used as an energy and carbon source. This energy is utilized for the uptake of soluble phosphorus from the bulk solution and its subsequent incorporation into intracellular poly-P reserves. Additionally, it supports PAO biomass growth and maintenance, and replenishment of glycogen. These processes result in phosphate accumulation within the cells. The amount of phosphorus uptake exceeds that of phosphorus release, which is called luxury phosphate uptake; therefore, net phosphorus removal occurs. Phosphorus is ultimately removed from the wastewater by discharging the polyphosphate-rich excess sludge (Chuang *et al.*, 2011; Tarayre *et al.*, 2016; Wei *et al.*, 2014; Zhang *et al.*, 2025; Y. Zhang *et al.*, 2024).

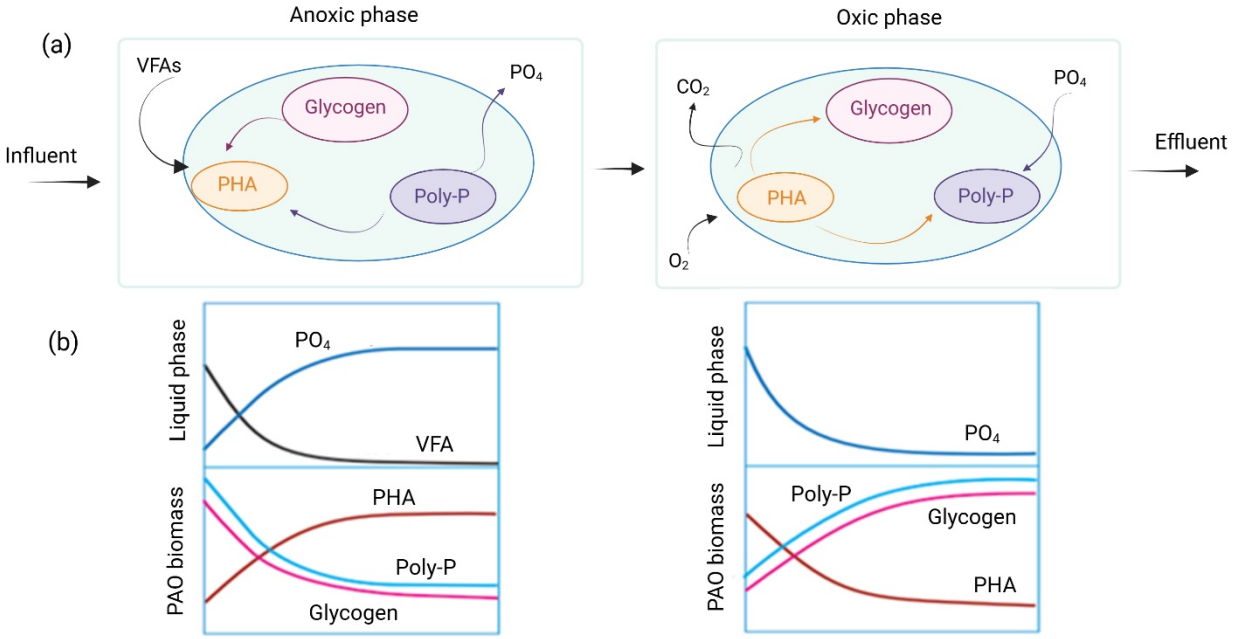

Figure 5. A schematic representation of the metabolism of PAOs under anoxic and oxic conditions. (a) In the anoxic phase, PAOs exhibit a metabolism in which VFA are assimilated and converted into PHA, utilizing energy derived from poly-P hydrolysis and glycogen degradation. The poly-P hydrolysis induces the release of PO_4^{3-} back into the liquid phase. When the environment switches to oxic conditions, these PAOs use the stored organic material for growth and take up more phosphorus than they previously released, storing it as poly-P inside their cells. The phosphorus-rich biomass (sludge) is then removed from the system, effectively reducing the phosphorus content in the treated water. (b) The changes in PAO biomass and liquid phase in EBPR under anoxic and oxic conditions is shown (modified from Loosdrecht 2016).

Glycogen-accumulating organisms (GAOs), which belong to γ- or α-proteobacteria, generally coexist with PAOs in the EBPR system. While they have similar metabolic pathways, GAOs lack the capability of phosphorus release and uptake. In both cases, VFAs are assimilated under anoxic conditions and stored as PHAs, which are subsequently oxidized under oxic conditions to support biomass growth and glycogen replenishment. However, the reducing equivalents and energy required for PHA synthesis are primarily derived from the use of glycogen, and not from the hydrolysis of intracellular poly-P, as in PAOs (Nittami *et al.*, 2011; Zhang *et al.*, 2025; Zhao *et al.*, 2022).

Interactions between PAOs and GAOs occur either as competition or cooperation, depending on the prevailing environmental conditions. This underscores the importance of managing microbial communities in activated sludge systems to optimize phosphorus removal performance. Generally, GAOs compete with PAOs for readily biodegradable carbon sources, which can diminish system efficiency. Nevertheless, GAOs are also implicated in endogenous denitrification, contributing to nitrogen removal. Thus, a balanced coexistence of PAOs and GAOs can facilitate the simultaneous removal of nitrogen and phosphorus, which remains an important direction in nutrient removal research (Izadi *et al.*, 2020; Oehmen *et al.*, 2007; Y. Zhang *et al.*, 2024; Zhao *et al.*, 2022). Moreover, the diverse metabolic pathways exhibited by different biomass under varying carbon sources may enable these communities to better adapt to complex environmental conditions and support more robust EBPR performance (Zhang *et al.*, 2025).

1.3.4. Major PAO and GAO populations in WWTPs

The most frequently identified PAOs in full-scale EBPR systems are *Candidatus Accumulibacter*, *Tetrasphaera*, *Dechloromonas*, *Thiothrix*, and *Comamonadaceae* (Nielsen *et al.*, 2019; Zhang *et al.*, 2025). While the most common GAOs are *Candidatus Competibacter*, *Candidatus Contendobacter*, *Propionivibrio*, *Defluviicoccus, and Micropruina.* They frequently coexist with PAOs in EBPR systems as recent research has shown (Izadi *et al.*, 2020; Nielsen *et al*., 2019; Zhang *et al.*, 2025; Zhao *et al.*, 2022).

Accumulibacter, which has been extensively studied, is widely recognized as the most important genus of PAOs, serving as the key functional organism in EBPR processes (Zhao *et al.*, 2022). Consistent with the well-established metabolic framework for conventional PAOs,

particularly as represented by *Accumulibacter,* intracellular poly-P concentrations are observed to be minimal following the anoxic phase and maximal after the oxic phase, although some plant-specific variations have been reported (Petriglieri *et al.*, 2021). This genus is phylogenetically classified based on the phosphate kinase gene (*ppk*) into two major groups, designated as Types I and II. Type I is further subdivided into five evolutionary clades (Types IA-E), while Type II encompasses seven evolutionary clades (Types IIA-G). These evolutionary clades exhibit distinct physiological traits; notably, clade IA is capable of coupling nitrate reduction with phosphorus uptake, whereas clade IIA lacks this ability. This genetic and functional diversity underscores the metabolic variability within *Accumulibacter* populations relevant to EBPR processes (Y. Zhang *et al.*, 2024).

After *Accumulibacter, Dechloromonas* was identified as the second most prevalent genus among both well-recognized and putative PAOs in EBPR systems (Petriglieri *et al.*, 2021; Y. Zhang *et al.*, 2024). The capacity of *Dechloromonas* for phosphorus removal was verified through metagenomic sequencing analysis of the *ppk* and phosphate hydrolaze genes (*ppx*) (Petriglieri *et al.*, 2021; Zhao *et al.*, 2022). Some *Dechloromonas* strains were identified as putative denitrifying polyphosphate-accumulating organisms (DPAOs), with the majority (8 out of 10) possessing genes encoding a complete denitrification pathway, indicating their potential involvement in denitrification processes (Chen *et al.*, 2024). In many studies, the co-occurrence of *Dechloromonas* and *Zoogloea* was identified as denitrifying bacteria (Chen *et al.*, 2024; Li *et al.*, 2020; Rong *et al.*, 2024). Moreover, *Zoogloea* has been recognized for its role in facilitating floc formation within activated sludge through the secretion of EPS, contributing to the stable operation (Fujii *et al.*, 2024; Liu *et al.*, 2024; Seguel Suazo *et al.*, 2024). EPS is essential for cell adhesion, biofilm formation, nutrient uptake and effective sludge settling in wastewater treatment systems (Banerjee *et al.*, 2021; Wang *et al.*, 2020; Yuan *et al.*, 2025). Owing to their capabilities for EPS synthesis and subsequent flocculation, PAOs can be enriched in activated sludge, thereby enhancing phosphorus recovery in the EBPR process (An *et al.*, 2016).

The correlation analysis between microbial genera and transcriptomic profiles indicated that *Zoogloea*, *Dechloromonas*, *Micropruina*, and *Tessaracoccus* were the dominant contributors to biofilm formation. Besides *Zoogloea*, *Micropruina,* and *Tessaracoccus* have roles in promoting EPS secretion (Wei *et al.*, 2023). Further, genomic interrogation of *Micropruina* and *Tessaracoccus* revealed an absence of the PHA synthase (*pha*C), which encodes the key

enzymatic function required for PHA biosynthesis. Correspondingly, neither poly-P nor PHA granules were detected in *Tessaracoccus*, as validated by the absence of these compounds in staining analyses (Elahinik *et al.*, 2022). Despite the lack of PHA and poly-P, glycogen was observed in *Micropruina* (Elahinik *et al.*, 2023). They appear to lack the classical GAO metabolism, as they are unable to produce PHA and are instead presumed to rely predominantly on fermentative metabolism within EBPR systems, as fermentative glycogen-accumulating organisms (fGAO) (Elahinik *et al.*, 2024, 2022; McIlroy *et al*., 2018; Tian *et al*., 2025).

Moreover, *Propionivibrio* are generally recognized as GAOs, as they perform PHA cycling without poly-P accumulation (Stokholm-Bjerregaard *et al.*, 2017; Yuan *et al.*, 2024). As a fermentative GAO, *Propionivibrio* is capable of fermenting organic substrates to VFAs. They utilize fermentatively derived energy and carbon sources to support cellular growth and facilitate glycogen accumulation (Dockx *et al.*, 2021; Pincam *et al.*, 2024). Besides, in situ studies have confirmed that *Ca. Competibacter* and *Ca. Contendobacter* stores VFAs as PHA without P-cycling under anoxic conditions, which is characteristic of the GAO metabolic phenotype (Stokholm-Bjerregaard *et al.*, 2017).

Irrespective of the specific type of PAOs, the cellular proliferation and phosphorus removal efficiency of PAOs are modulated by external factors, including the composition of feed characteristics, the chemical oxygen demand to phosphorus (COD:P) ratio, pH, and temperature (Erdal *et al.*, 2008; Oehmen *et al.*, 2007; Y. Zhang *et al.*, 2024). Specifically, municipal wastewater contains complex carbon sources, and understanding how PAOs and GAOs respond to these substrates under operating conditions is important, as carbon uptake directly governs their competitive interactions (Chen *et al.*, 2022).

1.3.5. Effect of the type of carbon source on the PAOs and EBPR efficiency

Optimal performance of EBPR systems and the composition of PAOs and GAOs in the population can vary depending on the type of carbon sources present in the wastewater. Typically, GAOs compete with PAOs for the anoxic uptake of carbon sources, thereby diminishing phosphorus removal efficiency because of the elevated carbon requirement (Oehmen *et al.*, 2007; Zhang *et al.*, 2025, 2024). The uptake of substrates under anoxic conditions is an energy-demanding process, and not all organic compounds are effectively assimilated in such an environment. Therefore, the availability of biodegradable organic carbon

is critical for supplying the energy necessary to support EBPR during the metabolic activity of PAOs (Hu *et al.*, 2018; Zhang *et al.*, 2025). While the addition of commercial organic compounds can serve as an external electron donor, this approach is often economically and environmentally unsustainable (Zhang *et al.*, 2025). Accordingly, it is essential to understand the influence of carbon sources to improve system efficiency.

1.3.5.1. Effect of volatile fatty acids

Volatile fatty acids (VFAs) are favored for enhancing the performance of EBPR, and most laboratory-scale experiments investigating it utilize VFAs as the primary carbon source due to their high degradability and diffusibility (Dockx *et al.*, 2021). Phosphorus removal efficiency in EBPR systems is strongly influenced by both the type and concentration of VFAs present (Zhao *et al.*, 2022). Both acetate and propionate are capable of supporting stable performance when applied individually, in combination, or through alternating dosing strategies, typically comprising 60% - 80% of the total VFA content (Zhang *et al.*, 2025). The proportion of acetate to propionate has been shown to influence the metabolic activity of PAOs, thereby affecting their phosphorus removal efficiency within treatment systems (Xie *et al.*, 2017). For instance, it was observed that influent containing a mix of acetate and propionate at ratios of 75:25% and 50:50%, combined with a pH of 7.5, is likely to support the metabolic activity of PAOs in preference to GAOs (Izadi *et al.*, 2020; Zhao *et al.*, 2022). Moreover, shifting the carbon source from solely acetate to a mixture of acetate and propionate in a 1:1 ratio increased the relative abundance of *Dechloromonas* from 1.5% to 4.8%. (Zhang *et al.*, 2025).

Propionate may be more favorable than acetate for promoting PAOs over GAOs, and appears to be more readily metabolized by PAOs than by other microbial populations (Chen and Gu, 2006; Wei *et al*., 2014). This can be attributed to the lower phosphorus release to carbon uptake (P/C) molar ratio of propionate, which reflects PAO activity and indicates that PAOs require less energy to assimilate propionate (0.42 mol P/mol C) than acetate (0.5 mol P/mol C) (Zhang *et al.*, 2025). Nonetheless, acetate remains advantageous in achieving high phosphate removal efficiency and supporting maximal PHAs production (Hu *et al.*, 2018; Wei *et al.*, 2014). In systems fed with acetate, poly-β-hydroxybutyrate (PHB) typically constitutes the dominant PHA component, accounting for approximately 60% to 100% of total PHA content. In contrast, propionate as the carbon source tends to favor the formation of poly-β-hydroxyvalerate (PHV), comprising 35% - 85%, and poly-β-hydroxy-2-methylvalerate (PH2MV), ranging from 40%

to 60% (Zhang *et al.*, 2025). Accordingly, the variation in oxic P-uptake can be attributed to differences in the intracellular storage polymer content (Ziliani *et al.*, 2023). VFAs enhance EBPR performance but can increase treatment costs, whereas other organic substrates may also be utilized as carbon sources under anoxic conditions (Oehmen *et al.*, 2007; Y. Zhang *et al.*, 2024).

1.3.5.2. Effect of non-volatile fatty acids

Different non-VFA substrates, including amino acids, sugars, and alcohols, have been used as potential organic substrates in experiments aimed at enriching PAOs under anoxic conditions (Mulkerrins *et al.*, 2004; Qiu *et al.*, 2019; Wei *et al.*, 2014). These complex carbon sources, which are abundant in WWTPs, may serve as complementary substrates for enhancing the EBPR (Zhang *et al.*, 2025). In municipal wastewater containing complex organic compounds beyond VFAs, fermentative organisms convert these substrates into VFAs and other fermentation products. These fermentation products are then taken up and stored by PAOs and, where present, GAOs (Elahinik *et al.*, 2023; Izadi *et al.*, 2020; Mulkerrins *et al.*, 2004).

One example of such compounds is proteins. They constitute over half of the organic matter in wastewater. The hydrolysates of protein, amino acids, have shown potential as carbon sources to enhance EBPR. Amino acids, sugars, and small amines are stored intracellularly to serve as energy sources during subsequent oxic metabolism. When amino acids were used, the PHA composition comprised roughly 20% PHB, 60% PHV, and 20% PH2MV; the pattern resembled that of a propionate-fed culture, with PHV being the dominant storage polymer (Zhang *et al.*, 2025). Further, both pure-culture and in situ studies have demonstrated that *Dechloromonas* species can grow on VFAs and casamino acids as substrates, enabling phosphate release under anoxic conditions (Petriglieri *et al.*, 2021).

Furthermore, glucose is commonly present in domestic wastewater and plays a significant role in the biochemical processes associated with substrate usage (Shen and Zhou, 2016). According to Zhang *et al.* (2025), glucose exhibits potential as a carbon substrate for EBPR systems under specific conditions, although its effectiveness is comparatively lower than that of acetate. Elahinik *et al.* (2023) reported that stable and sustained P-removal could be achieved in reactors using glucose as the sole carbon source. This performance was attributed to the metabolic cooperation between lactic acid-producing bacteria (*Micropruina,* fGAO) and PAOs.

Besides, alcohols have also been used as carbon sources in EBPR systems, such as glycerol and ethanol (Xie *et al.*, 2017). The application of glycerol as an additional carbon source for nutrient removal is both economically and technically feasible. Glycerol degradation to VFAs by fermentative bacteria and subsequent biological utilization of these VFAs represents a promising strategy to transform glycerol into a valuable resource rather than a waste product of biodiesel production (Zhang *et al.*, 2025). Moreover, ethanol is a readily biodegradable compound that has been reported to be directly assimilated by microorganisms, allowing for successful EBPR after prolonged acclimation. Ethanol is generally cheaper than both acetate and propionate, and thus offers an economic advantage as an alternative carbon source when a carbon surplus is needed in a wastewater treatment plant, especially COD-limited wastewater to improve denitrification (Hu *et al.*, 2018; Wei *et al.*, 2014; Zhang *et al.*, 2025). Besides the type of carbon sources, other external operational parameters should be taken into account to enhance system efficiency.

1.3.6. Effect of pH, COD:P ratio and temperature on the PAOs and EBPR efficiency

Optimizing operational parameters such as pH, COD:P ratio, and temperature directly influences the activity of PAOs and microbial competition in EBPR systems (Oehmen *et al.*, 2007). Once properly controlled, they promote stable and efficient phosphorus assimilation, which is essential for meeting effluent regulations and minimizing eutrophication risks in the receiving water bodies. Thus, fine-tuning these conditions plays a vital role in maximizing EBPR performance.

1.3.6.1. Effect of pH

In EBPR, pH plays a crucial role in the growth of PAOs and the P-removal process. pH can influence the permeability and surface chargeability of microbial cell membranes of PAOs, and it is associated with the growth and proliferation of microorganisms. Due to variations in the charge of the cell membrane, microorganisms exhibit different capacities for nutrient uptake, influencing their vital functions (Li *et al.*, 2018; Y. Zhang *et al.*, 2024). Moreover, pH can affect the biochemical reactions involved in P-removal by affecting the activity of enzymes, *ppk* and *ppx*, within the metabolic processes of PAO cells. For instance, the activity

of *ppk* increases with pH in the range of 6.5-8, leading to improved P-removal performance (Wang *et al.*, 2013; Y. Zhang *et al.*, 2024).

Li *et al.* (2018) indicated that acetic acid crosses cell membranes, is converted inside cells into ions and protons, and utilizes the proton motive force (PMF) during EBPR. This uptake causes PAOs to break down stored poly-P, which is regarded as the principal mechanism responsible for energy production, to compensate for the PMF losses, leading to phosphorus release (Wang *et al.*, 2013). Elevated pH reduces the proton gradient, making PMF restoration more energy demanding and requiring greater poly-P degradation to maintain acetate uptake, which results in more pronounced phosphorus release at higher pH. However, beyond a pH of 8.0, phosphorus removal occurred mainly through chemical precipitation, resulting in a decrease in phosphorus removal rate. Generally, the pH of the EBPR system is optimal under neutral to slightly alkaline conditions (Li *et al.*, 2018). Maintaining pH within these limits suppresses the proliferation of GAOs in phosphorus removal systems and confers a competitive advantage to PAOs, thereby also affecting the structure of the microbial community (Nguyen *et al.*, 2023; Y. Zhang *et al.*, 2024; Zhao *et al.*, 2022).

1.3.6.2. Effect of COD:P ratio

Stable wastewater composition and flow, along with accurate determination of optimal COD and P loading, are crucial to prevent deterioration in biological treatment performance. COD:P ratio (g COD:g PO_4-P) in the influent is a key factor influencing the enrichment of PAOs, conferring both a competitive advantage and enhanced capacity for effective EBPR (Chuang *et al.*, 2011; Oehmen *et al.*, 2007). The stoichiometric carbon demand required to remove one unit of phosphorus has been reported to typically range between 10 mg and 20 mg COD per mg of P removed. These lower COD:P ratios promote the proliferation of PAOs over GAOs. Despite this, as the influent COD:P ratio increases, the surplus carbon exceeding the stoichiometric demands of PAOs was redirected toward GAOs (Majed and Gu, 2019). Higher ratios, e.g. > 50 mg COD: mg P, are inclined to the growth of GAOs in place of PAOs, and the sludge shows substantially lower efficiency in P-removal (Izadi *et al.*, 2020; Mulkerrins *et al.*, 2004; Oehmen *et al.*, 2007). To maintain conditions conducive to the coexistence of both PAOs and GAOs, influent COD:P ratios in most municipal wastewater treatment plants are often in the range of approximately 5–40 mg COD per mg P, which is generally sufficient to support effective biological phosphorus removal (Gu *et al.*, 2008).

1.3.6.3. Effect of temperature

Temperature appears to be the least controllable parameter, especially under field conditions, among the various factors influencing system performance (Panswad *et al.*, 2003). It impacts the growth and phosphorus removal efficiency of PAOs by modulating the enzyme activity and the competition dynamics between PAOs and GAOs. Elevating temperatures to between 20 °C and 30 °C could enhance the activity of key enzymes involved in phosphate removal, and most PAO strains exhibit their highest productivity within this range. However, it is also observed that lower temperatures (5 - 20 °C) preferentially support the growth of PAOs over GAOs (Oehmen *et al.*, 2007; Zhang *et al.*, 2024). In this manner, the growth rate of PAOs increases, whereas GAOs are adversely affected by low temperature and their growth is restricted by the presence of PAOs. Therefore, these conditions result in phosphorus removal even at low temperatures, allowing EBPR processes to operate effectively during the winter. This suggests that other system parameters (i.e. C-sources and sludge retention time) mitigate the adverse effects of low temperatures, resulting in a limited impact on the P-removal performance of PAOs (Zhang *et al.*, 2024). To assess biomass activity under winter/cold climate conditions, tests are rarely performed below 5 °C because in practice the temperature of municipal wastewater is seldom colder and is usually around 7 - 12 °C (Loosdrecht *et al.*, 2016).

GAOs exhibit characteristics of mid-range mesophiles, with optimal growth observed between 25 °C and 32.5 °C. In contrast, PAOs have been identified as lower-range mesophiles, or potentially psychrophiles, with predominance occurring at temperatures around 20 °C or lower (Mulkerrins *et al.*, 2004; Panswad *et al.*, 2003). However, temperature effects on biological phosphorus removal remain inconclusive, with some studies indicating enhanced process efficiency at elevated temperatures (20 - 37 °C), whereas others have reported comparatively superior phosphorus removal performance under lower temperature conditions (5 - 15 °C) (Mulkerrins *et al.*, 2004).

1.4. Aim of thesis

BES technologies offer a promising approach for advancing the transition toward sustainable and clean energy production coupled with wastewater treatment. Nevertheless, the widespread industrial implementation of BES requires substantial improvements in the system

performance. The first part of this thesis aimed to optimize the interface between electroactive biofilms and the electrode surface to enhance biofilm formation and current generation. To this end, simple and cost-effective surface modification strategies were developed to enhance the feasibility of BES processes for future industrial applications. Accordingly, riboflavin and AQDS were selected for surface functionalization via physical adsorption due to their biocompatibility and high electron transfer efficiency with electrodes. Subsequently, the effect of surface roughness, ranging from smooth to rough, on the current production was investigated under optimized functionalization conditions.

The second part of the thesis aimed to deepen the understanding of how external conditions influence EBPR and to identify optimal operational parameters that improve phosphorus removal efficiency from wastewater. For this purpose, the 27,080 m³ biological treatment unit of the Langenhagen WWTP was downscaled to a 150 µL microfluidic model biofilm system (MMBS) based on the activated sludge process, enabling direct observation of biofilm formation. This system provided controlled simulation of alternating anoxic–oxic conditions and enabled the enrichment of PAOs as the targeted organisms, thereby allowing detailed investigation. To achieve this goal, a systematic analysis of key process parameters was performed using different carbon sources, COD:P ratios, pH values, and temperatures to examine their impact on PAO diversity and abundance, PAO-GAO interactions, phosphorus removal, and overall EBPR performance.

2. Materials and Methods

Unless otherwise noted, all chemicals and gases used were supplied by Westfalen AG (Münster), Saustein (Steinfurt), AppliChem (Darmstadt), Merck (Darmstadt), Carl Roth (Karlsruhe), Sigma-Aldrich Chemie (Taufkirchen), Cayman Chemical (USA) or Fisher Scientific (UK).

2.1. Construction of the microfluidic reactors

The microfluidic platform, already tailored (Hansen *et al.*, 2019), was used to cultivate microorganisms. In this study, straight and meandering channel microfluidic systems at the micro-scale were used to evaluate the removal of carbon and phosphorus, as well as energy and resource recovery, from wastewater. Both platform designs were based on the dimensions of standard microscope slides (76 × 26 mm^2 DIN ISO 8037–1:2003–05). PDMS (Sylgard^{TM} 184, Dow, Wiesbaden, Germany) was used to fabricate the different shapes of the cultivation platform following the relevant protocol. After casting silicone into a negative brass mold, it was polymerized at 60 °C for 2 h in the hybridization incubator (GFL, 7601). Access ports for the cultivation channel were created by inserting placeholder cannulas. The open channel of the silicone body was covalently bonded with a glass coverslip using oxygen plasma treatment (SmartPlasma 10 Pro, Plasma Technology GmbH, Herrenberg, Germany). To strengthen the bond between silicone and glass, reactors were incubated at 100 °C for approximately 20 min in the hybridization oven (HB 400-230 V, Hoefer Scientific Instruments, USA).

The reactor used in the BES was a straight channel with a length of 61.75 mm and a total volume of 354 µl. A brass insert was added to the mold to create a 1 × 1 cm recess in the silicone body for later insertion of a graphite electrode (Figure 6). A glass slide (1.0 mm, Epredia, ISO 8037/1) was used to cover the open PDMS channel.

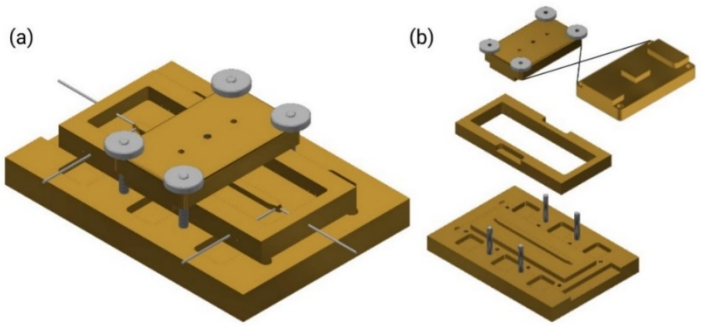

Figure 6. Casting mold for producing microfluidic reactors made of PDMS for the BESs. An assembled casting chamber with four inserted placeholder cannulas is shown in (a). (b) indicates the individual parts of the casting chamber. The mold is composed of a base with a negative straight channel, a frame with holes to insert cannulas. Additionally, a brass component is attached to create a 1 cm² recess in the silicone body for insertion of the electrode.

In the MMBS, the cultivation platform with meandering channels (Figure 7) was applied to mimic the EBPR process and enrich PAOs for phosphate elimination from wastewater.

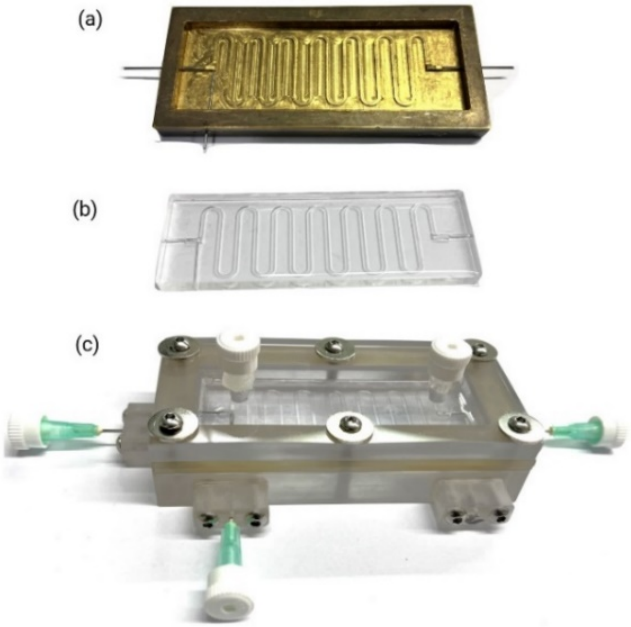

Figure 7. Production of meandering reactors for the MMBS. A casting chamber with three inserted placeholder cannulas is shown in (a). (b) and (c) show a PDMS reactor with bonded cover glass and assembled reactor, respectively.

The meandering cultivation channel had a total length of 296.9 mm, with a cross-section of 1 mm x 0.5 mm (width × height) and contained 13 turns. It included two prechambers, one at

each end, each with a volume of 5.36 µL, resulting in a total cultivation volume of 159.17 µL. Surface area (SA) was 296.9 mm x 3 mm (length × perimeter of the cross section), and the ratio of surface area to volume (SA:V) in a microfluidic reactor was approximately 5.6 * 10^3 m^{-1} (area in m^2 per volume in m^3). After casting, the meandering microfluidic channel geometry made of PDMS was covalently bonded with a cover glass (0.13-0.16 mm thickness, Thermo Scientific, Braunschweig, Germany) using oxygen plasma treatment.

2.2. Biofilm cultivation in BES

2.2.1. Cultivation medium

The bacterial strains used in this study are listed in Table 1 below with their respective strain numbers, and relevant genotypes.

Table 1. List of bacterial strains used in the BES experiment.

Strain	*Genotypes*	*Reference*
JG7	*Shewanella oneidensis* MR-1	(Venkateswaran *et al*., 1999)
JG407	*Geobacter sulfurreducens* PCA	(Caccavo *et al*., 1994)

The long-term storage of bacterial strains was carried out by cryopreservation. For this purpose, 1 ml of a densely grown liquid culture was mixed with 300 µL of glycerol in a cryotube and immediately deep-frozen in liquid nitrogen. Subsequent storage took place at -80 °C and in liquid nitrogen.

All media were prepared with ultrapure water (PURELAB Plus, Veolia Water Technologies Deutschland, Celle) (see Tables 2, 3, and 4). Anoxic media were anaerobized in a bottle with an anoxic rubber stopper and lid for an hour by repeated cycles of gassing (80% N_2/20% CO_2) and vacuuming. These were autoclaved subsequently for 20 min at 121 °C and 1 bar overpressure. Heat-sensitive substances in Table 4 were sterile-filtered (0.2 µm, Sarstedt AG & Co., Nümbrecht, Germany) and added to the autoclaved media.

The wild-type strain of *S. oneidensis* MR-1 was cultivated from frozen cultures, which were spread onto lysogeny broth (LB) agar plates and incubated at 30 °C. Single colonies from these plates were pre-grown overnight in LB medium under oxic conditions at 30 °C and 160 rpm. The overnight precultures were then transferred to anoxic minimal medium in Table 5.

To cultivate the wild-type strain of *G. sulfurreducens* PCA cultures, 2 ml of a cryo-culture was transferred into 1 L of anoxic preculture medium (see Table 6). This culture was pre-grown at 30 °C for at least 5 days and subsequently transferred up to a maximum of 5 times.

Table 2. NB trace mineral solution.

Component	*g L^{-1}*	*mM*
Nitrilotriacetic acid (with KOH to pH 6.5)	2.140	11.20
$MnCl_2 * 4\ H_2O$	0.100	0.51
$FeSO_4 * 7\ H_2O$	0.300	1.08
$CoCl_2 * 6\ H_2O$	0.170	0.71
$ZnSO_4 * 7\ H_2O$	0.200	0.70
$CuCl_2 * 2\ H_2O$	0.300	1.76
$AlK(SO_4)_2 * 12\ H_2O$	0.005	0.01
H_3BO_3	0.005	0.08
$Na_2MoO_4 * 2\ H_2O$	0.110	0.45
$NiSO_4 * 6\ H_2O$	0.110	0.41
$Na_2WO_4 * 2\ H_20$	0.200	0.61
pH = 7.0.		

Table 3. Selenite tungstate solution.

Component	*mg L^{-1}*	*µM*
NaOH	500	12.5
Na_2SeO_3	3	17
$Na_2WO_4 * 2\ H_2O$	4	12

Table 4. Vitamin solution.

Component	*mg L^{-1}*
Biotin	2.0
Folic acid	2.0
Pyridoxine-HCl	10.0
Thiamine-HCl	5.0
Riboflavin	5.0
DL-Ca-Pantothenate	5.0
Nicotinic acid	5.0
Vitamin B_{12}	0.1
p-Aminobenzoic acid	5.0
Lipoic acid	5.0

Table 5. Anoxic preculture medium for *S. oneidensis*.

Component	*g L^{-1}*	*mL L^{-1}*	*mM*
KH_2PO_4	0.42		3.09
K_2HPO_4	0.22		1.26
NH_4Cl	0.20		3.74
KCl	0.38		5.10
NaCl	0.36		6.16
$NaHCO_3$	1.80		21.43
Na_2CO_3	0.50		4.72
$MgCl_2$ * 6 H_2O	0.21		1.05
Na-D,L-Lactate (60%)	13.07		70
Casamino acids	1.00		
HEPES	11.92		50
Fumarate	11.60		100
NB trace mineral solution (see Table 2)		10	
Selenite tungstate solution (see Table 3)		1	

Autoclaved and then anaerobized with 80% N_2/20% CO_2. Complemented with 10 ml L^{-1} vitamin solution (see Table 4), 1 ml L^{-1} 0.2 M Na-Ascorbate and 1 ml L^{-1} 0.4 M $CaCl_2$ * 2 H_2O. pH = 7.0.

Table 6. Anoxic preculture medium for *G. sulfurreducens.*

Component	*g L^{1}*	*mL L^{-1}*	*mM*
KH_2PO_4	0.42		3.09
K_2HPO_4	0.22		1.26
NH_4Cl	0.20		3.74
KCl	0.38		5.10
NaCl	0.36		6.16
$NaHCO_3$	1.80		21.43
Na_2CO_3	0.50		4.72
$MgCl_2$ * 6 H_2O	0.21		1.05
Na-Acetate	1.23		15
Fumarate	4.64		40
NB trace mineral solution (see Table 2)		10	
Selenite tungstate solution (see Table 3)		1	

Autoclaved and then anaerobized with 80% N_2/20% CO_2. Complemented with 10 ml L^{-1} vitamin solution (see Table 4), 1 ml L^{-1} 0.2 M Na-Ascorbate, 1 ml L^{-1} 0.4 M $CaCl_2$ * 2 H_2O and 0.1% yeast extract (w/v). pH = 7.0.

The cultivation medium of the co-culture of *S. oneidensis* and *G. sulfurreducens,* and the required carbon sources based on the cultivation of the microorganisms are given in Tables 7 and 8.

Table 7. Cultivation medium for the co-culture of *S. oneidensis* and *G. sulfurreducens.*

Component	*g L^{-1}*	*mL L^{-1}*	*mM*
KH_2PO_4	0.42		3.09
K_2HPO_4	0.22		1.26
NH_4Cl	0.20		3.74
KCl	0.38		5.10
NaCl	0.36		6.16
$NaHCO_3$	1.80		21.43
Na_2CO_3	0.50		4.72
$MgCl_2$ * 6 H_2O	0.21		1.05
Na-D,L-Lactate (60%)	3.73		20
Casamino acids	0.10		
HEPES	11.92		50
NB trace mineral solution (see Table 2)		10	
Selenite tungstate solution (see Table 3)		1	

Autoclaved and then anaerobized with 80% N_2/20% CO_2. Complemented with 10 ml L^{-1} vitamin solution (see Table 4), 1 ml L^{-1} 0.2 M Na-Ascorbate and 1 ml L^{-1} 0.4 M $CaCl_2$ * 2 H_2O. pH = 7.0.

Table 8. Carbon sources for the cultivation of the microorganisms.

Utilization	*Microorganisms*	Lactate [mM]	Acetate [mM]	Fumarate [mM]	Yeast extract [g L^{-1}]
Pre-cultivation	*S. oneidensis*	70	-	100	-
	G. sulfurreducens	-	15	40	1
Cultivation medium	Co-culture	20	-	-	-

2.2.2. Inoculation and growth conditions of the model exoelectrogens

Cells were washed with the washing buffer listed in Table 9, which was anaerobized with an 80% N_2/20% CO_2 gas mixture. A suspension of the co-culture of *S. oneidensis* and *G. sulfurreducens* at a ratio of 10:1 was prepared from pre-grown cultures. An abundance of *S. oneidensis* cells was added since *G. sulfurreducens* relies on the acetate provided by *S. oneidensis*. The optical density (OD) of the inoculum was 2.0, measured by a spectrophotometer (Thermo Spectronic, Genesys 20, 4001/4, USA) at 600 nm. The whole system was first flushed with 70% ethanol, followed by equilibration with medium for a minimum of 12 hours before inoculation. Inoculation was performed using an L160 syringe pump (Landgraf Laborsysteme HLL GmbH, Langenhagen, Germany) at a flow rate of 2 mL h^{-1} through a separate side port of the microfluidic reactor over a 2-hour period with gastight fluororubber tubing (Cole-Parmer, Vernon Hills, IL, US).

Table 9. Washing buffer.

Component	*g L^{-1}*	*mM*
KH_2PO_4	0.42	3.09
K_2HPO_4	0.22	1.26
NH_4Cl	0.20	3.74
KCl	0.38	5.10
NaCl	0.36	6.16
Purged with 80% N_2/20% CO_2.		

Simultaneous pumping of the cultivation medium with a peristaltic pump (Ismatec, Reglo ICC, ISM4408, Materflex LLC, Barrington, IL) via the front access to the microfluidic reactor at 2 mL h^{-1} was intended to prevent the growth of microorganisms in the supply tubing upstream of the system. After inoculation, the cultivation medium flow rate was adjusted back to 4 mL h^{-1}.

2.2.3. Microfluidic BES and experimental setup

The microfluidic platform allowed the insertion of a 1 x 1 cm electrode for the anodic growth (Klein *et al.*, 2024). After the microfluidic straight channel reactor was produced, the graphite electrode was inserted into the PDMS, as shown in Figure 8. Its material consisted of a composite made from graphite and polypropylene (PPG 86), exhibiting an electrical conductivity of 60.15 S cm^{-2} (Eisenhuth GmbH & Co. KG, Osterode am Harz, Germany). The graphite material was subjected to corundum blasting to produce a rougher surface. The arithmetic average surface roughness (Ra) was 1.43 µm, while the average of the maximum peak-to-valley height of the profile in the surface (Rz) was 12.1 µm.

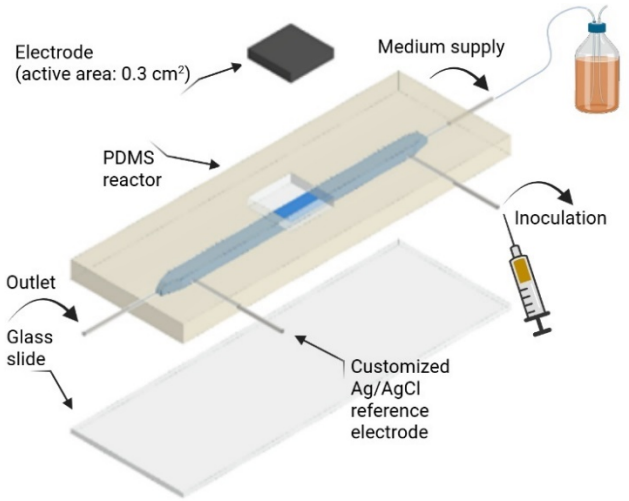

Figure 8. PDMS microfluidic reactor with a straight channel. Placeholder cannulas can be inserted into the brass mold during reactor production to create access points at any position. Cannulas can be inserted later for medium in/out, inoculation and reference electrode.

Blunt cannulas (B. Braun, Melsungen AG, Germany) with an inner diameter of 0.84 mm (18G) for medium supply and removal, as well as 0.51 mm (21G) for inoculation, were inserted at the position of the removed placeholder cannulas at the access points. In the frame, a 1 mm inner diameter silicone tubing (Carl Roth, Karlsruhe, Germany) was used to connect the reactors to each other and to the medium supply. Cannulas, 3-way stopcocks (BD Connecta™, Becton Dickinson, Franklin Lakes, New Jersey, USA), and luer lock fittings provided the connection between the tubing and the microfluidic reactors. Cultivation medium was supplied via a peristaltic pump (Ismatec, Reglo ICC, ISM4408, Materflex LLC, Barrington, IL) with a flow rate of 4 mL h^{-1}. Medium was provided to the reactors through an inner diameter of 1.5 mm silicone tubing (Carl Roth, Karlsruhe, Germany).

A complete BES was formed by connecting the anode and cathode reactors in series (Figure 9). The experiments were conducted in chambers, each containing triplicate reactors and comprising two sub-chambers: an anodic (anoxic) part and a cathodic (oxic) part (Figure 10).

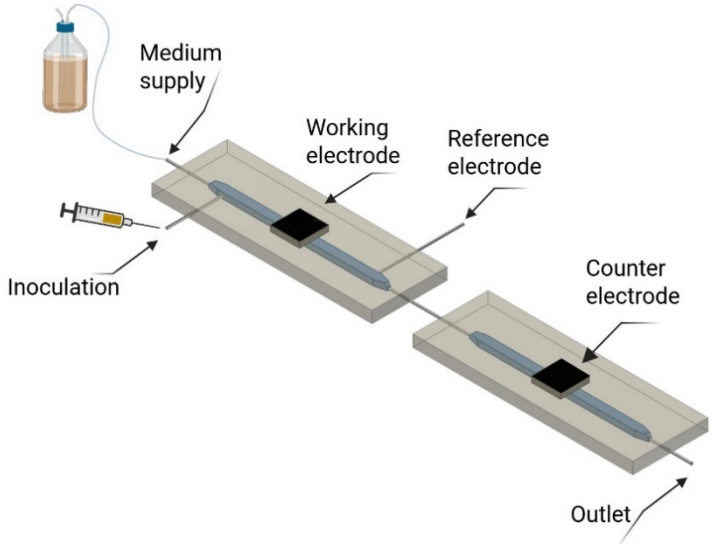

Figure 9. Schematic illustration of the BES reactors, showing the anodic compartment with the working and reference electrodes, and the cathodic compartment with the counter electrode.

The upstream reactor functioned as the working electrode and was equipped with a custom-made silver/silver chloride (Ag/AgCl) reference electrode. Due to the dimensions of the access points to the microfluidic reactors, reference electrodes were electrochemically produced at room temperature. In this regard, silver wire, 3 cm long and 0.8 mm in diameter (ChemPur, Karlsruhe, Germany), was first cleaned with ethanol. The dry silver wire, encircled with a fine platinum mesh, was subsequently submerged in a beaker filled with 0.1 M degassed hydrochloric acid (HCl). A potential was applied to the silver wire, which functioned as the working electrode, with the platinum mesh serving as the counter electrode. A commercial Ag/AgCl electrode served as the reference electrode. For the equilibration of electrochemical systems, an open-circuit voltage (OCV) was initially maintained for 5 min, followed by an overpotential of +50 mV (vs. OCV) for 50 min (Klein *et al.*, 2024). Within this method, Cl^- was attracted to positively charged Ag^+, resulting in the formation of a layer of AgCl on the silver wires. After drying, the freshly prepared Ag/AgCl electrode was used for each anodic reactor.

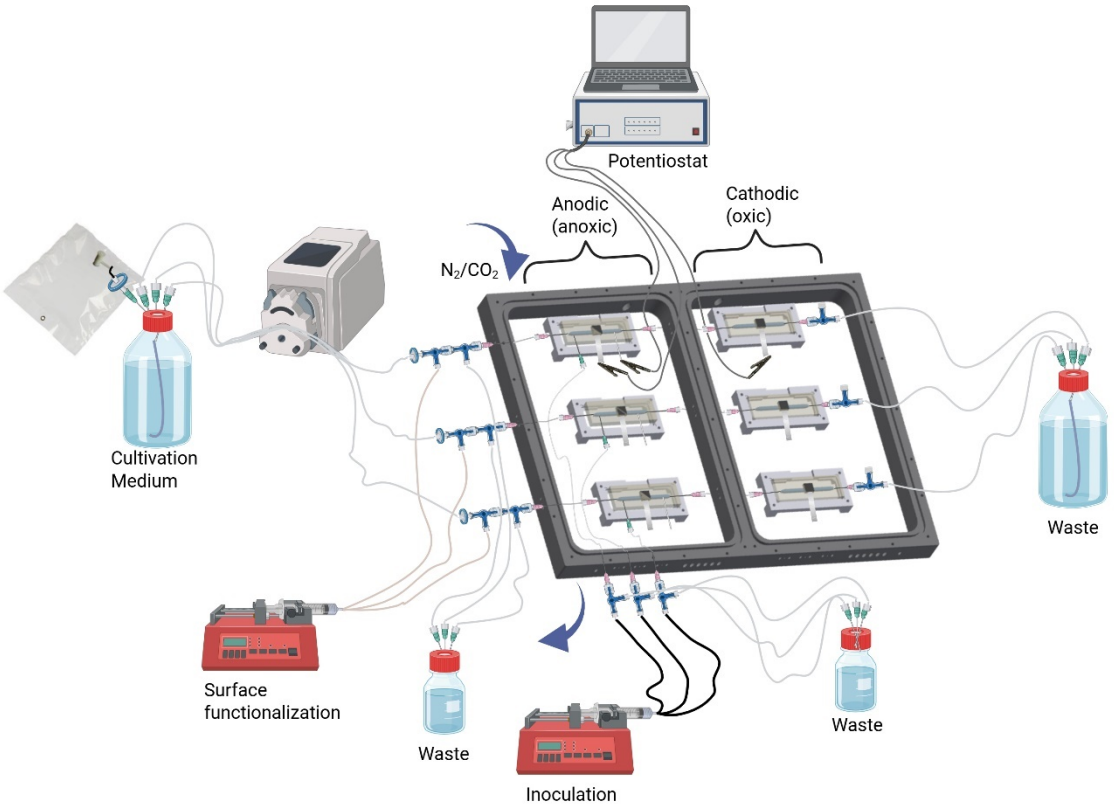

Figure 10. Schematic diagram of the BES system with microfluidic reactors.

A transparent lid was placed on the anodic side to provide anoxic conditions, and the working electrode on this side was used as the anode. The lid, frame, and bottom plate were made of a gas-tight polycarbonate (Figure 11). The chamber was continuously fed with a mixture of N_2/CO_2 (80:20, v:v) at a rate of 30 mL min^{-1} via side ports. Meanwhile, the cathode side was maintained under oxic conditions.

The working electrodes were attached to a potentiostat (VMP-300, BioLogic, Science Instruments, France) with EC-Lab software V11.43. A 0.1-mm-thick silver foil (Chempur, Karlsruhe, Germany) was used for the connection. Chronoamperometric analyses with an applied potential of 0 V (vs. SHE) were used to measure the current density produced by the biofilm on the electrode surface to correlate with the biofilm growth.

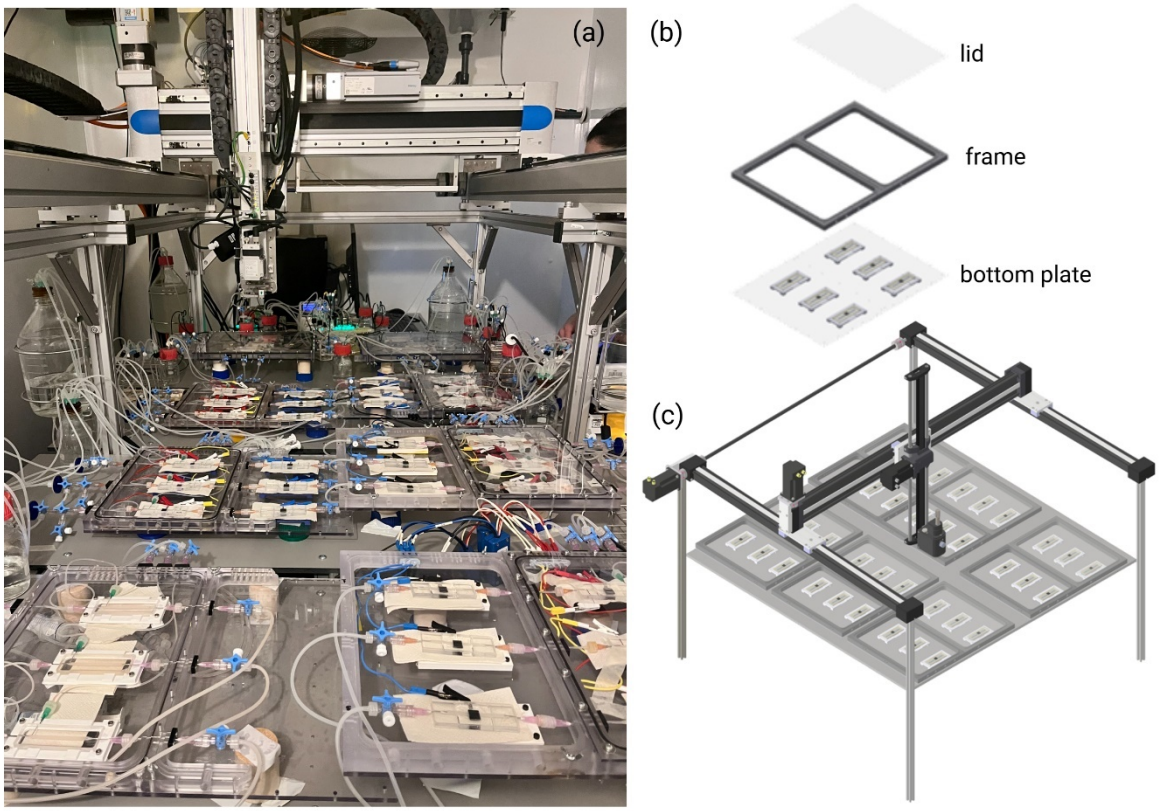

Figure 11. OCT platform components. Microfluidic cultivation experiments were conducted in a 30-degree room. All platform components were designed to be modular, enabling multiple parallel experiments with customized conditions and non-destructive in-situ analysis. An automated OCT platform for biofilm cultivation and imaging is shown in (a). The system consists of a bottom plate, frame and lid in (b). The platform allows simultaneous operation of up to six triplicate sets for the continuous biofilm growth in (c).

In BES experiments, two different approaches were evaluated: (I) to improve the biofilm-electrode interaction by electrode surface functionalization and (II) to test the effect of surface roughness on the generated current density and biofilm formation. For the first approach, riboflavin and AQDS were used for surface functionalization (Table 10).

Table 10. Biocompatible compounds for surface functionalization.

Component		*g 100mL^{-1}*	*mM*
$C_{17}H_{20}N_4NaO_9P * xH_2O$	FMN-Na (Riboflavin 5′-monophosphate sodium salt hydrate)	0.72	15
$C_{14}H_6Na_2O_8S_2$	AQDS (Anthraquinone-2,6-disulfonic acid disodium salt)	0.62	15

Besides, the surface roughness of the graphite electrode influences the efficiency of BES. For the surface roughness experiments, graphite electrodes with three different roughness levels were used for anodic biofilm growth. Scanning electron microscopy (SEM) (Zeiss Supra 55 VP with Gemini column) was used to compare the surface morphology and roughness of the electrodes at the microscale.

2.2.4. Biofilm imaging using optical coherence tomography (OCT)

Methods to examine biofilm structure optically can be based on the scales of the images. This distinction into individual cells, cell clusters, microscopic, mesoscopic, and macroscopic structures was made by Wagner *et al.* (2010). OCT is a non-invasive, in-situ imaging technique that enables online investigation of mesoscopic biofilm structures at the millimeter scale directly in the cultivation platform. The focus is on the development of the biofilm over time under operational conditions (Wagner and Horn, 2017) on the anode with parallel measurements. The tomograph includes a light source, a beam splitter, a reference arm, and a sample arm, as seen in Figure 12.

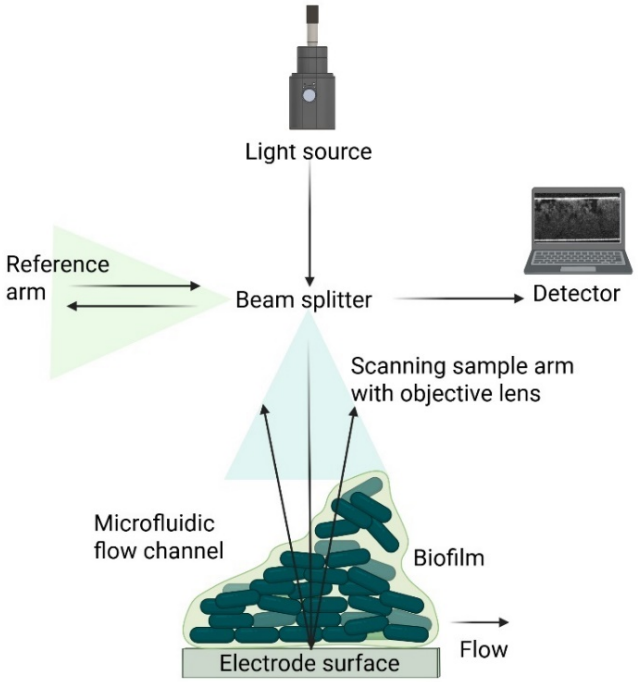

Figure 12. Schematic overview of the imaging biofilm with OCT.

The sample arm has an objective lens focusing on the biofilm. OCT is based on light reflection, scattering, and interference with materials. Light reflected and scattered from the biofilm interferes with the light from the reference arm at the beam splitter. These interference signals from the biofilm are captured digitally in a greyscale image and analyzed for structural information (Wagner and Horn, 2017).

2D images consist of pixels, and 3D images consist of voxels. OCT raw images have a bit depth of 32 means each voxel has a value between 0 and 2^{32}, where biofilms are white (0) and voids are black (2^{32}), and between 0 and 2^{32} has grey values. Due to the resolution of the monitors used, firstly, the images were converted to 8-bit image (2^8). This means that each voxel can take a value between 0 and 256, from white to many shades of grey to black. To straighten images and cut away the surface, "untilt" was then applied. In the binarization step, an appropriate threshold value between 0 and 255 must be applied to separate biomass from the background signal. After binarization, the images have a bit depth of 1 (2^1). At the end, there are only black (background) voxels or white (biofilms) voxels. All further OCT image processing steps and calculations were based on these binary image datasets.

The biofilm development of the co-culture of the two model organisms, *S. oneidensis* and *G. sulfurreducens*, on the graphite electrodes in the BES was monitored with automated OCT using a Ganymede (GAN611, Thorlabs GmbH, Dachau, Germany). An LSM03 objective lens and software version 5.7.3 were used. The nominal central wavelength of the light source was 930 nm. The 3D OCT datasets (C-scans) were 9 mm x 2.5 mm x 1.4 mm (L x W x H) with pixel size in x-y plane = 4 μm/pixel and a pixel height of 2.14 μm. The acquisition speed was 100 kHz with a refractive index of water n = 1.33.

Biofilm quantification was conducted by calculating the biofilm volume by correlating the white pixel numbers with the voxel size derived from the binary OCT images (Klein *et al.*, 2024, 2022), as shown in Equation 1. The resulting biovolume values were then normalized by dividing the total biofilm volume by the frame of view (FOV: L x W) area (0.225 cm^2), as described in Equation 2, which also provides the mean biofilm height. This method allows for the homogenization of structural heterogeneities within the biofilm (Wagner and Horn, 2017).

$$Biovolume\ (mm^3) = The\ number\ of\ white\ pixels\ x\ voxel\ size \quad (1)$$

$$Normalized\ biovolume\ (mm^3\ cm^{-2}) = \frac{Biovolume}{FOV} \quad (2)$$

Further, current data were normalized to the projected surface area of the working electrode (0.3 cm^2). The current density was calculated by dividing the generated current by the anode surface area (Equation 3).

$$Current\ density\ (\mu A\ cm^{-2}) = \frac{Current}{Analyzed\ area} \quad (3)$$

Additionally, biofilm porosity, surface coverage, and biofilm surface roughness were calculated for the BES as described below. Biofilms can be porous and have holes. The mean height of the biofilm is the real height (h_{real}) from height maps. Calculating biovolume per area gives a theoretical biofilm height ($h_{theoretical}$). The porosity of the biofilms was calculated by correlating h_{real} with $h_{theoretical}$ (Klein *et al.*, 2024) with Equation 4. The obtained data revealed the proportion of voids within the biofilm.

$$Porosity\ \% = \frac{hreal - htheoretical}{hreal}\ x\ 100 \quad (4)$$

Further, graphical height profiles of the biofilms on the anodes were generated based on Wagner and Horn (2017). These height maps were used to evaluate surface coverage. While the amount of black pixels indicated no coverage, all other colors showed that biofilm coverage was present. The percentage of the surface area covered by the biofilm was determined using Equation 5. Moreover, biofilm roughness indicates the degree of heterogeneity of the biofilm surface and was calculated as the mean biofilm height divided by its standard deviation (Equation 6).

$$Coverage\ \% = \left(1 - \frac{Black\ pixels}{All\ pixels}\right)\ x\ 100 \quad (5)$$

$$Roughness = \frac{mean\ thickness}{standard\ deviation\ of\ thickness} \quad (6)$$

2.3. Biofilm cultivation in MMBS

2.3.1. Cultivation medium

All experiments were conducted with synthetic wastewater (see Tables 11 and 12) as a feed to control the experimental conditions precisely, provide different wastewater compositions, and evaluate the effects of individual compounds (Loosdrecht *et al*., 2016). The system was continuously fed with cultivation medium prepared separately, consisting of a carbon source during the anoxic phase (Table 13) and a phosphate source supplied in the oxic phase (Table 14).

Table 11. Trace element solution.

Component	*g L^{-1}*	*mM*
EDTA	10.0	26.87
$FeCl_3$ * 6 H_2O	1.50	5.55
H_3BO_3	0.15	2.43
$CuSO_4$ * 5 H_2O	0.03	0.12
$MnCl_2$ * 4 H_2O	0.12	0.61
Na_2MoO_4 * 2 H_2O	0.06	0.25
$ZnSO_4$ * 7 H_2O	0.12	0.42
KI	0.18	1.09
CoCl * 6 H_2O	0.15	0.63

Table 12. Synthetic wastewater.

Component	*mg L^{-1}*	*mM*
NH_4Cl	107	2
$MgSO_4$ * 7 H_2O	90	0.37
$CaCl_2$ * 2 H_2O	14	0.10
KCl	36	0.48
Yeast extract	1	

Autoclaved and then anaerobized with N_2. Complemented with 0.3 mL L^{-1} trace element solution (see Table 11). pH = 7.5.

Table 13. Anoxic medium (C-source).

Carbon Source	*Formula*	*g L^{-1}*	*ml L^{-1}*	*mM*
D(+)-Glucose-Monohydrat	$C_6H_{12}O_6 * H_2O$	0.10		0.52
Casein hydrolysate	$C_{21}H_{41}N_5O_{11}$	0.07		0.12
Glycerol	$C_3H_8O_3$	0.08		0.90
Ethanol	C_2H_6O		0.06	1.04
Na-Acetate (75%)	$C_2H_3NaO_2$	0.10		1.17
Na-Propionate (25%)	$C_3H_5NaO_2$	0.02		0.20

Table 14: Oxic medium (PO_4-P source).

PO_4-P Source	*mgP L^{-1}*	*COD/P*	*g L^{-1}*	*µM*
$NaH_2PO_4 * 2H_2O$	1.25	80	0.006	40.4
$NaH_2PO_4 * 2H_2O$	2.5	40	0.013	80.8
$NaH_2PO_4 * 2H_2O$	10	10	0.050	323

2.3.2. Inoculation and growth conditions of PAOs

Langenhagen wastewater treatment plant (30853 Langenhagen, Germany) contains nitrification, denitrification, and biological phosphorus removal processes. After metagenomic studies, including analyzing the community composition and identifying PAOs, activated sludge was used from the anoxic (Bio-P) tank as an inoculum (see Appendix, Figure S2).

The wastewater was pretreated before inoculation to prevent clogging of the microfluidic system. For pretreatment, 1 L of activated sludge was concentrated to 30% by allowing the sludge to settle and then decanting the supernatant. Subsequently, it was diluted 1:10 (v:v) (sludge to ultrapure water) with ultrapure water and filtered through a 160 µm glass filter (Por. 1, P 160, 100-160 µm, ISO 4793-80). This filtration step removed larger particles, leaving only planktonic cells and smaller biofilm flocs, essential for the inoculation process in a microfluidic cultivation system. Before inoculation, the complete system was stabilized with the cultivation medium.

The inoculation was performed via a separate side entrance at a flow rate of 0.6 mL h^{-1} with a syringe pump (LA160, Landgraf Laborsysteme HLL GmbH, Langenhagen, Germany) for 22 h (Klein *et al.*, 2022). In order to prevent heterotrophic growth and the growth of microorganisms in the supply tubing upstream of the system, the P-containing cultivation medium was simultaneously pumped with N_2 using a peristaltic pump (Ismatec, ISM404B, Cole-Parmer, Barrington, IL, US) through the front access to the microfluidic reactor at a flow rate of 2 mL h^{-1}.

2.3.3. MMBS and experimental setup

After the microfluidic meandering channel reactor was produced, it was placed inside the chamber, which can be continuously purged with N_2 or compressed air to maintain anoxic or oxic conditions (Figures 13 and 14). To connect with the chamber and tubing, specially manufactured blunt cannulas (ID: 0.8 mm, BD Microlance, Spain), luer lock fittings and 3-way stopcocks (BD Connecta™, Becton Dickinson, Franklin Lakes, New Jersey, USA) were used. Inner diameter of 1.5 mm silicone tubing (Carl Roth, Karlsruhe, Germany) and fluorinated rubber (FPM) tubing (Reichelt Chemietechnik GmbH & Co., Heidelberg, Germany) were employed for the medium supply as well as for inoculation, respectively. In the meandering reactor, three access points allowed for medium inlet, outlet, and inoculation of the microorganisms. Additionally, valves functioned as the implementation of alternating cycles of anoxic and oxic cultivation media, as well as for the supply of N_2 and compressed air. With this aim, all media and gas tubings were connected to miniature active 2/2 normally closed valves (SMV-2R–BN1F; Takasago Kōryō Kōgyō, Tokyo, Japan). The valves were controlled by a custom-built control unit, which contained the programmable logic module. Additionally, the gas flow rate was monitored by gas sensors (Honeywell, Airflow Sensor, 50CC/MIN, 25PSI, 5VDC).

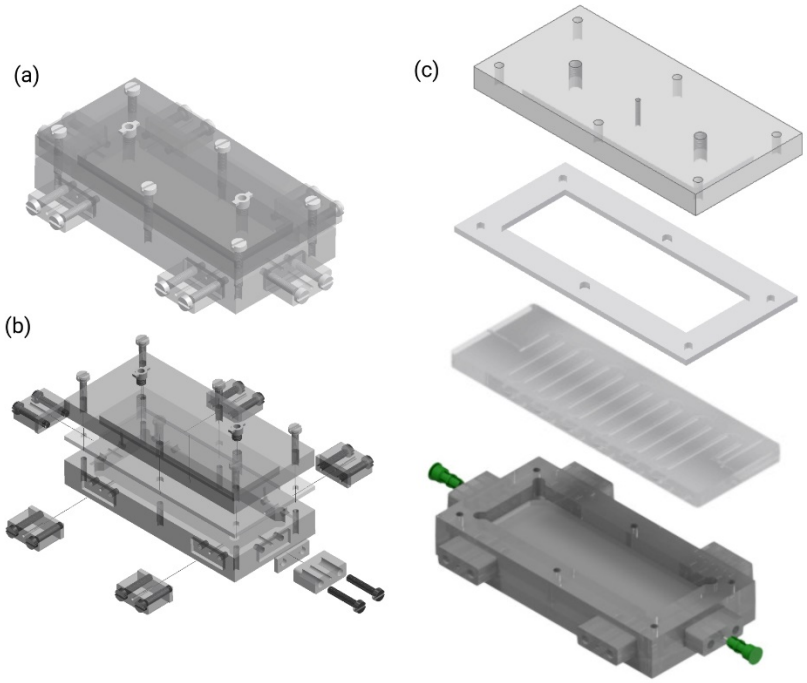

Figure 13. Cultivation platform setup in MMBS is shown: the assembled frame (a), components of the chamber (b), and individual parts of the microfluidic platform, including the base chamber with inserted cannulas, the PDMS meandering reactor with cover glass, the frame for gastight connection, and the top of the chamber for gas connection via tubing (c).

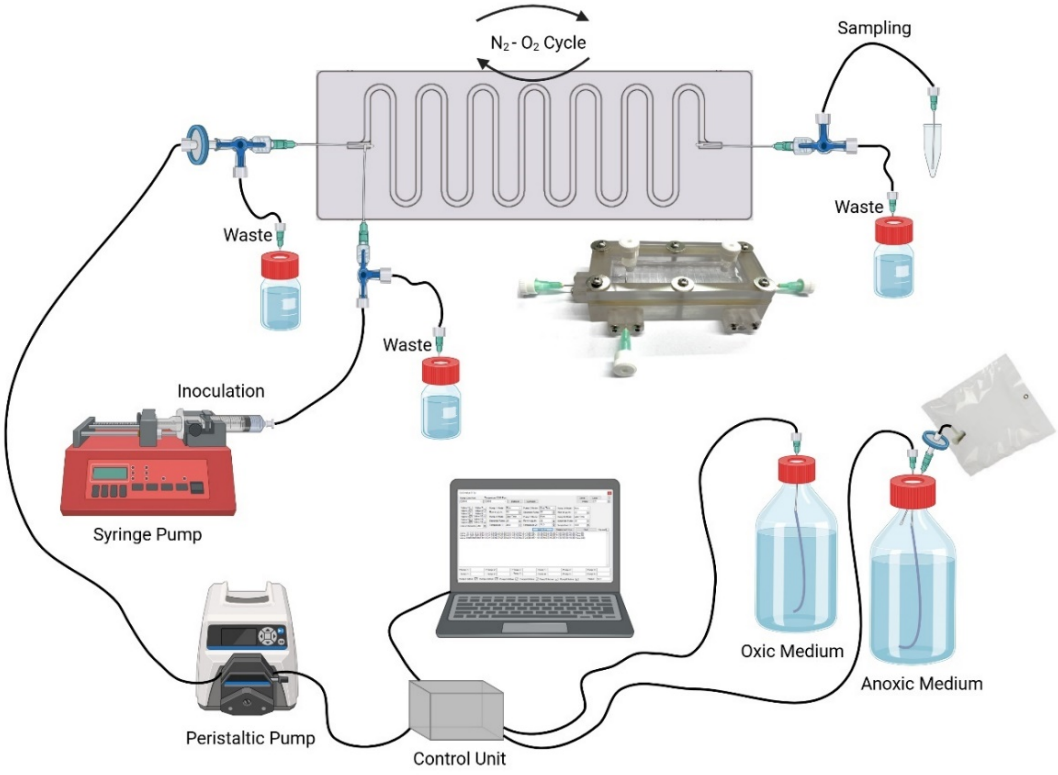

Figure 14. Schematic overview of the experimental setup for the cultivation of PAOs in MMBS.

The system was continuously fed with cultivation medium prepared separately, consisting of a carbon source (100 mg COD L^{-1}) during the anoxic phase with N_2, and a phosphate source (2.5 mg PO_4-P L^{-1}) supplied under aeration with compressed air in the oxic phase. The system consisted of anoxic/interphase/oxic/interphase stages with durations of 3/1/4/1 h, respectively, and a cycle was 9 h. At the interphase, an oxic medium was supplied under an anoxic gas (N_2) to ensure strict separation of the two main phases. Besides, interphase was implemented to prevent carbon from being available to the microorganisms simultaneously with oxygen as an electron acceptor for their growth. Cultivation was conducted for 20 days, and 2/3 of the time was with an oxic medium. The cultivation medium was supplied via the front port with a flow rate of 2 mL h^{-1} using a peristaltic pump. The system has been developed to perform three different experiments in triplicate (Figure 15).

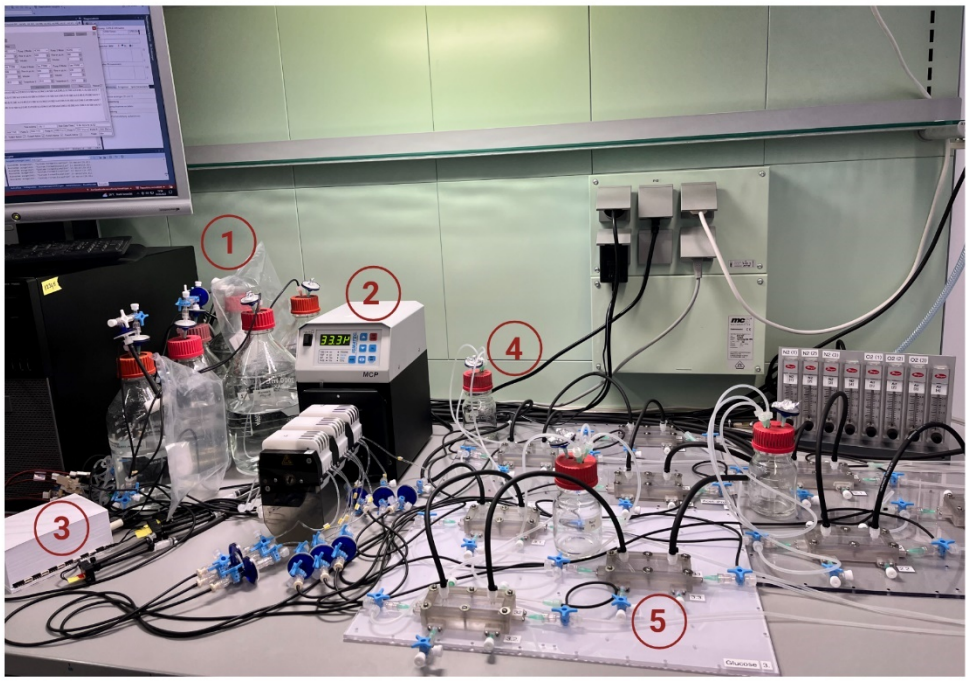

Figure 15. MMBS setup during the experiment. It shows (1) the oxic and anoxic medium bottles, (2) a peristaltic pump, (3) a custom-built programmable control box, (4) waste collection bottles, and (5) microfluidic reactors in the chambers.

The biofilm-based microfluidic reactor operated as a continuous flow-through system with a low working volume (µL). Due to the system's structure and scale, the sludge retention time (SRT) was not actively controlled and instead depended solely on the inconsistent washout of cells in the effluent. Further, hydraulic retention time (HRT) was 4.8 min (HRT = Reactor volume (V) / Flow rate (Q) = 159.17 µL / 33.33 µL min^{-1}).

As seen in Table 15, the impact of several factors on the efficiency of PAOs was analyzed. The key conditions selected for this study include the type of available carbon sources: glucose as a sugar, NZ-Amine as an amino acid, glycerol and ethanol as alcohols, as well as acetate and propionate as VFAs; pH values of 6.5, 7.5 and 8.0; COD:P ratio of 10, 40 and 80; as well as room temperature and 12 °C.

Table 15. Tested parameters in MMBS.

Carbon Source	*pH*	*COD (mg L^{-1})*	*PO_4 -P (mg L^{-1})*	*COD:P*	*Temperature (^oC)*
Glucose	7.5	100	2.50	40	RT[a]
NZ-Amine	7.5	100	2.50	40	RT[a]
Glycerol	7.5	100	2.50	40	RT[a]
Ethanol	7.5	100	2.50	40	RT[a]
HAc/HPr	7.5	100	1.25	80	RT[a]
HAc/HPr	7.5	100	10.0	10	RT[a]
HAc/HPr	7.5	100	2.50	40	RT[a]
HAc/HPr	7.5	100	2.50	40	12
HAc/HPr	8.0	100	2.50	40	RT[a]
HAc/HPr	6.5	100	2.50	40	RT[a]

HAc/HPr : 75% Acetate and 25% Propionate

a. RT=Room temperature

In the temperature experiment, a recirculating chiller (VWR 1160S refrigerated heated circulating bath, USA) and aluminium water cooling block (40 x 120 x 12 mm, Uxcel) were used to reduce the temperature to the desired degree (Figure 16). The cooling block was connected to the circulation bath with a silicone tubing (ID:6.0 mm, Carl Roth, Karlsruhe, Germany). The tube of the cultivation medium was inserted into the main connection tubing to maintain a stable temperature, preventing influence from external fluctations.

The temperature variance might occur between the circulating bath and the microfluidic channels due to factors of the long tubing connections and the room temperature. Therefore, the canula of the custom-built temperature sensor was inserted into the inoculation port (Figure 16a). Then, the temperature in the meandering channel was set to 12 ^{o}C with the sensor using the program of Arduino IDE 2.1.0 before commencing the experiment.

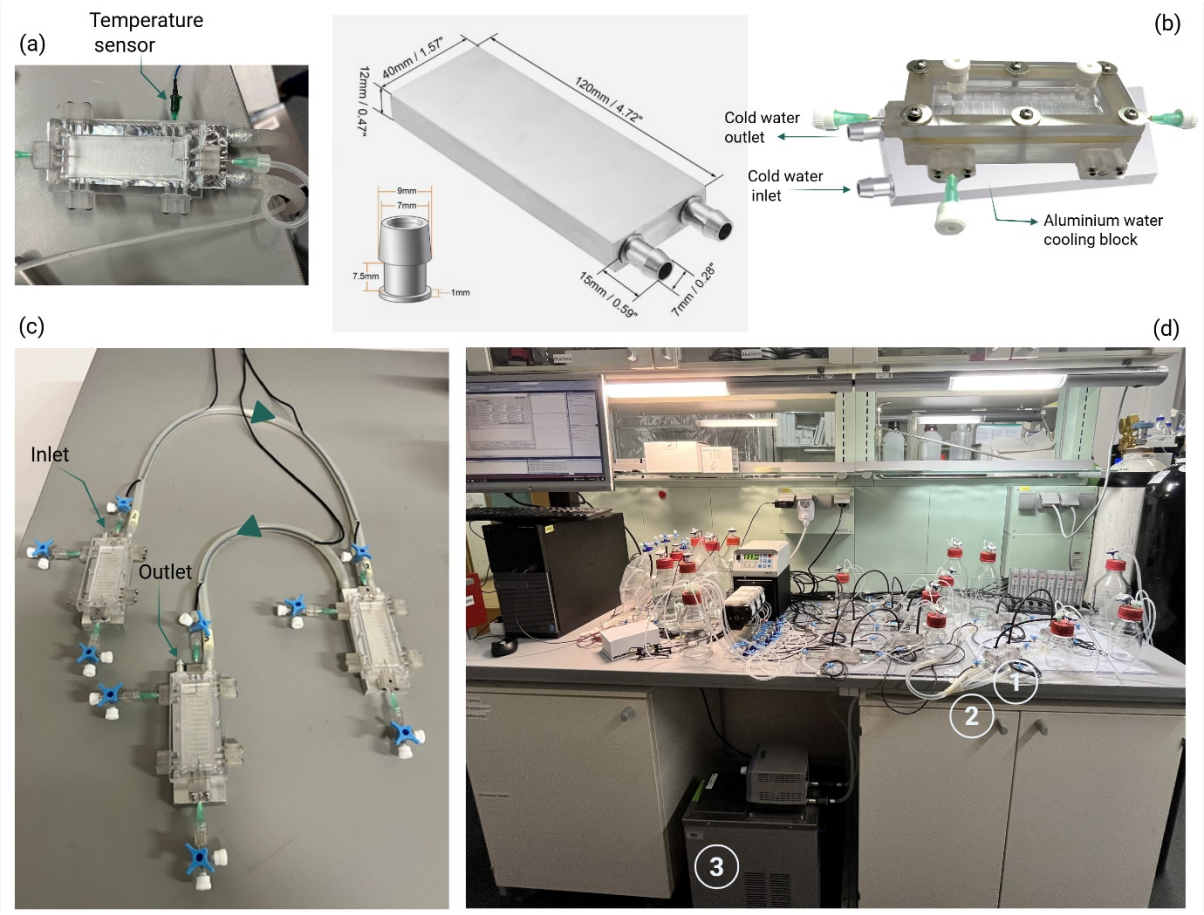

Figure 16. Temperature experiment with the cooling unit. The temperature sensor is shown in (a), an illustration of the aluminium water cooling block with assembled frame in (b), the frame and main tubing connection with inserted fluororubber medium tubings in (c) and a photo of the running temperature experiment in (d): (1) the cooling block under the frame, (2) the main tubing connection with circulation bath and (3) recirculating chiller are shown.

2.3.4. Biofilm imaging using OCT

In MMBS, the biofilm development of the mix-culture in the meandering channels was observed via a Ganymede (GAN200, Thorlabs GmbH, Dachau, Germany) with an LSM03 objective lens and software version 5.6.0. The 3D OCT datasets (C-scans) were 4 mm x 1 mm x 1.4 mm (L x W x H) for the straight sections and 6 mm x 3 mm x 1.4 mm (L x W x H) for the corners with pixel size in x-y plane = 4 µm/pixel and a pixel height of 2.15 µm at an acquisition speed of 36 kHz. The biovolume was divided by the imaging frame area of 0.04 cm^2 for the straight sections and 0.059 cm^2 for the corners, respectively, to obtain the normalized biovolume.

The images were taken after removing the lid from the frame at the end of the 20-day cultivation period. OCT images were primarily captured from three positions along the meandering channel: front, middle, and back. Biofilm height maps were generated from images captured at the 2nd, 7th, and 12th curve. Furthermore, at each position, two images of the straight sections (lines 1, 2, 7, 8, 13, and 14) and one image of the corner (curves 2, 7, and 12) were taken, as shown in Figure 17. In total, these nine separate imaging scans were used to quantify the average biovolume for each cultivation reactor.

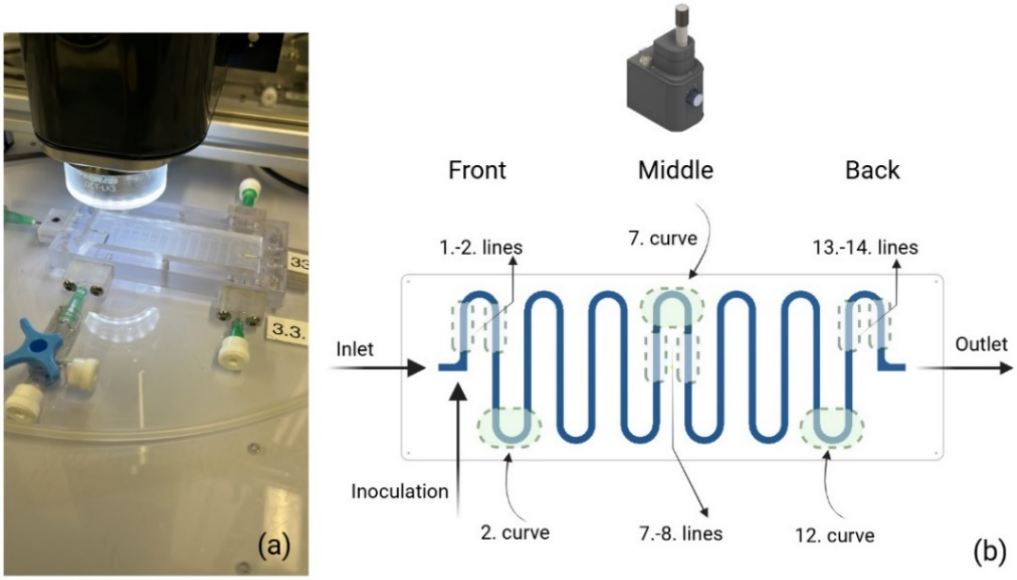

Figure 17. OCT imaging in meandering channels: imaging biofilm growth (a) and OCT positions in the meandering channel from front to back (b).

2.3.5. Fluorescence in situ hybridization (FISH) and confocal imaging

Fluorescence in situ hybridization (FISH) protocol involving the fixation of cultured cells was implemented as an endpoint analysis in MMBS. At the end of the cultivation period, the fixation step was manually applied to meandering reactors. In this regard, the biofilm was fixed by using 4% formaldehyde for an hour, then washed with 1xPBS for 30 min and with 1xPBS:ethanol (v:v) for another 30 min using an L160 syringe pump at a flow rate of 4 mL h^{-1} and stored +4 °C.

Afterwards, the automated FISH protocol was performed based on a previously described (Klein *et al.*, 2024) with rRNA-targeted probes Dechlo2 (Mcilroy *et al.*, 2016; Ziegler *et al.*, 2016) and GAM42a (Manz *et al.*, 1992), with the addition of unlabelled Gam42a-Competitor

(Klein *et al.*, 2022). The FISH experiment was performed using the probes, as listed in Table 16. The cells were counterstained with 4′, 6-diamidino-2-phenylindole (DAPI; Merck KGaA, Darmstadt, Germany). The FISH protocol was carried out by sequentially pumping solutions into the meandering reactor. To this end, miniature active 2/2 normally closed valves (SMV-2R–BN1F; Takasago Kōryō Kōgyō, Tokyo, Japan) were used for the connection of solution tubes and the reactor. The valves were operated using a custom-built control unit. Using Y-branches, the tubing system (ID:1.0 mm silicone tube, Carl Roth, Karlsruhe, Germany) carrying the solutions was connected to the reactor via a single tubing (ID:1.5 mm silicone tube, Carl Roth, Karlsruhe, Germany). A 0.38 mm inner diameter Ismatec tube (Idex, Wertheim, Germany) was used for the peristaltic pump (Ismatec, Reglo ICC, ISM4408, Materflex LLC, Barrington, IL) with a flow rate of 4 ml h^{-1}. All prepared solutions are listed in Tables 17-21. The detailed steps of the FISH protocol are shown in Table 22. During the experiment, the microfluidic reactor was placed inside the hybridization oven (Biometra OV4, Biomedizinische Analytik GmbH, Göttingen, Germany) in the dark, and the required temperatures were set manually. The illustration of the FISH setup can be seen in Figure 18.

The images of the probe-labelled cells were taken via an LSM 800 confocal laser scanning microscope (CLSM) with a Plan-Apochromat 63x/1.40 Oil DIC M27 objective (Carl Zeiss, Oberkochen, Germany). Digital image analysis in microbial ecology (Daime), based on Daims *et al.* (2006), was used to determine the biovolume fraction of the detected microbial community in boundary conditions. Images were analyzed following the protocol of Daims (2009) using Daime version 2.2.

Table 16. Used FISH probes.

Component	*Target*	*Specificity*	*Position*	*Sequence (5′-3′)*	*Dye*	*FA-concentration*	*Reference*
Gam42a	23S rRNA	γ-Proteobacteria	1027-1043	GCC TTC CCA CAT CGT TT	Cy5	35	(Manz *et al.*, 1992)
Dechlo2	16S rRNA	β-Proteobacteria	211-230	GCT CAA TCA GCG CAA GGT CT	TAM	40	(Mcilroy *et al.*, 2016; Ziegler *et al.*, 2016)
Gam42a-competitor	-	-	-	GCC TTC CCA CTT CGT TT	-	-	(Klein *et al.*, 2022)

Table 17. Phosphate-buffered saline (PBS, 10x).

Component	*g L^{-1}*	*mM*
NaCl	80	1368.93
KCl	2	26.83
Na_2HPO_4	14.4	101.44
KH_2PO_4	2.4	17.64

Table 18. Hybridization buffer.

Component	*20 % FA (mL)*	*30 % FA (mL)*	*35 % FA (mL)*	*40 % FA (mL)*
5 M NaCl	1.08	1.08	1.08	1.08
1 M TrisHCl (pH 8)	0.12	0.12	0.12	0.12
ddH_2O	3.6	3	2.7	2.4
20% SDS	0.003	0.003	0.003	0.003
Formamide (FA)	1.2	1.8	2.1	2.4

Table 19. Embedding buffer.

Component	*mL L^{-1}*
Citifluor	11
Vectashield	2
1xPBS (see Table 17)	1

Table 20. SSC buffer (20x).

Component	*g L^{-1}*	*M*
NaCl	175.3	3
Tri-Na-Citrat-Dihydrat	88.2	0.3
pH 6 with 7 N HCl.		

Table 21. Washing buffer.

Component	*20 % FA (mL)**	*30 % FA (mL)**	*35 % FA (mL)**	*40 % FA (mL)**
5 M NaCl	2.15	1.02	0.7	0.46
1 M TricHCl (pH 8)	1	1	1	1
0.5 M EDTA (pH 8)	0.5	0.5	0.5	0.5
20% SDS	0.025	0.025	0.025	0.025
ddH_2O	46.5	47.5	47.8	48
Add 20% SDS at the end, otherwise it will precipitate.				

* Depends on the concentration of hybridization buffer used.

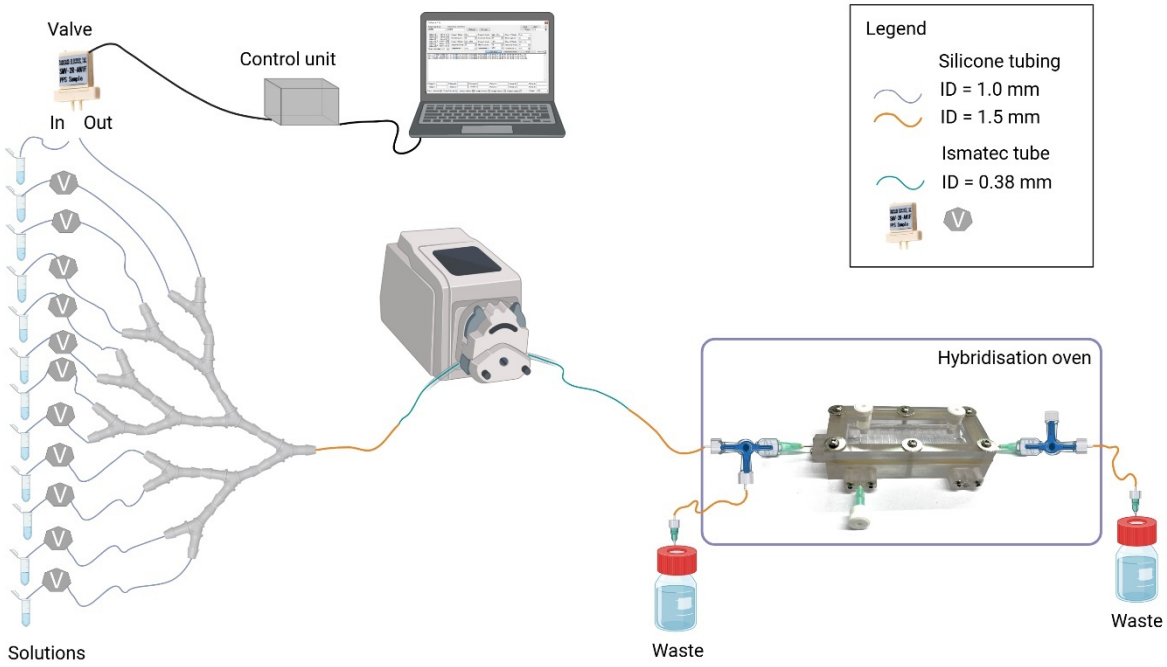

Figure 18. Illustration of the FISH setup. The experiment was conducted in a humid chamber and in the dark.

Table 22. Automated protocol of FISH. The fixation step was performed manually.

Work step	**Solution**	**Flow rate** *[µL min^{-1}]*	**Pumping time** *[min]*	**Incubation time** *[min]*	**Temp.** *[°C]*
Fixation	4% formaldehyde in PBS (137 mM NaCl, 2.7 mM KCl, 10.1 mM Na_2HPO_4, 1.8 mM KH_2PO_4; v/v)	67	-	60	RT[a]
Wash	PBS	67	29	-	RT[a]
Permeabilization	0.1 M HCl	67	29	-	RT[a]
		-	-	10	RT[a]
Wash	ddH_2O	67	29	-	RT[a]
Hybridization I	6.6 ng µL^{-1} (add 28 µL of a 500 ng µL^{-1} stock solution to a total volume of 2100 µL) Dechlo2 (Mcilroy *et al.*, 2016; Ziegler *et al.*, 2016) probe in 40% hybridization buffer (0.9 M NaCl, 20 µL mL^{-1} 1 M TrisHCl pH 8 (v/v), 0.01 %SDS (w/v), 40% formamide (v/v))	67	29	-	48
		-	-	90	48
Wash	Washing buffer 40% (46 mM NaCl, 20 µL mL^{-1} 1 M TrisHCl pH 8 (v/v), 5 mM EDTA, 0.01% SDS (w/v))	67	29	-	48
Hybridization II	6.6 ng µL^{-1} (add 28 µL of a 500 ng µL^{-1} stock solution to a total volume of 2100 µL) Gam42a (Manz *et al.*, 1992) and Gam42a competitor (Klein *et al.*, 2022) probe in 35% hybridization buffer (0.9 M NaCl, 20 µL mL^{-1} 1 M TrisHCl pH 8 (v/v), 0.01% SDS (w/v), 35% formamide (v/v))	67	29	-	48
Wash	Washing buffer 35% (70 mM NaCl, 20 µL mL^{-1} 1 M TrisHCl pH 8 (v/v), 5 mM EDTA, 0.01% SDS (w/v))	-	-	90	48

Table 22. Automated protocol of FISH (continued).

Work step	Solution	Flow rate *[µL min^{-1}]*	Pumping time *[min]*	Incubation time *[min]*	Temp. *[°C]*
Wash	SSC (3 M NaCl, 0.3 M trisodium citrate dihydrate, pH adjusted to 6 with 7 M HCl)	67	29	-	RT[a]
Wash	PBS	67	29	-	RT[a]
Counterstaining	1 µg mL^{-1} DAPI	67	29	-	48
		-	-	5	48
Embedding	Embedding buffer (785.7 µL mL^{-1} CitiFluor™ AF3 (Science Services GmbH, München, Germany), 142.9 µL mL^{-1} VECTASHIELD® Antifade Mounting Medium (vector Laboratories, Newark, California, United States), 71.4 µL mL^{-1} PBS)	67	29	-	RT[a]
Storage	-	-	-	∞	4

a. RT=Room temperature

2.3.6. Phosphorus quantification

In MMBS, the phosphate content of the flow-through media was investigated by Dionex™ ICS-1100 Ion Chromatography (IC, Thermo Fisher Scientific, Waltham, Massachusetts, USA) to shed light on the metabolic activities and growth of microorganisms within the microfluidic system at different time points. Dionex IonPac AS9-HC (2 x 250 mm) anion exchange column, including Dionex IonPac AG9-HC (2 x 50 mm) pre-column with 9 mM sodium carbonate (Na_2CO_3) as an eluent, was used for the detection of the phosphate concentrations.

The ions in a sample can be identified and quantitated with IC. First of all, the calibration was performed using a standard solution of monosodium phosphate (NaH_2PO_4 * $2H_2O$) at concentrations ranging from 1 to 100 µM. The analytical measurement was then performed. Eluent flow helped to separate the sample ions and carried the sample through the system. The

instrument method for IC involved injecting a liquid sample, separating ions on an ion-exchange column, detecting the separated ions by conductivity, and analyzing data. The concentration of each ion was determined by quantifying peak areas or heights against calibration standards.

As previously stated, the system comprised anoxic/interphase/oxic/interphase stages with durations of 3/1/4/1 h, respectively, and a cycle was 9 h. Samples from the microfluidic cultivation platforms were taken in the anoxic and oxic phases every 30 minutes. In order to estimate P-release and uptake amounts, the periods between 30 and 90 minutes (anoxic phase) and 210 to 330 minutes (oxic phase) were considered as active time.

The abiotic control values were subtracted from the measured phosphate concentrations (ΔP). The flow rate (Q) was 2 ml h^{-1}. The selected active time (T) was an hour in the anoxic phase and 2 hours in the oxic phase. The amounts of P-release and uptake were correlated with the biofilm volume (BV) to evaluate the system`s capacity using Equations 7 and 8. P-removal amount and removal capacity were obtained by subtracting the release values from the uptake values using the following Equations 9 and 10. All these experiments were performed in three biological replicates.

$$P - release\ and\ uptake\ (\mu g\ PO_4 - P) = \Delta P\left(\frac{mg\ P}{L}\right) x\ Q\left(\frac{mL}{h}\right) x\ T(h) \quad (7)$$

$$P - release\ and\ uptake\ capacity\ (\mu g\ PO_4 - P\ mm^{-3}) = \frac{\Delta P\left(\frac{mg\ P}{L}\right) x\ Q\left(\frac{mL}{h}\right) x\ T(h)}{BV\ (mm^3)} \quad (8)$$

$$P - removal\ (\mu g\ PO_4 - P) = P_{uptake}(\mu g) - P_{release}(\mu g) \quad (9)$$

$$P - removal\ capacity\ (\mu g\ PO_4 - P\ mm^{-3}) = \frac{P_{uptake}(\mu g) - P_{release}(\mu g)}{BV\ (mm^3)} \quad (10)$$

2.3.7. Metagenomic analysis

Metagenomic sequencing is required to identify the diversity and abundance of microbial communities. In MMBS, biofilm samples from meandering channels were collected after 20 days of cultivation by flushing the channels with minimal media, followed by storage at -20 °C for the metagenomic analysis. The biomass was collected through centrifugation at 13,000g for 2 minutes. DNA isolation was carried out with the Qiagen DNeasy PowerBiofilm kit (Qiagen, Hilden, Germany) according to the manufacturer's protocol. A NanoDrop 2000 spectrophotometer (Thermo Scientific, Waltham, MA, USA) and the Qubit dsDNA assay kit (Life Technologies, Carlsbad, CA, USA) were used to determine the total concentration and purity of the extracted DNA. With the Native Barcoding Kit 24 V14, SQK-NBD114.24 (Oxford Nanopore Technologies, Oxford, UK), 400 ng of Qubit double-stranded DNA were used per sample to prepare the library. A MinION Mk1b and an R10.4.1 flow cell using MinKNOW software version 24.02.6 (Oxford Nanopore Technologies, Oxford, UK) were used for sequencing. Basecalling and demultiplexing were performed with dorado version 7.3.9 in super accuracy mode. Sequencing reads were aligned against metagenome-assembled genomes (MAGs) from the MiDAS database (Singleton *et al.*, 2021) with BLAST v2.12 for taxonomic identification and abundance estimation. In order to enable subsequent analysis, metagenomic bins were prepared. Accordingly, a sample-based read assembly was performed with Flye v2.9.1.-b1768 (Kolmogorov *et al.*, 2020) including the parameters -nano-hq and -meta. Read mapping was then performed using Minimap2 v2.24 (Li, 2016). By Metabuli v1.9.0.2 (Kim and Steinegger, 2024) and the GTDB database r214 (Parks *et al.*, 2022), contigs were annotated. Contig coverage was evaluated with Minimap2 as well as Samtools 1.13. Binning was conducted with taxvamb v4.1.4 (Kutuzova *et al.*, 2024).

2.3.8. Principal components analysis (PCA) and spearman-based co-occurrence network analysis

Principal component analysis (PCA) was employed as a multivariate analysis technique with Minitab 19.0 to investigate variations in microbial communities and their associated key performance indicators under the studied operational conditions. Additionally, a spearman-based co-occurrence network analysis was carried out with R and Gephi 0.10. In the network construction, only statistically significant correlations ($p < 0.05$) were considered.

3. Results

Many potential industrial applications, including anode-assisted fermentation and wastewater treatment, are designed to operate as continuous flow-through processes. However, biofilms exhibit complex and temporally dynamic compositions; therefore, cultivating and controlling them in their environment can be challenging. Microfluidic flow-through systems address these challenges by enabling the sustained cultivation of biofilms under controlled conditions, while also allowing for real-time, in situ analysis. Biofilm cultivation experiments were conducted at the microscale in a BES and an MMBS, respectively. These experiments targeted carbon and phosphorus removal from wastewater, energy and resource recovery, and the direct observation of biofilm formation.

In the first part of the study, process parameters governing BES, including electrode surface functionalization and roughness, were examined for their impact on biofilm development and current density generation by using exoelectrogens, known for EET. The performance of the system following surface modification was compared to that of a naturally formed biofilm in BES. Additionally, optical analysis was performed to assess the behavior of a co-culture of *S. oneidensis* and *G. sulfurreducens*. Furthermore, SEM analysis provided insights into surface morphology.

The second part of this thesis focused on improving the previously established microfluidic cultivation platform by Klein *et al.* (2022) and enriching PAOs for P-removal. Accordingly, four cultivation series were conducted to assess their impact on the efficiency of PAOs in MMBS. Moreover, optical analyses were performed to observe the development of PAOs under different conditions and to identify their genus. Further, P-release and uptake concentrations measured using chromatographic analysis provided valuable insights into PAOs activity. In addition, metagenomic, multivariate and network analysis were used to evaluate interactions between PAOs and GAOs under different operating conditions. The tested parameters are shown in Figure 19.

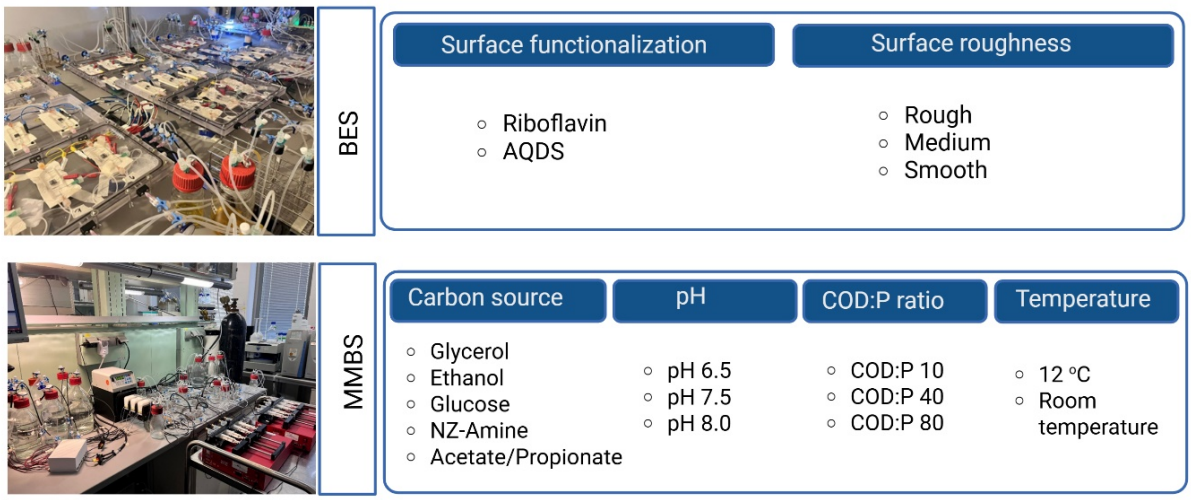

Figure 19. Tested process parameters in BES and MMBS. An experimental setup was designed to investigate the influence of surface functionalization and surface roughness on anodic biofilm development and current generation in BES. Additionally, a series of experiments was conducted in the MMBS to evaluate the impact of process conditions, such as carbon source, pH, COD:P ratio, and temperature, on PAO efficiency.

3.1. Carbon elimination and energy recovery with exoelectrogens in BES

BES offers an effective approach for removing organic pollutants by facilitating carbon elimination through the activity of specialized microorganisms known as exoelectrogens. In the anodic side of BES, they oxidize organic carbon compounds, transferring electrons to the anode via EET mechanisms. These electrons then flow through an external circuit to the cathode, resulting in current density generation. This process not only purifies wastewater but also enables energy recovery from it. To improve the overall BES performance, the impact of surface functionalization and surface roughness using a mixed species of *S. oneidensis* and *G. sulfurreducens* was analyzed.

3.1.1. Effect of surface functionalization on the efficiency of BES

Biocompatible compounds, riboflavin and AQDS, were utilized for the functionalization of the electrode surface to improve the interactions between biofilm and anode by aiming to increase electron transfer from cells to the electrode surface. As illustrated in Figure 20, using riboflavin and AQDS with a rough-surface graphite electrode improved both the current density and biofilm formation. The results demonstrated that employing a rough-surface electrode functionalized with riboflavin and AQDS led to peak current densities of

125.92 ± 8.38 µA cm^{-2} and 121.01 ± 8.95 µA cm^{-2}, respectively. These generated current densities were approximately 3.4-fold and 3.2-fold higher than those of the non-functionalized control (37.46 ± 14.87 µA cm^{-2} after 7 days) and developed more rapidly. The observed shorter lag phase in current density development might be attributed to an improved connection between the basal biofilm layer and the anode surface. Furthermore, higher current densities were associated with increased biovolume, and both parameters rose concurrently. When riboflavin was used, the maximum biofilm volume reached 5.84 ± 0.11 mm^3 cm^{-2} on day 7, whereas with AQDS, it peaked at 4.99 ± 0.55 mm^3 cm^{-2} on day 6 and subsequently declined to 3.33 ± 0.87 mm^3 cm^{-2} by day 7. In the control experiment, the biovolume remained low, at around 0.6 mm^3 cm^{-2} until the last day of the experiment, reaching a maximum of 0.78 ± 0.32 mm^3 cm^{-2} on day 7. The 7.5-fold and 4.3-fold increases in biofilm volume indicate that using surface modification enhanced the density of electroactive biofilm cells on the anode.

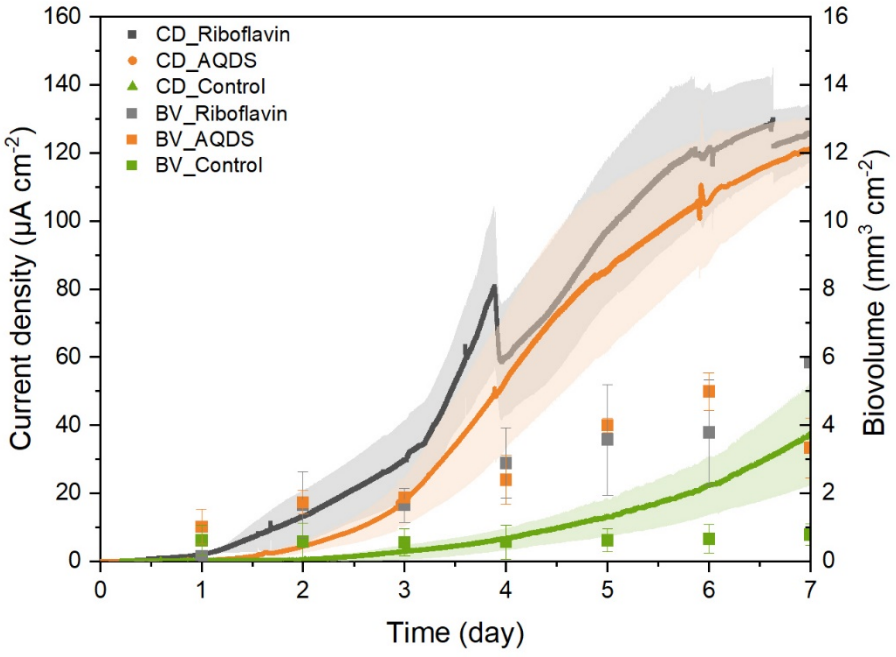

Figure 20: The effects of riboflavin- and AQDS-functionalized electrodes compared with naturally grown biofilms without functionalization in terms of current density and biovolume in BES. Surface functionalization markedly increased current density and accelerated biofilm growth, as quantified by OCT. Data for biovolume represented as mean ± standard deviation from triplicate experiments, whereas shaded regions in the current density profiles indicate the standard deviation (n=3; CD, current density; BV, biovolume).

Further, Figure 21 presents the mean current densities over a 7-day operation period. Riboflavin-functionalized reactors achieved mean current densities of 55.22 ± 9.78 µA cm^{-2}, AQDS-functionalized electrodes reached 47.13 ± 10.63 µA cm^{-2}, whereas the control attained only 9.94 ± 4.01 µA cm^{-2}. These values correspond to a 5.6-fold increase in mean current density with riboflavin and a 4.7-fold increase with AQDS relative to the control.

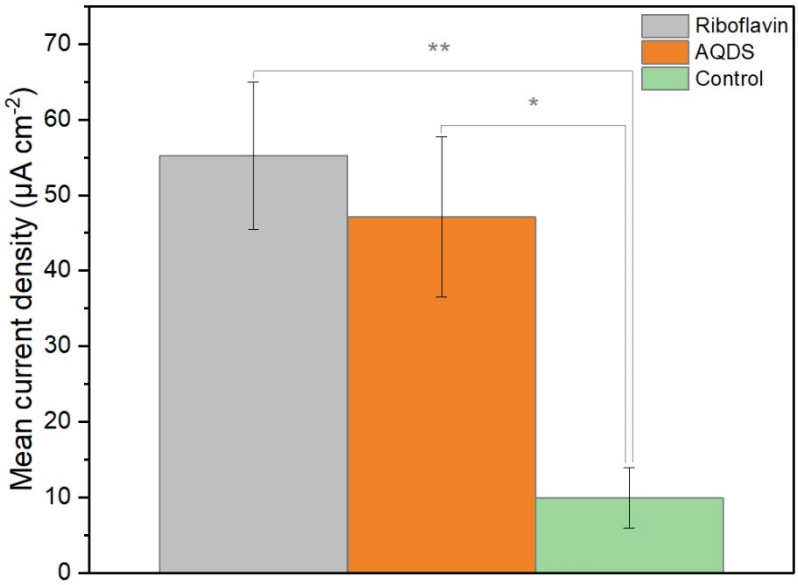

Figure 21. Effect of surface modification on the mean current densities over the 7-day operation period, compared with the non-functionalized electrode. Both riboflavin- and AQDS-modified surfaces substantially increased the generated mean current densities. Statistical significance is indicated as * $p<0.05$; ** $p<0.01$. A two-sample Welch's t-test (unequal variances) was used to compare groups. The values represent the mean of triplicate measurements, and the error bars indicate the corresponding standard deviations.

Non-invasive OCT imaging during ongoing flow and anoxic cultivation provided the correlation between current density and biofilm formation. The use of riboflavin and AQDS enhanced biovolume formation, compared to the control experiment, as seen in Figure 22.

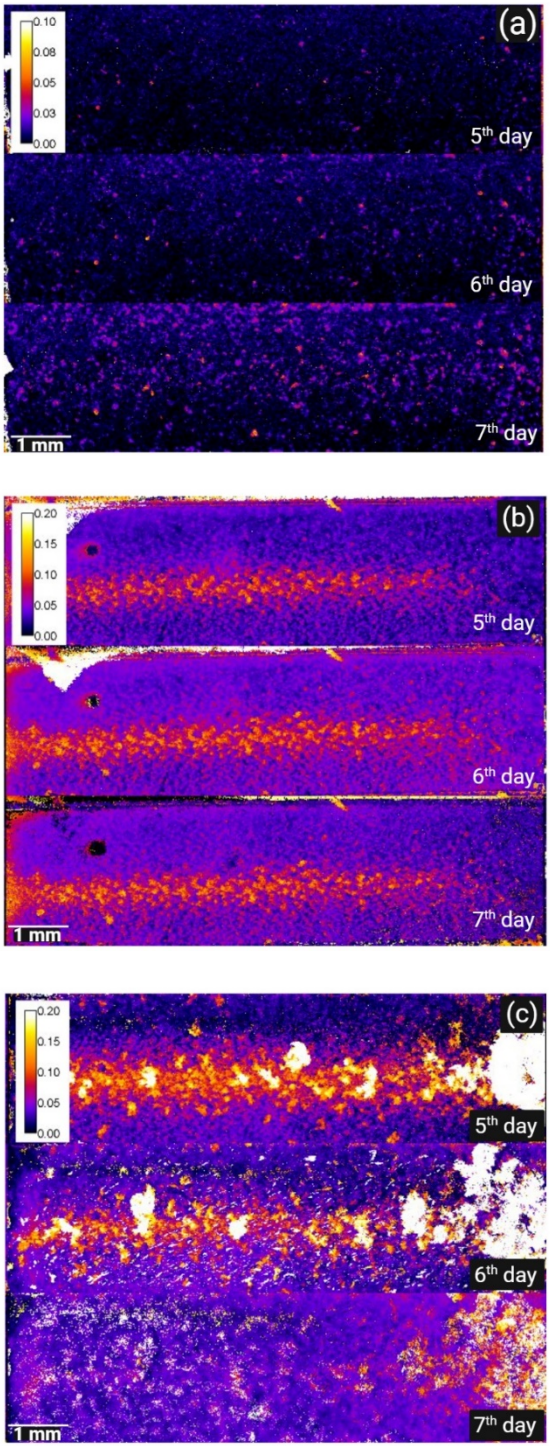

Figure 22. Representative height maps from days 5, 6, and 7 show distinct biofilm growth patterns and thickness of biofilms for the control (a), as well as for electrodes functionalized with riboflavin (b) and AQDS (c) with rough surface material. The pre-treatment of riboflavin and AQDS promoted increased biovolume formation. The scale bar indicates biofilm height in mm. Scale bar = 1 mm.

In addition to enhancing biofilm formation and current density, surface modification also improved biofilm porosity, surface coverage, and biofilm surface roughness. The porosity of the biofilm formed on the non-functionalized electrode remained consistently low throughout the experiment, averaging approximately 30% (Figure 23a), suggesting a thinner and more compact structure with fewer voids. In contrast, functionalization with AQDS increased the porosity more than twofold to around 63%. Further, once riboflavin was used, the biofilm porosity decreased from approximately 81% at the start to 67% by the end of the experiment. Although porosity decreased throughout the experiment following riboflavin application, surface functionalization with riboflavin and AQDS collectively resulted in approximately a 2-fold increase in porosity compared to the control condition without functionalization. This enhanced porosity may have promoted greater biofilm growth and a higher accessibility of the substrate within the biofilm matrix.

Besides, surface coverage increased alongside current density, reaching 61% on day 7 in the control experiment. For both riboflavin and AQDS treatments, the electrode surface was almost completely covered by biofilm (Figure 23b). The increased surface coverage compared with the control is likely due to improved electroactive biofilm attachment on the functionalized electrode, thereby contributing substantially to the pronounced current increase observed with EAB.

Furthermore, the roughness of the biofilm without functionalization remained stable at approximately 0.39 throughout the experiment (Figure 23c). In contrast, functionalization with riboflavin and AQDS led to a steady increase in biofilm surface roughness. With riboflavin treatment, roughness increased from 0.47 ± 0.22 at the beginning to 0.83 ± 0.29 by the end of the experimental period. Functionalization with AQDS produced the highest roughness values, peaking at 0.98 ± 0.18 on day 6 before decreasing to 0.67 ± 0.13. These topographical variations resulting from increased biofilm roughness on the functionalized electrode can reduce detachment by generating localized low-shear regions.

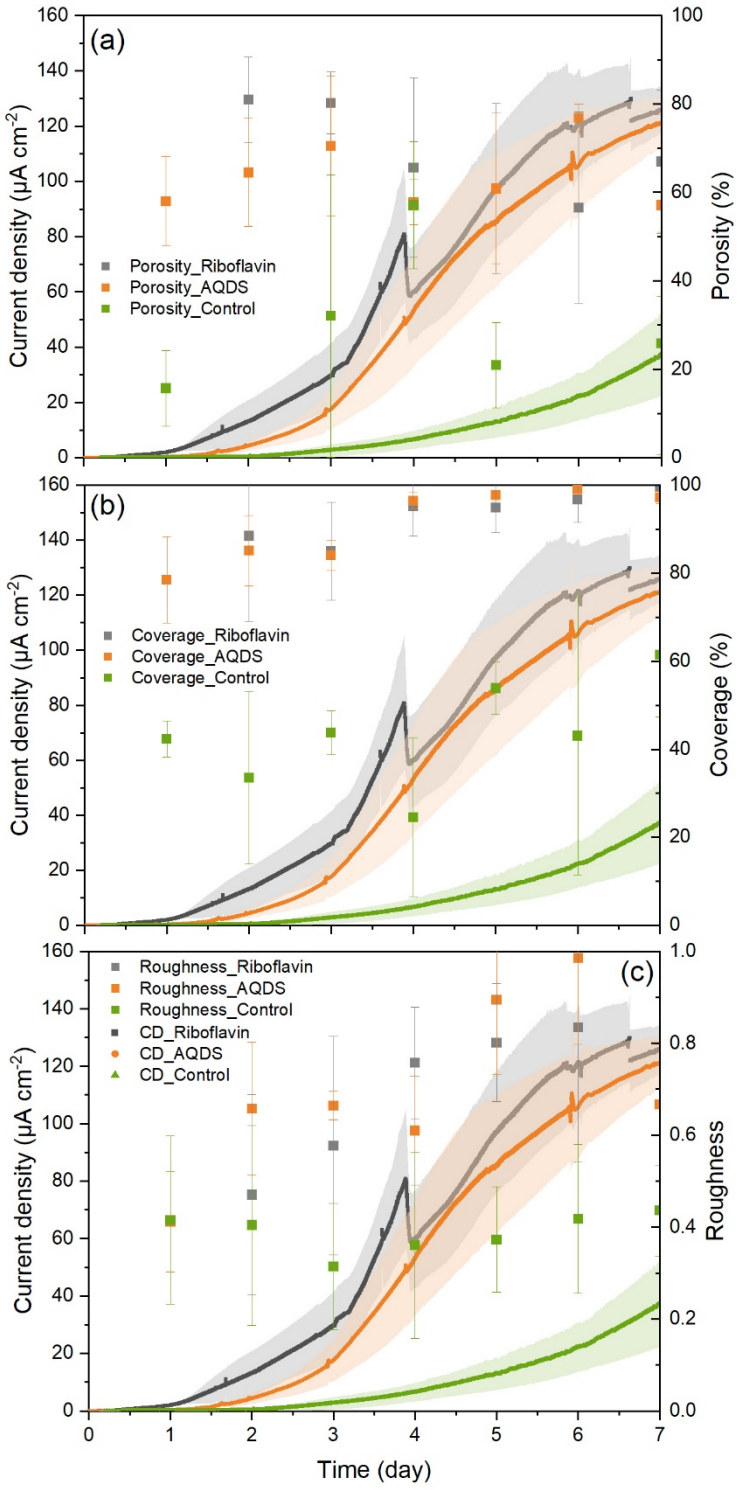

Figure 23. Presented biofilm porosity, coverage and roughness over time in relation to the current density. (a) Biofilms on non-functionalized anodes maintained a porosity of approximately 30%, whereas riboflavin- and AQDS-functionalized electrodes showed more than a 2-fold higher porosity, indicating a consistently different internal biofilm structure. (b) Riboflavin and AQDS rapidly achieved near-complete biofilm surface coverage, indicating significantly greater colonized area on functionalized electrodes. while the control remained distinctly lower (61% by day 7). (c) Biofilm roughness remained stable at around 0.39 on non-functionalized electrodes; however, riboflavin and AQDS treatments induced a progressive increase in biofilm roughness, reflecting more pronounced microtopographical development on the functionalized surfaces (n=3; CD, current density).

3.1.2. Effect of surface roughness on the efficiency of BES

The surface roughness of graphite electrodes influences the efficiency of BESs. In this study, the electrode surfaces were functionalized using riboflavin and AQDS. Riboflavin demonstrated greater effectiveness in enhancing current production. Subsequently, graphite electrodes with three distinct surface roughness levels - rough, medium, and smooth - were tested to investigate the impact of surface roughness on anodic biofilm growth in the presence of riboflavin. As demonstrated in Figure 24, a decrease in electrode surface roughness corresponded to a reduction in current density. The results showed that using a rough-surface electrode functionalized with riboflavin yielded a peak current density of 125.92 ± 8.38 μA cm^{-2}. When a medium surface roughness electrode was used, the current density decreased approximately 4-fold, reaching 32.13 ± 10.22 μA cm^{-2} on day 7. In contrast, the smooth-surface electrode exhibited no measurable current generation.

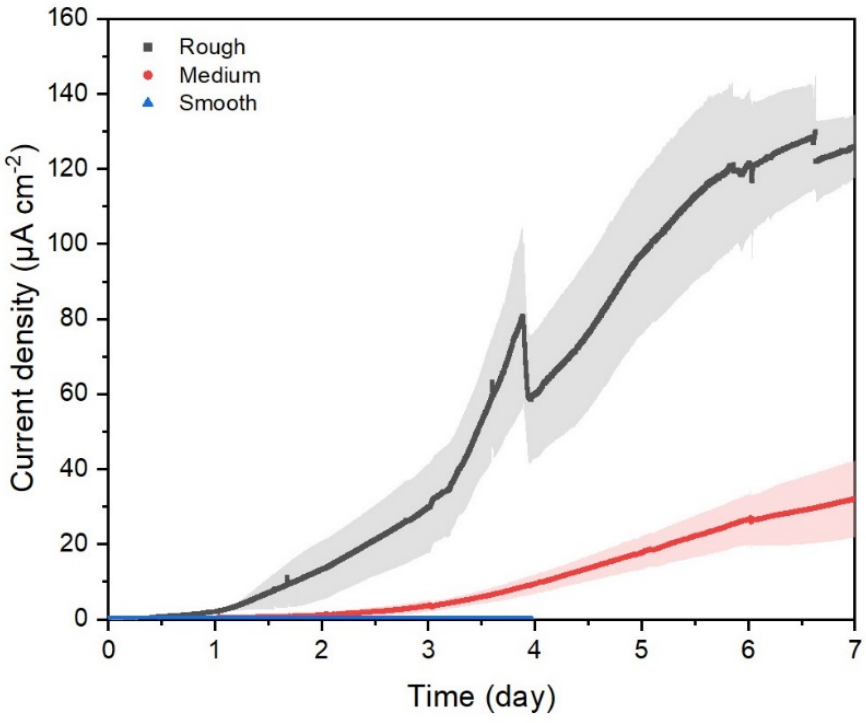

Figure 24. Effects of different surface roughness on the current generation. Electrode roughness strongly promoted current generation, with the smooth surface showing negligible current, the medium giving a clear increase, and the rough electrode yielding the highest current density.

Moreover, as demonstrated in Figure 25, rough electrodes achieved a mean current density of 55.22 ± 9.75 µA cm^{-2} over a 7-day operation period, whereas medium electrodes reached only 10.56 ± 2.96 µA cm^{-2}, corresponding to a 5.2-fold increase for the rough electrodes.

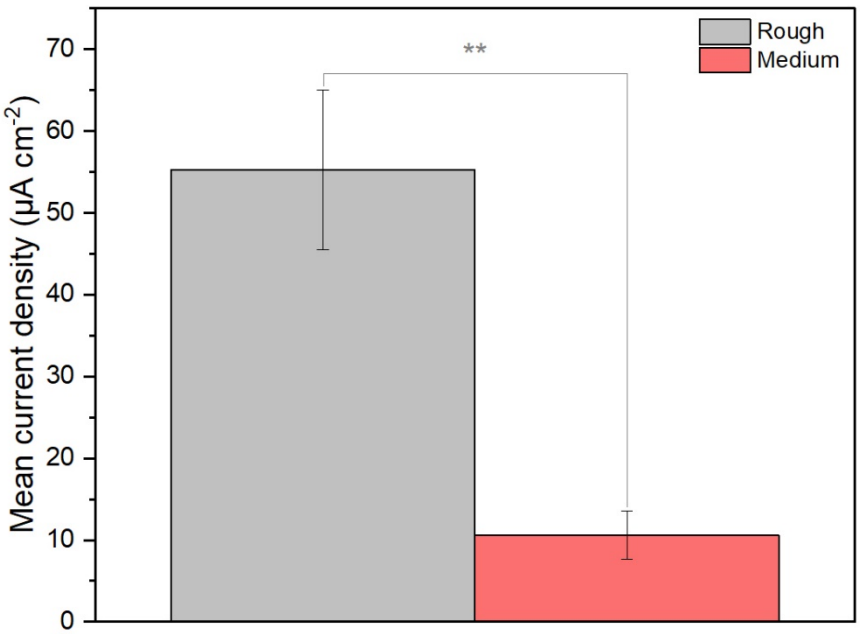

Figure 25. Mean current densities with rough and medium electrodes over the experimental period. Using rough electrodes (n=3) with riboflavin functionalization resulted in substantially higher mean current densities than medium electrodes with riboflavin functionalization (n=2), corresponding to more than a 5-fold improvement in performance (statistical significance: ** $p<0.01$).

As presented in Figure 26, the surface roughness of the graphite electrode was characterized using SEM. The peaks and valleys depict the micro-scale texture, with the vertical distance between the highest peak and lowest valley decreasing from the rough to the smooth surface.

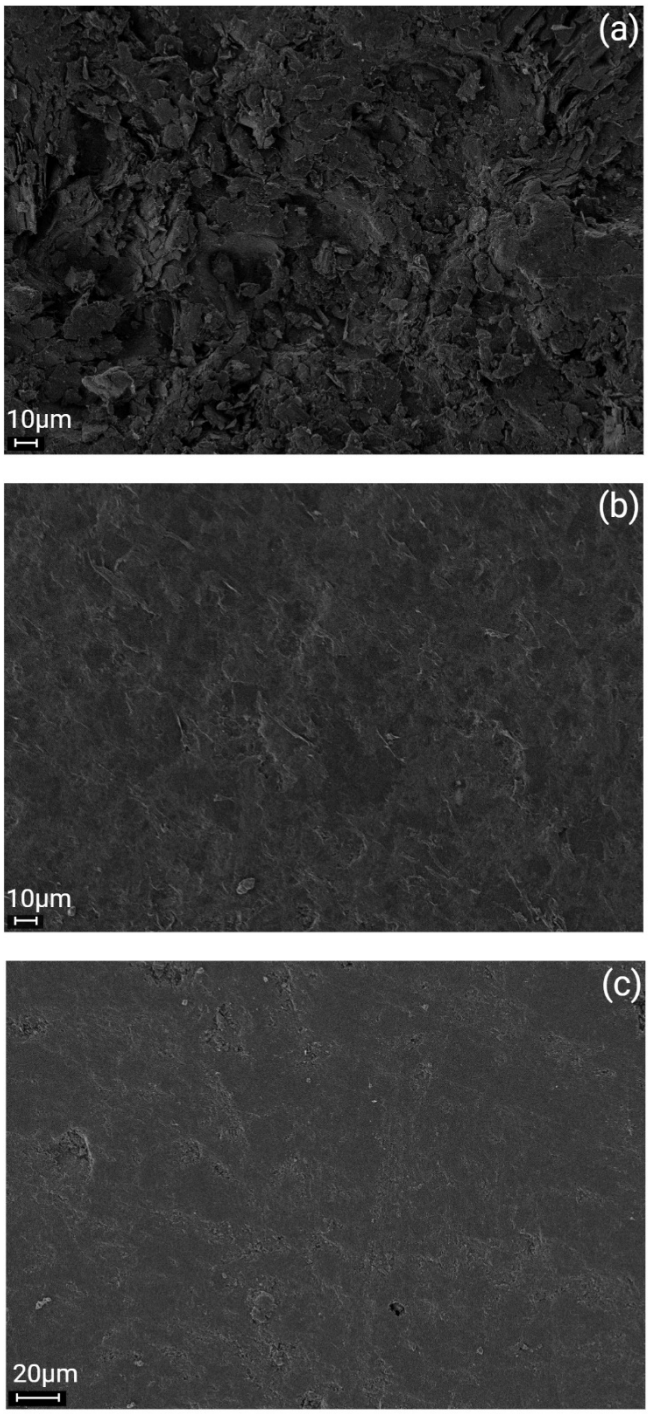

Figure 26. SEM analysis to compare electrodes with different surface roughness: rough (a), medium (b), and smooth (c).

3.2. Phosphate elimination and resource recovery with PAOs in MMBS

Phosphate elimination in microfluidic reactors involves the unique metabolic capabilities of PAOs to achieve phosphorus removal in a highly controlled and miniaturized environment. The performance of the system and the activity of PAOs are influenced by various process conditions, including the type of carbon source, pH, COD:P ratio or temperature. Their effects on PAO efficiency were evaluated at the end of a 20-day cultivation period by measuring phosphate concentrations in the effluent and quantifying biofilm volume from OCT-based analysis.

3.2.1. Impact of carbon sources on the efficiency of MMBS and PAO-GAO abundance

A micro-scale microfluidic flow-through system was used to cultivate PAOs containing communities and to monitor the effect of various growth conditions in parallel. The type and availability of carbon source influence biological phosphorus removal performance and PAO activity through metabolic pathways, substrate uptake rates, and microbial competition (Zhang *et al.*, 2025). To investigate the impact of external carbon sources on the PAO efficiency and phosphate removal, as depicted in Figure 27, six different organic compounds from four categories, including glycerol and ethanol as alcohols, glucose as a sugar, NZ-Amine as a mixture of amino acids and peptides, as well as acetate and propionate as VFAs, were tested. P-release and P-uptake measurements confirmed the activity of PAOs across all tested carbon sources (see Appendix, Figure S3). The experiments showed a clear influence of the tested C-sources on P-removal, biofilm growth and biofilm P-release/uptake capacity.

The use of acetate and propionate as VFAs resulted in higher P-release (1.89 ± 0.96 µg PO_4- P), whereas glucose yielded a comparatively lower P-release of 1.24 ± 0.61 µg PO_4-P. Among all tested conditions, acetate/propionate and glucose yielded the highest P-uptake amounts, reaching 4.65 ± 0.48 µg PO_4-P and 4.52 ± 0.24 µg PO_4-P, respectively. Accordingly, the highest phosphate removal was observed with glucose, resulting in a removal value of 3.27 ± 0.40 µg PO_4-P when employed as an alternative to VFAs among the complementary carbon sources (Figure 27a). Then, the acetate/propionate mixture achieved a phosphate removal of 2.76 ± 0.58 µg PO_4-P.

Further, glycerol use in the system resulted in low P-release (0.38 ± 0.16 µg PO_4-P) and similarly low P-uptake of 2.63 ± 0.52 µg PO_4-P, while ethanol only modestly stimulated anoxic P-release (0.97 ± 0.21 µg PO_4-P), limiting subsequent P-uptake to 2.90 ± 0.35 µg PO_4-P. Accordingly, glycerol and ethanol exhibited minimal P-release and P-uptake overall, with corresponding phosphate removal values of 2.25 ± 0.36 µg PO_4-P and 1.93 ± 0.52 µg PO_4-P, respectively. Notably, NZ-Amine induced the highest P-release among all carbon sources (2.45 ± 0.63 µg PO_4-P) and relatively low P-uptake with 3.89 ± 0.16 µg PO_4-P, yet resulted in the lowest phosphate removal among all tested C-sources, measured at 1.44 ± 0.48 µg PO_4-P.

In addition to quantifying P-removal, biofilm volume in the MMBS can serve as an indicator of overall system performance. As illustrated in Figure 27b, a distinct influence of the C-source on biofilm growth was observed. Glycerol supported the highest biofilm growth, reaching 5.18 ± 5.82 mm^3 cm^{-2}, followed by ethanol (3.42 ± 2.10 mm^3 cm^{-2}). In contrast, NZ-Amine resulted in the lowest biofilm volume, at 1.01 ± 1.38 mm^3 cm^{-2}. Moreover, while the acetate/propionate mixture supported robust, PAO-dominated communities (2.77 ± 1.65 mm^3 cm^{-2}), reactors fed with glucose exhibited weaker biofilm development (1.52 ± 1.39 mm^3 cm^{-2}). Additionally, due to substrate availability, the biofilm volume decreased from the front to the back positions in the reactor. At the front position in the meandering channel, glycerol again yielded the highest biofilm (11.49 ± 4.33 mm^3 cm^{-2}), while NZ-Amine produced the lowest (2.60 ± 1.56 mm^3 cm^{-2}).

The selected carbon source has a pronounced influence on the phosphate removal capacity of biofilm-based systems. Glucose and NZ-Amine exhibited the highest net P-removal capacities per unit biofilm volume, with values of 0.75 ± 0.09 µg PO_4-P mm^{-3} and 0.47 ± 0.15 µg PO_4-P mm^{-3}, respectively, due to the higher P-uptake and lower biofilm volumes. Moreover, acetate/propionate-fed biofilms (0.32 ± 0.07 µg PO_4-P mm^{-3}) showed a higher P-removal capacity than the thicker biofilms cultivated with glycerol and ethanol. Accordingly, glycerol, despite supporting the largest biofilm volume, showed the lowest P-removal capacity (0.14 ± 0.02 µg PO_4-P mm^{-3}) among the tested carbon sources, followed by ethanol with 0.18 ± 0.05 µg PO_4-P mm^{-3} (Figure 27c). These findings suggest a negative correlation between biofilm volume and P-removal capacity, except for NZ-Amine, which demonstrated the highest P-release capacity (0.79 ± 0.21 µg PO_4-P mm^{-3}).

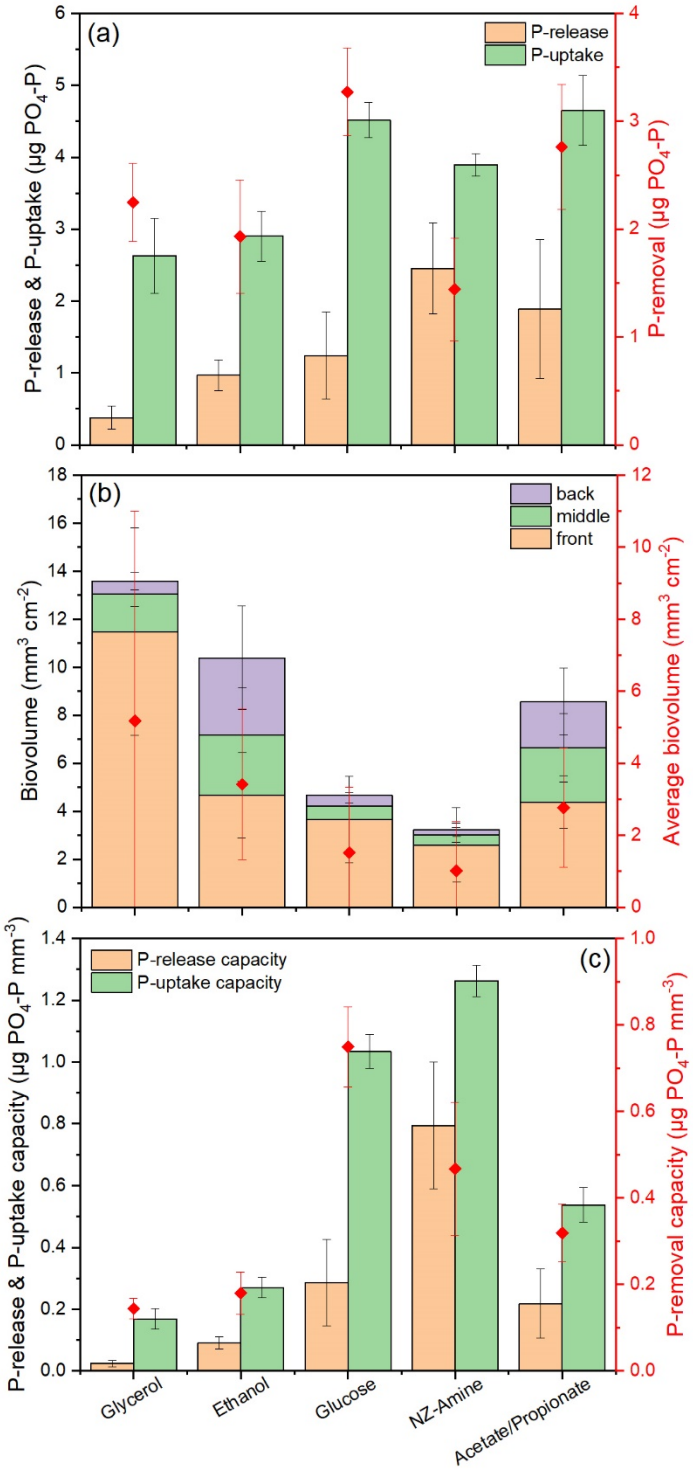

Figure 27. PAO efficiency and overall system performance using various C-sources. Experiments were conducted at a COD:P ratio of 40, pH 7.5, and room temperature. (a) Among all tested carbon sources, NZ-Amine induced the highest P-release during the anoxic phase but resulted in the lowest P-removal. In contrast, glucose and acetate/propionate supported the highest rates of P-uptake and P-removal. (b) Owing to superior substrate availability, the biovolume was highest at the front position compared with the middle and back positions in the meandering channels. Among the carbon sources, glycerol promoted the highest biofilm development, whereas NZ-Amine yielded the lowest biovolume. (c) Due to the observed negative correlation between biovolume and P-removal capacity, glycerol demonstrated the lowest P-removal capacity among the carbon sources tested. In contrast, glucose and NZ-Amine exhibited the highest P-removal capacities, which can be attributed to their greater P-uptake and comparatively lower biofilm volumes (n=3).

During cultivation in the microfluidic flow channel, the mesoscopic structures of the biofilms were directly observed within the reactor using OCT. Experiments were carried out in a flow-through system to reflect the conditions commonly employed in wastewater treatment applications. In addition to monitoring and visualizing the biofilm structure, data were collected to assess the relationship between biofilm volume and P-removal. As shown in the illustrative height map in Figure 28, the biofilm thickness generally declined from the front to the back of the channel, likely due to substrate consumption. Local thickness measurements confirm that the entrance of the microfluidic channels typically exhibited the highest biofilm volume.

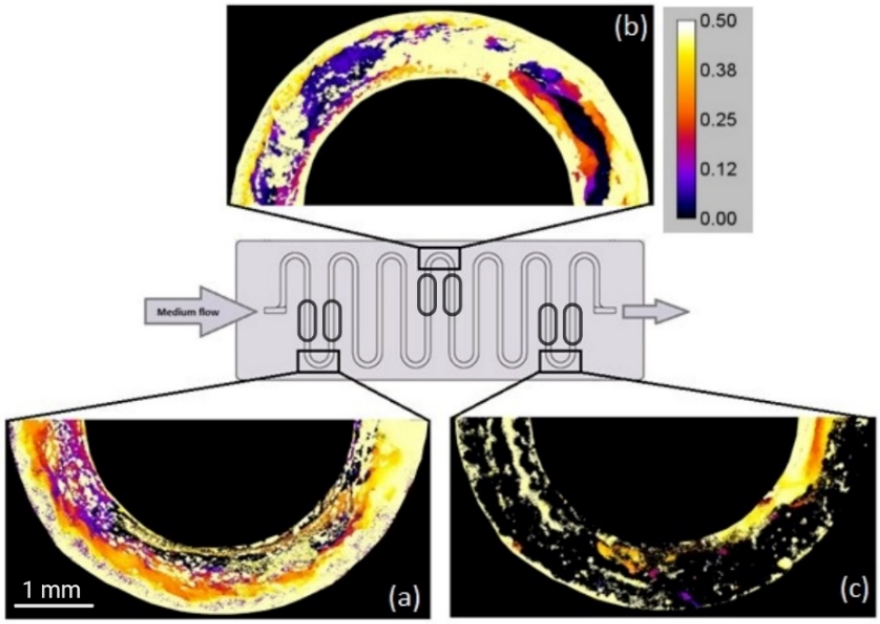

Figure 28. Representative maps of mesoscopic biofilm structures using OCT in MMBS. In three sections of the meandering channels are shown to illustrate biofilm topography and local thickness: front (a), middle (b), and back (c) positions (the experiment was conducted with acetate/propionate as the carbon sources, pH 8.0, COD:P of 40, and at room temperature). In the height map, colors represent biofilm height within the meandering channel: white areas correspond to the maximum biofilm height of 0.5 mm, while black areas indicate the absence of biofilm. The scale bar on the right indicates biofilm height in mm. Scale bar = 1 mm.

At the end of the PAO enrichment experiment with a microfluidic cultivation platform, metagenomic analyses based on whole native DNA sequencing were performed to assess the microbial community composition and to identify PAOs. The abundance of PAOs was compared to the initial inoculum (see Appendix, Tables S2 and S3). Figure 29 indicates the microbial community composition under different carbon sources. Sequencing results demonstrate that *Dechloromonas*, a recognized PAO genus, exhibited the highest relative

abundance when acetate/propionate (3:1 ratio) was used as the carbon source (25.24%), closely followed by ethanol (24.09%). The abundance of *Dechloromonas* was lowest under NZ-Amine supplementation, reaching only 1.05%. Co-enrichment of *Zoogloea*, a potential GAO, was observed in both cases. Ethanol utilization notably promoted *Zoogloea* growth, resulting in a relative abundance of 30.19%, followed by acetate/propionate at 22.82%. *Zoogloea* abundance also increased under amino acid feeding but remained at a moderate level of 11.37%.

In the experiments with glucose and acetate/propionate, *Dechloromonas* was more abundant than *Zoogloea*. However, in the glycerol, ethanol, and NZ-Amine experiments, *Zoogloea* surpassed *Dechloromonas* in abundance, which could impact P-removal due to the competitive dynamics between PAOs and GAOs.

Although a slight preference for ethanol was observed, *Accumulibacter*, a well-known PAO, exhibited a relatively low abundance (1.10%) under this condition and showed no enrichment across the tested carbon sources. Besides, in the glucose experiment, the relative abundance of *Micropruina* and *Tessaracoccus,* as fGAOs, reached 2.14% and 2.21%, respectively. However, their relative abundances declines 0.35% and 0.29% in the glycerol-fed system, and further to 0.07% and 0.03% under acetate/propionate feeding conditions. Further, the use of glycerol led to *Propionivibrio, Competibacter and Contendobacter,* all considered GAOs, reaching relative abundance of 0.82%, 0.71% and 0.50% in the community. Additionally, these genera were also detected in the glucose-fed system, with relative abundances of 0.37%, 0.47% and 0.30%, respectively. Further, in contrast to *Competibacter and Contendobacter,* the relative abundance of *Propionivibrio* increased from 0.35% to 0.66% under acetate/propionate-fed condition.

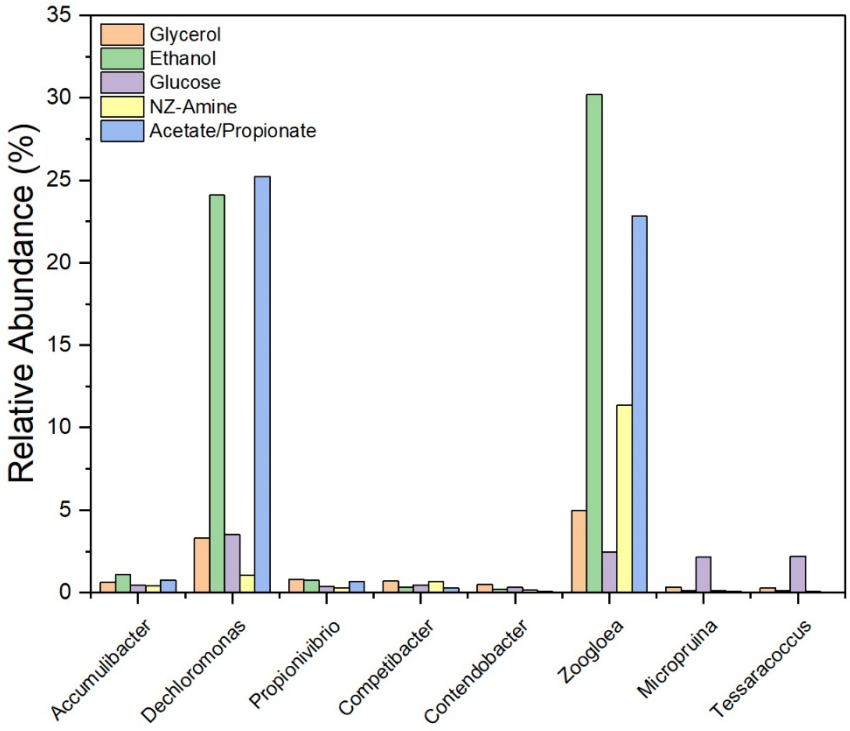

Figure 29. The relative abundances of potential PAOs and GAOs across different carbon sources were compared between the initial inoculum and the samples obtained at the end of cultivation in the MMBS. Abundance values are expressed as percentages of the total microbial community. Standard process conditions in the MMBS were maintained at a COD:P ratio of 40, pH 7.5, and room temperature. *Dechloromonas* reached the highest relative abundance when acetate/propionate was supplied, with a marginally lower abundance observed under ethanol treatment. Under both substrate conditions, co-enrichment of *Zoogloea*, a putative GAO, was detected, with ethanol notably favoring its proliferation, followed by acetate/propionate. Under glucose supplementation, *Micropruina* and *Tessaracoccus*, identified as fGAOs, were enriched. Although *Accumulibacter* (PAO) did not show enrichment across the tested carbon sources, except in the ethanol-fed system, *Propionivibrio*, *Competibacter* and *Contendobacter*, as GAOs, were only scarcely enriched in the glycerol-fed system.

3.2.2. Impact of pH, COD:P ratio and temperature on the efficiency of MMBS and PAO-GAO abundance

The effects of pH (6.5, 7.5 and 8.0), COD:P ratio (10, 40 and 80), as well as temperature (room temperature and 12 °C) on the efficiency of PAOs were analyzed. Figure 30 demonstrates the effects of these process conditions on P-removal, biofilm growth and biofilm P-removal capacity. Initially, pH values - 6.5, 7.5, and 8.0 - were compared to assess their impact on system performance. At an elevated pH level from 6.5 to 7.5, the P-release by PAOs slightly increased from 1.80 ± 0.62 µg PO_4-P to 1.89 ± 0.9 µg PO_4-P. However, when the pH was further raised to 8.0, the P-release declined to 1.13 ± 0.04 µg PO_4-P. Furthermore, the results indicated that P-uptake was lowest at pH 7.5, reaching 4.65 ± 0.48 µg PO_4-P. In contrast, the

P-uptake values observed at pH 6.5 and 8.0 were comparable, measuring 6.53 ± 0.75 µg PO_4-P and 6.00 ± 0.60 µg PO_4-P, respectively. The pH experiments revealed no significant differences in overall P-removal. However, variations in P-removal were associated with changes in biofilm thickness. Minimal differences were observed at pH 6.5 and 8.0, with P-removal values of 4.73 ± 0.74 µg PO_4-P and 4.87 ± 0.57 µg PO_4-P, respectively (Figure 30a). However, the lowest P-removal amount was recorded at pH 7.5 (2.76 ± 0.58 µg PO_4-P), which also corresponded to the lowest biovolume (2.77 ± 1.65 $mm^3\ cm^{-2}$), likely due to reduced P-uptake. In contrast, at pH 8.0, biofilm formation was promoted, resulting in a biovolume of 7.57 ± 3.78 $mm^3\ cm^{-2}$, followed by pH 6.5, which yielded a biovolume of 6.58 ± 3.73 $mm^3\ cm^{-2}$, as shown in Figure 30b. Further, as indicated in Figure 30c, both anoxic phosphate release and oxic uptake capacities increased with rising pH from 6.5 to 7.5, in parallel with P-removal capacity (from 0.24 ± 0.04 µg PO_4-P mm^{-3} to 0.32 ± 0.07 µg PO_4-P mm^{-3}). An optimum in terms of P-removal capacity appears to be reflected at 7.5 due to the reduced biovolume. However, at pH 8.0, the P-removal capacity declined to 0.21 ± 0.02 µg PO_4-P mm^{-3}, reflecting the negative correlation between biofilm volume.

Secondly, the effect of varying phosphate concentrations on the system with a fixed carbon concentration of 100 mg COD L^{-1} is shown in Figure 30. Experiments were conducted at room temperature using acetate/propionate as the carbon source, with phosphate concentrations of 2.5 mg L^{-1} (the standard for all other experiments), 1.25 mg L^{-1} and 10 mg L^{-1}. An increased phosphate concentration (10 mg L^{-1}, COD:P 10) improved both P-release and P-uptake, reaching 5.23 ± 1.56 µg PO_4-P and 10.90 ± 2.43 µg PO_4-P, respectively. Under this condition, increased P-removal (5.67 ± 2.33 µg PO_4-P) and enhanced biofilm growth (8.99 ± 3.73 $mm^3\ cm^{-2}$) were observed, likely due to the greater P-availability. However, owing to the high volume of biofilm, P-removal capacity (0.22 ± 0.08 µg PO_4-P mm^{-3}) was lower than that observed at COD:P ratio of 40. In contrast, low P-concentration (1.25 mg L^{-1}, COD:P 80) resulted in reduced poly-P formation during the oxic phase, limiting P-release in the anoxic phase. P-removal and P-removal capacity were negligible (0.043 ± 0.27 µg PO_4-P and 0.002 ± 0.01 µg PO_4-P mm^{-3}, respectively), as P-release and P-uptake values were similar. Nevertheless, the biovolume remained relatively high (6.84 ± 3.52 $mm^3\ cm^{-2}$), indicating that the COD:P ratio does not directly affect biofilm growth in the absence of nutrient limitation. Besides, a COD:P ratio of 40 yielded improved P-removal capacity (0.32 ± 0.07 µg PO_4-

P mm^{-3}), due to the higher P-uptake capacity (0.54 ± 0.06 µg PO_4-P mm^{-3}) and lower biofilm volume (2.77 ± 1.65 mm^3 cm^{-2}), compared to COD:P ratios of 10 and 80 (in Figure 30c).

Lastly, in the temperature experiment conducted at room temperature and 12 ^oC, P-release levels were comparable (1.88 ± 0.96 µg PO_4- P and 2.04 ± 0.85 µg PO_4-P, respectively). However, P-uptake was enhanced at 12 ^oC, with uptake values of 6.88 ± 0.31 µg PO_4-P compared to 4.65 ± 0.48 µg PO_4-P at room temperature (Figure 30a). Temperature experiments, shown in Figures 30a and b, demonstrated that both P-removal and biovolume were slightly higher at 12 °C (4.84 ± 1.05 µg PO_4-P; 3.79 ± 2.68 mm^3 cm^{-2}) compared to room temperature (2.76 ± 0.58 µg PO_4-P; 2.77 ± 1.65 mm^3 cm^{-2}). Similarly, P-removal capacity appeared to be higher at low temperature (0.43 ± 0.09 µg PO_4-P mm^{-3}) due to increased P-uptake than at room temperature (0.32 ± 0.07 µg PO_4-P mm^{-3}). The results showed that operating at a lower temperature did not adversely affect biological phosphorus removal performance.

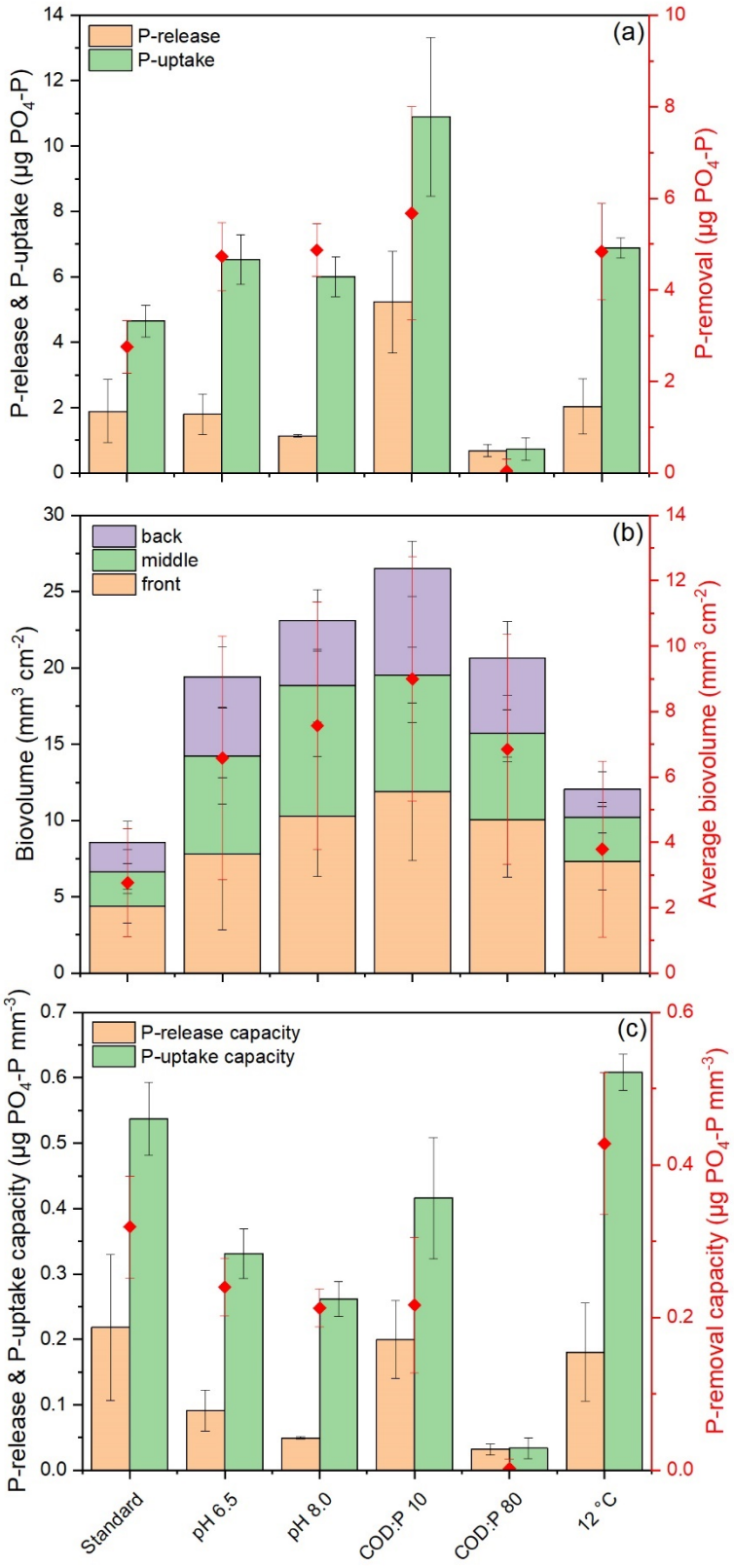

Figure 30. The efficiency of PAOs and the overall system performance under varying pH conditions (6.5, 7.5 and 8.0), COD:P ratios (10, 40 and 80), and temperatures (room temperature and 12 °C). Standard process conditions were defined using acetate/propionate (3:1) as the carbon source, at a pH of 7.5, a COD:P ratio of 40, and room temperature.

(a) The pH experiments indicated no significant differences in overall P-removal among the tested conditions; however, slight variations were observed, with similar behavior at pH 6.5 and 8.0, which differed slightly from pH 7.5. Under the low COD:P ratio of 10, both P-release and P-uptake increased substantially, resulting in enhanced P-removal. Conversely, at the increased COD:P ratio of 80, P-removal was negligible. Additionally, P-removal was higher at 12 °C than at room temperature. (b) The lowest biovolume was observed at pH 7.5, likely due to reduced P-uptake, whereas pH 8.0 promoted biofilm development. At a COD:P ratio of 10, biofilm growth was enhanced, presumably due to increased phosphate availability; however, despite the markedly low P-removal at a COD:P ratio of 80, the biovolume remained comparatively high, suggesting that the COD:P ratio does not exert a direct influence on biofilm growth in the absence of nutrient limitation. Additionally, biovolume was also greater at 12 °C compared to room temperature. (c) Reflecting the negative correlation between biofilm volume and phosphate removal capacity, pH 7.5 and a COD:P ratio of 40 (standard) yielded the highest P-removal capacity. Furthermore, the biofilm-based phosphate removal capacity was marginally higher at 12 °C than at room temperature (n=3).

Figure 31 presents the microbial community composition under various process conditions, with acetate/propionate as carbon sources. Experiments at pH levels of 6.5 and 7.5 showed that growth of *Dechloromonas* was preferentially enhanced in the system, which reached relative abundances of 27.28% and 25.24%, respectively. Besides, at pH 7.5, *Zoogloea* became more dominant, reaching a relative abundance of 22.82%, indicating that neutral pH conditions favour its proliferation. *Accumulibacter* was slightly enriched at pH 6.5 and 8.0, with relative abundances of 1.13% and 1.03%, respectively. Moreover, at pH 8.0, the GAO genera *Propionivibrio, Competibacter and Contendobacter* reached relative abundances of 1.27%, 0.39% and 0.22% in the community, respectively.

A phosphate concentration of 2.5 mg L^{-1} (COD:P 40) promoted the proliferation of *Dechloromonas*, which reached a relative abundance of 25.24%. This condition also supported the growth of *Zoogloea*, with a relative abundance of 22.82%. At a higher P concentration of 10 mg L^{-1} (COD:P 10), *Dechloromonas* remained dominant (22.48%), while the relative abundance of *Zoogloea* decreased to 13.26%. In contrast, limited P-loading at 1.25 mg L^{-1} (COD:P 80) appeared to suppress PAO growth, as the relative abundance of *Dechloromonas* declined to 14.13%. Additionally, the abundance of *Zoogloea* decreased slightly to 12.01%.

Moreover, analysis of the biofilm microbial composition revealed a decrease in the relative abundance of *Dechloromonas* from 25.24% at room temperature to 12.92% at 12 °C, and a decline in *Zoogloea* from 22.82% to 10.78%. Despite reductions of approximately half in both genera, system performance, as measured by P-removal, remained unaffected at the lower temperature. In contrast, the relative abundance of *Accumulibacter* (PAO) was 0.77% at room temperature and increased slightly to 0.81% at 12 °C, a pattern consistent with that of *Propionivibrio*, *Competibacter*, *Contendobacter*, *Micropruina* and *Tessaracoccus*.

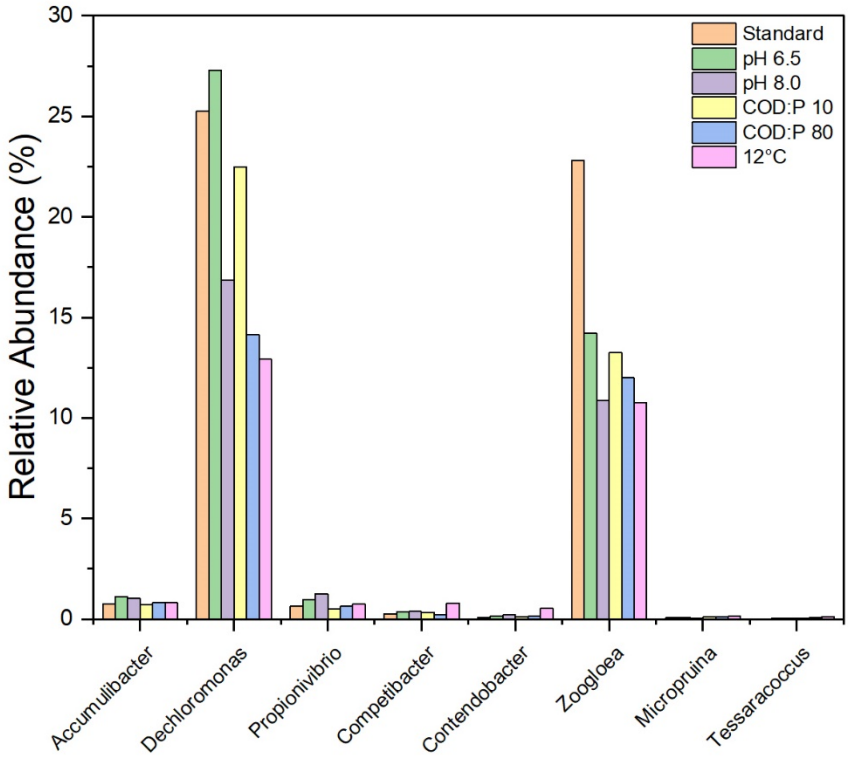

Figure 31. The relative abundances of potential PAOs and GAOs under different pH values, COD:P ratios, and temperatures at the end of cultivation and compared with the initial inoculum in the MMBS. Relative abundances are expressed as percentages of the total microbial community. Standard process conditions in the MMBS were maintained using acetate/propionate as the carbon source (3:1 ratio), pH 7.5, COD:P ratio of 40, and room temperature. At pH≤7.5, preferential enrichment of *Dechloromonas* was observed. Further, *Zoogloea* was more dominant at pH 7.5, suggesting that neutral pH conditions favour its proliferation. A phosphate concentration of 2.5 mg L^{-1} (COD:P ratio of 40) effectively promoted the growth of both *Dechloromonas* and *Zoogloea*, whereas a lower phosphate loading of 1.25 mg L^{-1} (COD:P ratio of 80) led to a reduction in their relative abundances. Moreover, analysis of the microbial composition of biofilms revealed that the relative abundances of *Dechloromonas* and *Zoogloea* decreased at the lower temperature.

3.2.3. FISH analysis

A FISH protocol (see Table 22) involving the fixation of cultured cells was implemented as an endpoint analysis after 20 days of cultivation in MMBS to verify the metagenomic results by detecting the presence of key microorganisms. Following the cultivation period, metagenomic analysis indicated that *Dechloromonas* became the dominant PAO, exhibiting a higher relative abundance (25.24%) compared to the initial inoculum. A representative fluorescence microscopy image of probe-labelled cells within a mature biofilm, formed in the microfluidic flow channel, is presented in Figure 32. These images were obtained under defined experimental conditions: a mixture of acetate and propionate as VFAs, a pH of 7.5, a COD:P ratio of 40, and at room temperature. Images were acquired at curve 7, corresponding to the

middle position of the meandering channel. FISH was performed using rRNA-targeted probes; specifically, the Dechlo2 probe was employed to detect *Dechloromonas*, while the γ-proteobacteria-targeted probe Gam42a was used to identify GAOs. The presence and abundance of *Dechloromonas*, as revealed by metagenomic sequencing, were confirmed by FISH through the quantification of cells belonging to this genus. Additionally, digital image analysis of FISH images using Daime estimated the proportion of *Dechloromonas* cells to be 28.03%. This finding was consistent with the metagenomic analysis of mature biofilms. Together, these results provide valuable insights into the predominant microbial populations within the microfluidic platform.

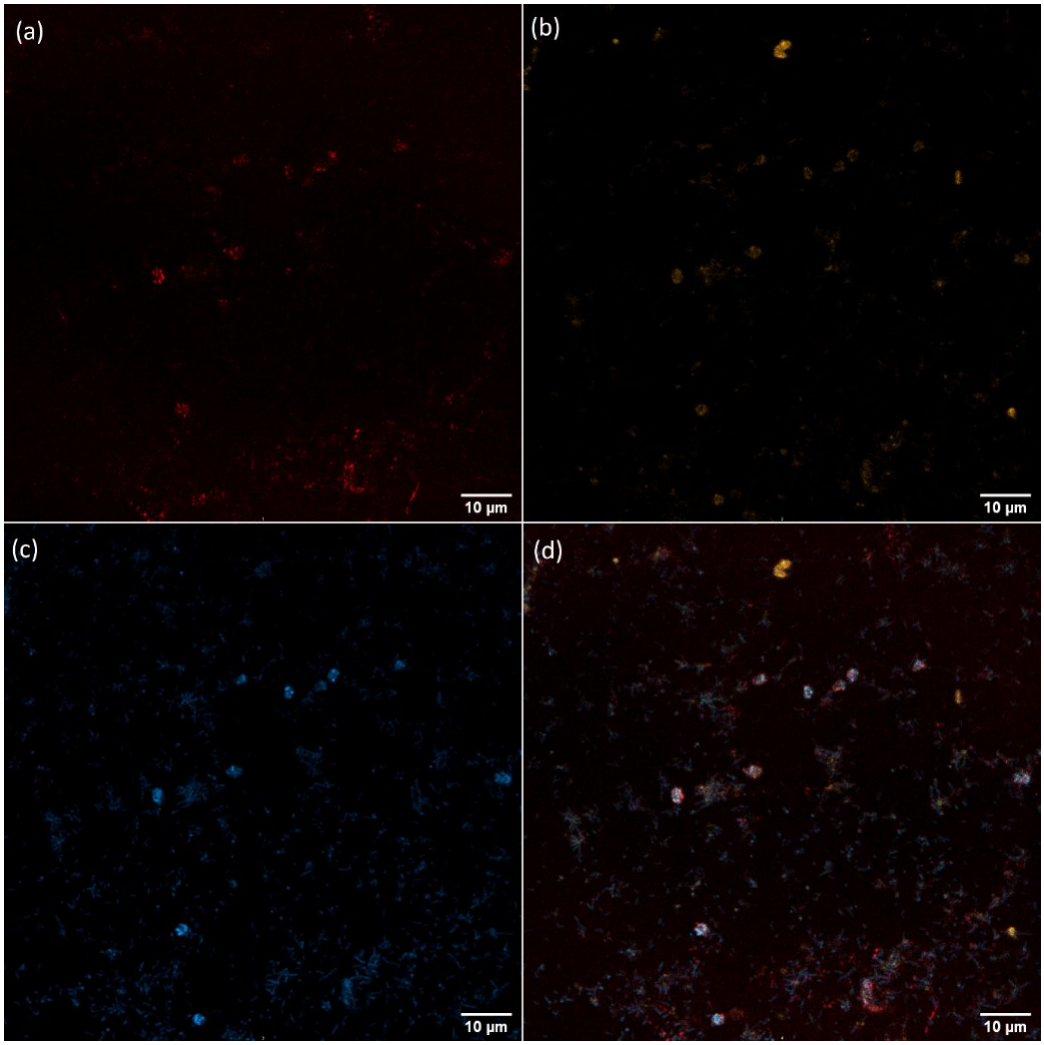

Figure 32. Representative fluorescence microscopy image of mature biofilm in the microfluidic flow channel in curve 7 using (a) the γ-proteobacteria-specific Gam42a (5'-[Cy5]-GCC TTC CCA CAT CGT TT-3′) probe (Manz *et al*., 1992; red) and addition of unlabelled Gam42a-Competitor (5′-GCC TTC CCA CTT CGT TT-3′) probe (Klein *et al*., 2022); (b) *Dechloromonas*-specific Dechlo2 (5'-[TAM]-GCT CAA TCA GCG CAA GGT CT-3′) probe (Mcilroy *et al*., 2016; Ziegler *et al*., 2016; orange-red); and (c) 4′, 6-diamidino-2-phenylindole (DAPI; blue) as counterstain. The merged image is shown in (d).

3.2.4. Multivariate and network analyses

A PCA was conducted to provide insights into the interactions between multiple process conditions in relation to the corresponding diversity of major PAOs/GAOs, as well as biofilm formation and activity. This analysis was based on the relative abundance of major PAOs and GAOs, biofilm volume and P-removal. As shown in Figure 33, PC1 and PC2 together explained 56.9% of the total variance.

The score plot (Figure 33a) indicates that the use of acetate/propionate as carbon sources resulted in minimal variation across different pH and temperature values, compared to the effects observed with varying COD:P ratios and with other carbon sources, excluding glycerol and ethanol. Glycerol and ethanol exhibited minimal impact on variations. In contrast, glucose and NZ-Amine induced larger variation, as glucose achieved the highest P-removal, while NZ-Amine resulted in the lowest among all tested carbon sources. Furthermore, changing COD:P ratio (80 and 10), by using different P-concentrations (1.25 and 10 mg L^{-1}), showed substantial variation (highlighted by the arrows), as indicated by the increased distance between samples in the PCA plot.

The loading plot (Figure 33b) confirms a strong negative correlation between P-removal and COD:P ratio, which is more pronounced than the correlation observed for pH and temperature. However, P-removal was positively correlated with both biovolume and relative abundance of *Dechloromonas*. Although *Zoogloea* did not directly contribute to P-removal, its presence exhibited a positive correlation with the dominant genus *Dechloromonas*. As a filamentous organism, *Zoogloea* may enhance the extracellular matrix, thereby promoting the robust growth of *Dechloromonas* within the biofilm microbial composition. Further, *Accumulibacter,* the well-known PAO, and *Dechloromonas* were also positively correlated with biofilm formation. In contrast, other potential GAOs, such as *Micropruina*, displayed negative correlations with the dominant *Dechloromonas* and *Zoogloea* populations.

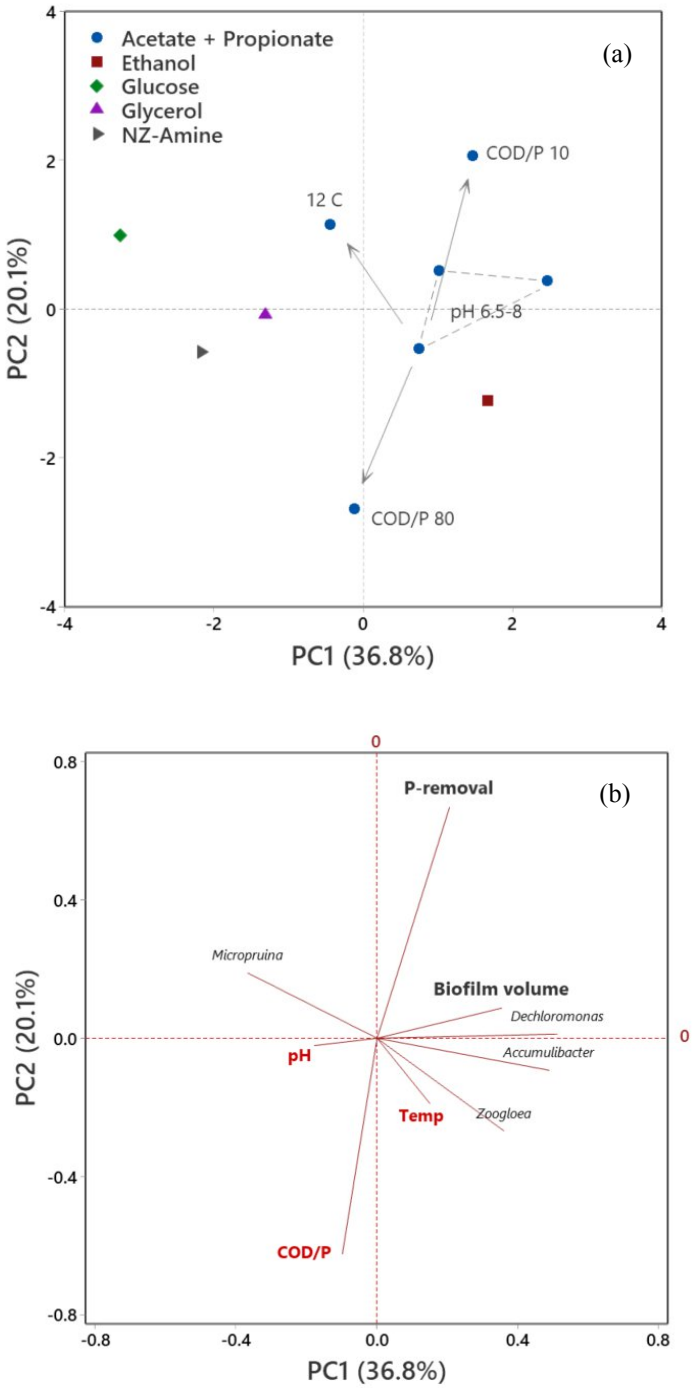

Figure 33. Principal component analysis (PCA) based on the relative abundances of major PAOs and GAOs in the MMBS under varying C-sources, pH values, COD:P ratios, and temperatures, as well as the corresponding biofilm volume and P-removal. (a) The score plot reveals that acetate/propionate as carbon sources produced minimal variability across different temperature and pH conditions, in contrast to the more pronounced effects associated with varying COD:P ratios and other C-sources. Notably, glycerol and ethanol demonstrated a limited impact on variation, whereas glucose and NZ-Amine elicited greater variability in the observed responses. (b) The loading plot demonstrates that variations in the COD:P ratio within the acetate/propionate experiments exerted a more pronounced influence on system performance than various pH and temperature conditions. A negative correlation was observed between the COD:P ratio and P-removal, wherein increasing the COD:P ratio corresponded with a decline in removal of P. Conversely, P-removal showed a positive correlation with both biovolume and *Dechloromonas*. Further, although *Zoogloea* did not seem to contribute directly to P-removal, its abundance showed a positive correlation with that of *Dechloromonas*. PC implies the principal component; arrows, in the score plots, are used to highlight the variance between samples.

Spearman-based co-occurrence network analyses, shown in Figure 34, were performed for genera with a relative abundance greater than 1% in samples collected before enrichment (four inoculum samples; see Appendix, Figure S1) and after enrichment under different conditions, including carbon source, pH, COD:P ratio, and temperature, to assess the overall distribution patterns and potential clusters. Node size represents the maximum relative abundance observed among all samples, while green and red edges indicate positive and negative correlations, respectively.

The correlation analysis and corresponding network construction aimed to identify co-occurrence patterns indicative of associations within the microbial community, including PAOs and GAOs, for each system operated under different process conditions. Combined with the relative abundance data, these patterns provide a basis for hypothesizing how the microbial community responds to varying operating conditions. In addition, to reduce potential uncertainties associated with relative abundance data, the following measures were implemented: (1) samples from each system were analyzed and interpreted separately for correlations, (2) whole native DNA sequencing was applied to enable an accurate assessment of the relevance of specific microorganisms and to avoid potential PCR amplification bias in the estimation of relative abundance, and (3) only statistically significant correlations among genera ($p < 0.05$) were considered.

Modularity clusters are groups of nodes in a network that are more strongly connected to each other than to the rest of the network. By analyzing the modularity clustering within the constructed network, including samples before enrichment, four distinct modularity clusters were found (Figure 34a). Notably, *Dechloromonas* and *Zoogloea,* considered potential PAOs/GAOs, were grouped within the same cluster (highlighted in light blue), suggesting potential ecological or functional associations. This cluster exhibited predominantly negative correlations with other clusters, which included either dominant genera from the inoculum or major GAOs, underscoring the effectiveness of the enrichment process under P-accumulating conditions.

When inoculum samples were excluded from the network construction and nodes (representing genera) were ranked by betweenness centrality, *Dechloromonas* exhibited a high rank, indicating its more central role compared to other genera in the community structure within the network (Figure 34b).

(a)

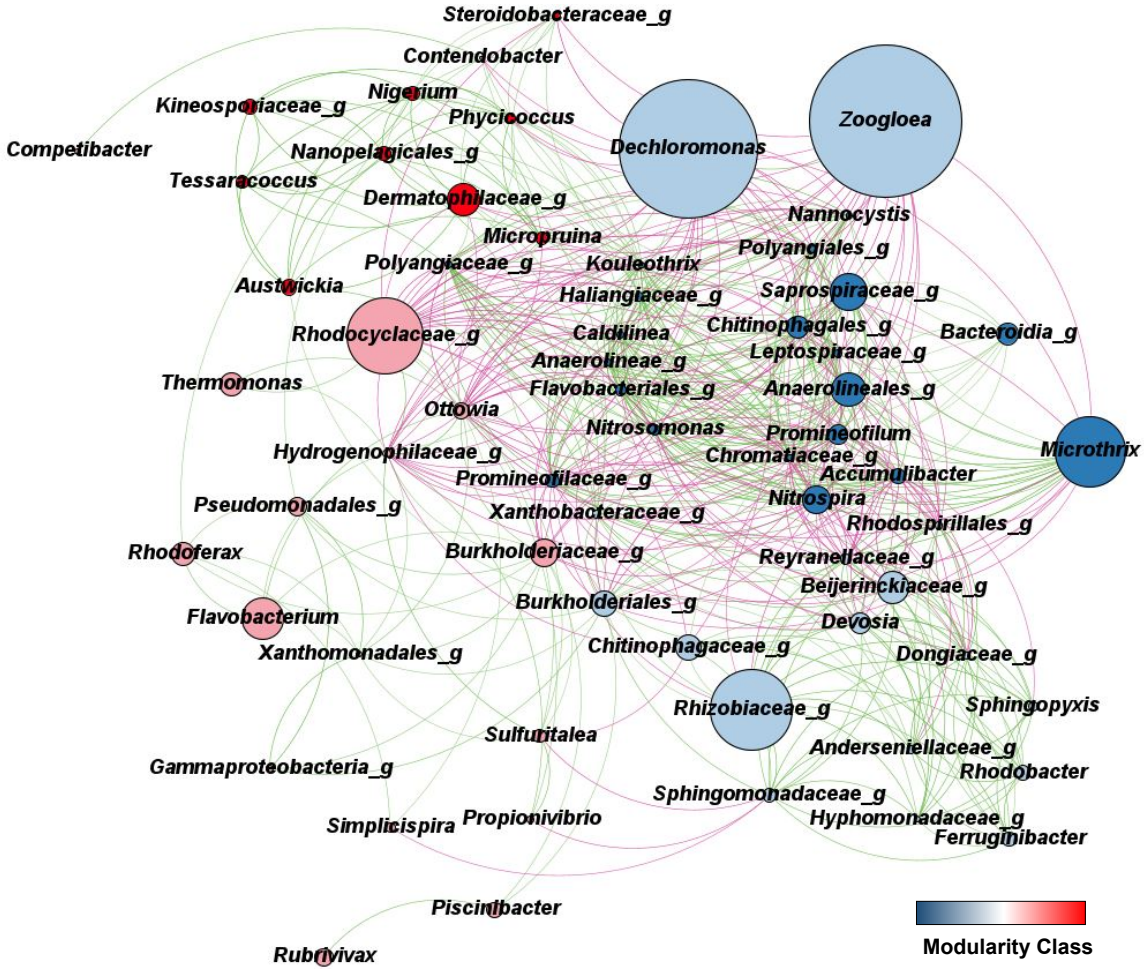
Steroidobacteraceae_g
Contendobacter
Nigerium
Kineosporiaceae_g
Phycicoccus
Competibacter
Nanopelagicales_g
Tessaracoccus
Dermatophilaceae_g
Micropruina
Polyangiaceae_g
Kouleothrix
Austwickia
Haliangiaceae_g
Rhodocyclaceae_g
Caldilinea
Anaerolineae_g
Thermomonas
Flavobacteriales_g
Ottowia
Nitrosomonas
Hydrogenophilaceae_g
Promineofilaceae_g
Pseudomonadales_g
Xanthobacteraceae_g
Rhodoferax
Burkholderiaceae_g
Flavobacterium
Burkholderiales_g
Xanthomonadales_g
Chitinophagaceae_g
Rhizobiaceae_g
Sulfuritalea
Gammaproteobacteria_g
Sphingomonadaceae_g
Simplicispira
Propionivibrio
Piscinibacter
Rubrivivax
Dechloromonas
Zoogloea
Nannocystis
Polyangiales_g
Saprospiraceae_g
Chitinophagales_g
Bacteroidia_g
Leptospiraceae_g
Anaerolineales_g
Promineofilum
Chromatiaceae_g
Accumulibacter
Nitrospira
Rhodospirillales_g
Reyranellaceae_g
Beijerinckiaceae_g
Devosia
Dongiaceae_g
Sphingopyxis
Anderseniellaceae_g
Rhodobacter
Hyphomonadaceae_g
Ferruginibacter
Microthrix
Modularity Class

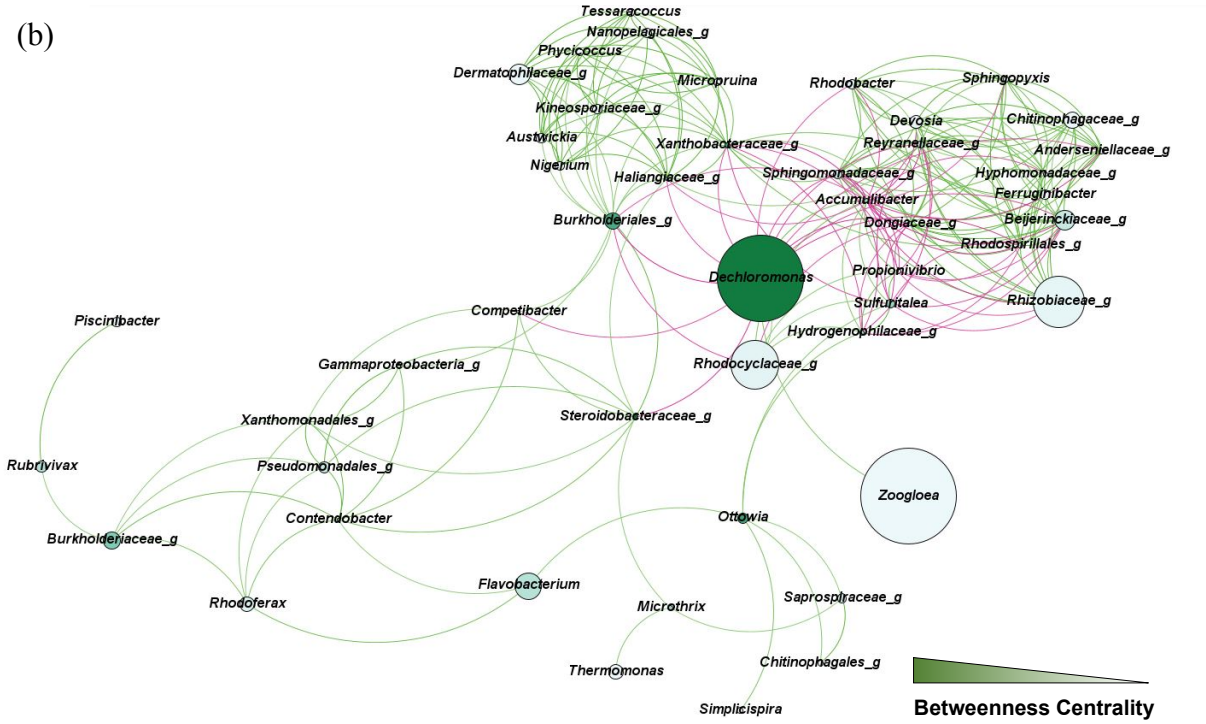

Figure 34. Spearman-based co-occurrence networks showing microbial interactions among the identified genera with relative abundances greater than 1% in the MMBS, based on samples collected before and after enrichment under various conditions. Node size indicates the maximum relative abundance observed across all samples, as well as green and red edges indicate positive and negative correlations, respectively. (a) After enrichment, four distinct modularity clusters were identified. *Dechloromonas* and *Zoogloea* were grouped within one cluster (highlighted in light blue), which exhibited negative correlations with the other clusters. (b) Excluding inoculum samples from network construction and ranking genera by betweenness centrality revealed that *Dechloromonas* attained a high betweenness centrality rank, indicating a more central structural role within the network than other genera in the community. In contrast, *Zoogloea* ranked lower and exhibited only a positive correlation (with Dechloromonas), suggesting potential mutualism between these genera. Only significant correlations ($p<0.05$) are displayed.

It was also found that most of the significant correlations between *Dechloromonas* and other genera were negative, highlighting its major role in P-removal across various conditions tested. In contrast, *Zoogloea* showed a lower betweenness centrality rank and displayed a positive significant correlation only with *Dechloromonas*. This positive correlation suggests that *Dechloromonas* and *Zoogloea* likely benefit from each other's presence.

4. Discussion

Rising energy consumption and intensifying environmental concerns necessitate the development of more sustainable and efficient approaches to wastewater treatment (Ghimire *et al.*, 2021). The BES represents a promising technology for the removal of organic contaminants from wastewater through the facilitation of carbon oxidation processes. This strategy not only achieves water purification but also enables concurrent energy recovery during the treatment process, thereby decreasing the energy requirements of the treatment process (Mier *et al.*, 2021). To this purpose, microorganisms colonize the BES electrode as a biofilm, enabling the transfer of respiratory electrons to the electrode surface. Yet, this biofilm–electrode interaction represents a critical limitation of the technology, as its current efficiency does not meet the demands (Martinez and Alvarez, 2018). To strengthen the biofilm–electrode interface, surface modifications can be used to improve biofilm attachment to the anode surface, resulting in improved current generation. In the first part, surface functionalization with biocompatible chemicals, riboflavin and AQDS, and different roughness of electrodes were evaluated with the model exoelectrogenic organisms *S. oneidensis* and *G. sulfurreducens* in microfluidic BES reactors.

Further, employing microfluidic systems as microliter-scale research tools enables comprehensive investigation of system optimization, thereby advancing the understanding of key operational parameters, particularly in complex treatment processes such as biological phosphorus removal from wastewater. Studies indicate that around 1.3 Mt of phosphorus is directed to wastewater treatment plants annually, with the recoverable fraction from municipal wastewater capable of supplying 15–20% of global phosphorus demand (X. Wang *et al.*, 2024). PAO-oriented EBPR is a biological strategy for highly efficient phosphorus removal, which addresses strict effluent quality standards and supports phosphorus recycling.

The share of poor-quality receiving water bodies has generally decreased over time, reflecting improvements in phosphorus management. However, a significant proportion still fails to meet the required phosphorus concentration status, according to the latest measurements in Germany. For instance, Figure 35 shows the river sampling sites where total phosphorus levels exceed the threshold for "good status" (defined as water quality class II-III or worse) from 1982 to 2023, along with a projected target for 2030 from the German Environment Agency (Arle *et al.*, 2017). This figure highlights the ongoing challenge of phosphorus-

induced river eutrophication, quantifies water bodies that do not meet the phosphorus target, and tracks progress toward national sustainability goals. It reflects both improvements over the decades and the need for continued efforts to reduce phosphorus pollution to achieve the 2030 target of the German Sustainable Development Strategy.

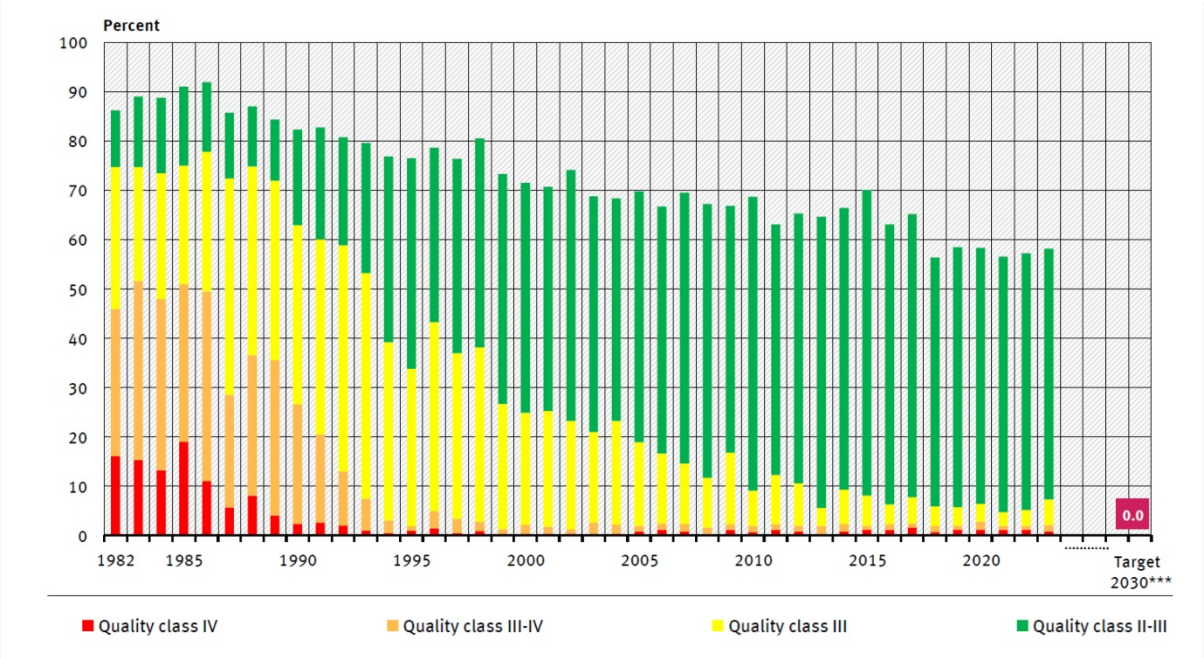

Figure 35: River sites in Germany exceeding total phosphorus standards. The data shows the percentage of monitoring sites exceeding the 'good status' target value relative to the total number of sites according to the German Environment Agency (modified from Arle et al., 2017).

Phosphorus removal plays a critical role in biological wastewater treatment, as it prevents eutrophication and deterioration of receiving water bodies, and ensures compliance with regulatory standards, with PAOs representing a key microbial group capable of achieving this. The subsequent part of this thesis aims to comprehensively assess the impact of external operational conditions and to establish optimal operational parameters that maximize the efficiency of biological phosphorus removal in WWTPs. To accomplish this objective, a previously established MMBS developed by Klein (2018) was further developed and applied based on the principles of the activated sludge process at the microliter scale, and to enrich the targeted PAOs. To investigate how process conditions affect the diversity and abundance of PAOs and their interactions with GAOs, a series of experiments was performed using various carbon sources - glycerol, ethanol, glucose, amino acids, and acetate/propionate. The effects of different COD:P ratios (10, 40, and 80), pH levels (6.5, 7.5, and 8.0), and temperatures (room

temperature and 12 °C) were also examined to assess their influence on PAO activity and the overall performance of EBPR.

To this end, the two wastewater treatment approaches of interest in this study, i.e., carbon elimination and energy recovery by exoelectrogens in BES (section 4.1) as well as phosphate elimination and resource recovery by PAOs in MMBS (section 4.2), were evaluated for system optimization and to improve treatment efficiency. A comprehensive investigation of how operational conditions affect biofilm formation, using a multi-parallel microfluidic cultivation platform, is fundamental to understanding process dynamics and to the development of optimized, energy-efficient wastewater treatment systems.

4.1. Carbon elimination and energy recovery with exoelectrogens in BES

The BES is a technology that integrates biological and electrochemical processes through the interplay of chemical and electrical energy conversion, and offers the potential for a sustainable bioeconomy. One of the major limitations to moving such technology to real-world applications is optimizing the electrode-biofilm interaction. Meanwhile, approaches to provide robust and highly conductive biofilms are essential (Klein *et al.*, 2024). Surface functional groups are key determinants in promoting the attachment and development of electroactive biofilms. Furthermore, materials exhibiting pronounced topography and larger surface area have been shown to provide superior support for biofilm development (Fernández-Ávila Cobo *et al.*, 2025). Accordingly, key operational parameters of BESs, notably electrode surface functionalization and roughness, were systematically investigated with respect to their effects on biofilm formation and current density generation by EABs capable of EET.

4.1.1. Effect of surface functionalization on the efficiency of BES

The anode surface was functionalized with biocompatible compounds to enhance interactions between the biofilm and the electrode by increasing electron transfer from cells to the electrode surface. In this thesis, riboflavin and AQDS were used to modify the graphite electrode surface via a simple physical adsorption procedure prior to inoculation of the corresponding microorganisms, *S. oneidensis* and *G. sulfurreducens*. The riboflavin functionalized electrode resulted in a maximum biofilm volume of 5.84 mm^3 cm^{-2} on day 7, whereas the control

condition maintained low biofilm volumes of approximately 0.6 mm^3 cm^{-2} throughout the experiment, with only a modest maximum of 0.78 mm^3 cm^{-2} on day 7 (see section 3.1.1, Figure 20). The 7.5-fold increase in biofilm volume suggested that riboflavin, used for surface functionalization, contributed to the increase in the number of electroactive biofilm cells on the anode surface.

According to the publication by Edel *et al.* (2021), the addition of riboflavin induces a concentration-dependent activation of the speC promoter, which encodes the ornithine decarboxylase, thereby promoting biofilm formation and increasing cell density on the anode, resulting in higher current densities. Among the proteins significantly influenced by SpeC, UDP-N-acetylglucosamine C4 epimerase WbpP is distinguished as the only one with a recognized direct function in EPS formation. The protein could act as a catalyst for chemical alterations in the composition of the EPS. The alteration in EPS composition may account for the enhanced cell attachment observed on the anode, potentially as a consequence of riboflavin-mediated quorum sensing. Beyond acting as a redox mediator and cofactor, riboflavin thus also serves as a quorum-sensing molecule. This messenger molecule enhances biofilm development in the absence of oxygen in *S. oneidensis*, dependent on cell density (Edel *et al.*, 2021; Klein *et al.*, 2025). In most microbial electrochemical systems, such regulatory effects are particularly relevant because only a small fraction of microorganisms remains planktonic in the electrolyte, while the majority grow as electroactive biofilms embedded in a self-secreted EPS matrix on the electrode surface, which ensures adhesion, structural integrity, and long-term stability as well as contributes to electron transfer (Angelaalincy *et al.*, 2018; Klein *et al.*, 2023). Additionally, electron mediators such as flavin mononucleotide, 9,10-anthraquinone, and 2-hydroxy-1,4-naphthoquinone have likewise been reported to enhance biofilm development by stimulating EPS production (Q. Zhao *et al.*, 2022). These findings suggest a potential riboflavin–SpeC–WbpP mechanism, in which redox-active molecules might act simultaneously as mediators, cofactors, and signaling compounds to link EPS regulation with electroactive biofilm formation.

Immobilizing riboflavin on the anode surface clearly enhanced biofilm formation compared to naturally developed biofilms. This approach relied on the physical adsorption (physisorption) of electroactive organic molecules onto graphite electrodes. Specifically, the isoalloxazine ring, constituting the core of riboflavin, plays a central role in enzyme-catalyzed electron transfer processes in biological systems (Malinauskas, 2008; Wu *et al.*, 2007). This

electroactive unit contributes to redox reactions by interacting with cellular components via non-covalent forces, including π–π stacking interactions (Răsădean *et al.*, 2021). In this context, the spontaneous non-covalent physical adsorption of redox-active compounds onto graphite surfaces offers a simpler and faster immobilization route than covalent attachment procedures (Andrés *et al.*, 2021; Ta *et al.*, 1999).

The improved interactions between the biofilm and the anode surface, achieved through riboflavin immobilization, not only enhanced biofilm formation but also accelerated current density generation. The biofilm formed on the non-functionalized surface generated a current density of 37.46 μA cm^{-2} after 7 days. On the contrary, surface functionalization with riboflavin yielded a current density of 125.92 μA cm^{-2}, corresponding to an approximately 3.4-fold increase (Figure 20). Besides, riboflavin substantially enhanced mean current density (55.22 μA cm^{-2}) compared with the control (9.94 μA cm^{-2}) over the 7-day operational period, representing a 5.6-fold increase (Figure 21). Immobilizing a redox mediator on the anode surface has proven to be an effective strategy for enhancing extracellular electron transfer efficiency and, consequently, increasing power output (Feng *et al.*, 2010b).

Besides enhancing overall system efficiency once *S. oneidensis* and *G. sulfurreducens* are both present, which employ distinct EET mechanisms, the characteristics of *c*-type cytochromes (*c*-Cyts) on the outer membrane complex are of central importance in electron transfer. In exoelectrogens, outer membrane cytochromes (OMCs) constitute the primary redox-active components mediating transmembrane electron transfer and are strongly affected by the physicochemical properties of the anode surface. Therefore, modification of the electrode surface with functional groups represents a key and effective approach to control the redox state of OMCs and thereby regulate EET activity (Li and Cheng, 2019). Riboflavin, which plays an important role in EET, can be bound to outer membrane *c*-Cyts (Zhao *et al.*, 2023). Further, it has been identified as a bound cofactor of the terminal reductases MtrC and OmcA, thereby promoting more efficient direct electron transfer (Erben *et al.*, 2021a; Klein *et al.*, 2025). Moreover, the binding of riboflavin to cytochromes, a newly-formed flavocytochrome exhibiting high electrochemical activity, significantly enhances electron exchange both among cytochromes and at the cytochrome–electrode interface (Huang *et al.*, 2018; Yi *et al.*, 2021). Flavins have been recognized as cofactors not only of the outer membrane cytochromes in *S. oneidensis* but also in those of *G. sulfurreducens* (Edel *et al.*, 2021). After riboflavin pre-treatment prior to inoculation, cells located closest to the residual flavins on the anode surface

may gain an advantage for attachment and initial biofilm formation, particularly if the flavins function as cofactors for outer-membrane cytochromes involved in electron transfer. According to Erben *et al.* (2021b), this role may explain the current enhancement observed at minimal flavin concentrations, which cannot be fully explained by diffusive MET.

The other possible effect of the specific surface functional groups introduced via surface pre-treatment may also improve surface properties and electron transfer, thereby reducing electron transfer resistance (ETR) (Li and Cheng, 2019; Vassilev *et al.*, 2022). Functional groups present on surfaces can establish bonds with the bacterial outer membrane or EPS, acting as intermediates that facilitate EET. Such bonding interactions may lead to a direct reduction in ETR on a molecular scale (Li and Cheng, 2019). Accordingly, riboflavin improves the electrical conductivity of *S. oneidensis* biofilms by reducing charge transfer resistance, thereby facilitating more efficient EET (Arinda *et al.*, 2019; Erben *et al.*, 2021a).

In addition to riboflavin, AQDS was used as a surface functionalization for the graphite anode. In the presence of AQDS, the biofilm volume reached 3.33 mm^3 cm^{-2} over the 7-day operational period, compared with only 0.78 mm^3 cm^{-2} on the non-functionalization surface. Correspondingly, the biofilm formed on the surface without AQDS generated a current density of 37.46 μA cm^{-2}, whereas surface functionalization with AQDS resulted in a current density of 121.01 μA cm^{-2}. A 4.3-fold increase in conductive biofilm volume, accompanied by a 3.2-fold increase in electricity generation, indicates that AQDS substantially contributes to enhancing system performance at the anode surface (Figure 20). Further, AQDS substantially improved the mean current density (47.13 μA cm^{-2}) compared to the control (9.94 μA cm^{-2}), resulting in a 4.7-fold increase (Figure 21).

Immobilizing an electron mediator such as AQDS that forms a conductive film on the anode surface enhances anode performance by increasing the effective surface area and improving the biocompatibility of the electrode material, thereby promoting bacterial adhesion and facilitating more efficient electron transfer, which collectively leads to higher bioelectroactivity of the anode system (Feng *et al.*, 2010a, 2010b; Mier *et al.*, 2021). Additionally, Li *et al.* (2024) demonstrated that the addition of AQDS stimulated EPS secretion within the biofilm, particularly protein fractions, thereby enhancing the activity and electrochemical performance of the electroactive biofilms.

Initial evidence implicating the Mtr pathway in the reduction of extracellular shuttles was provided by a study investigating the capacity of *S. oneidensis* to reduce AQDS, a structural analog of the redox-active components of humic acid (Brutinel and Gralnick, 2012). Further, according to Li *et al.* (2012), the anthraquinone ring appears to be the most effective structure for facilitating electron transfer with the OMCs of *G. sulfurreducens,* as well as AQDS facilitates long-range electron transfer from *G. sulfurreducens* to the electrode.

Most quinone derivatives readily adsorb on a variety of electrode materials, typically exhibiting well-defined, reversible redox behavior and highly stable electrochemical responses, thereby catalyzing EET to the anode (Heydorn *et al.*, 2020; Shi and Shiu, 2004). For instance, in the study by Feng *et al.* (2010b), an AQDS-modified graphite electrode produced a power density that was five times higher than that of the unmodified electrode. Furthermore, immersing a graphite anode to immobilize AQDS on its surface increased the power output of sediment-type MFCs by 1.5–1.7-fold (Li and Cheng, 2019). According to Ta *et al.* (1999), once adsorbed from micromolar concentrations onto highly oriented pyrolytic graphite (HOPG), 2,6-AQDS exhibits electrochemical behavior characteristic of an almost ideal, quasi-reversible, and surface-bond redox species.

The microfluidic BES enables the simultaneous measurement of biovolume and current density, and the results showed that anode surface pre-treatment with riboflavin and AQDS enhanced both biofilm formation and current generation. Further, this surface modification improved biofilm porosity, coverage, and roughness. The porosity of biofilms developing on non-functionalized anode surfaces remained at around 30% (Figure 23a), with variability in the measured values comparable to that reported by Klein *et al.* (2024). The non-functionalized anode had thinner and more compact biofilm with fewer voids. In contrast, surface functionalization led to an average biofilm porosity that was more than twice that of the non-functionalized surfaces. The increased porosity may have promoted the development of thicker and more structured biofilms. This likely enhanced the diffusional accessibility of substrates within the biofilm matrix and lower pH gradients (Klein *et al.*, 2024).

Moreover, surface functionalization with riboflavin and AQDS resulted in almost complete biofilm surface coverage, whereas the control reached only 61% coverage (Figure 23b). This higher surface coverage compared to the control occurred due to the improved electroactive biofilm attachment on the functionalized electrode surface by altering the physicochemical properties of the substratum. These alterations can enhance the initial attachment of cells by

reducing ETR, thereby enabling improved biofilm coverage over the electrode surface, which is essential for effective EET in BES. The extensive biofilm coverage is very likely a principal contributor to the pronounced increase in current provided by EAB (Champigneux *et al.*, 2019).

Additionally, the roughness of the biofilm on the non-functionalized surface remained essentially constant at around 0.39 over the course of the experiment (Figure 23c). Conversely, surfaces functionalized with riboflavin or AQDS exhibited a progressive increase in biofilm roughness. Functionalization of electrode surfaces creates micro- or nanoscale patterns that provide distinct microbial adhesion sites. Bacteria that attach directly to heterogeneous regions of the substratum exhibit localized, attachment-dependent responses that deviate from the behavior of the surrounding population. This, in turn, gives rise to the formation of a biofilm with pronounced microscale topographical variations (Ren *et al.*, 2018). Increased biofilm roughness promotes adhesion by enhancing the interception of flowing cells with the uneven biofilm surface. Moreover, rough biofilms may protect mixed-culture biofilms by generating extended low-shear regions that help reduce detachment (Shen *et al.*, 2015).

To sum up, functionalization of the anode surface with specific organic molecules is particularly attractive because it offers a low-cost, resource-efficient, and highly tunable strategy compared with external dosing or endogenous overproduction of soluble compounds. These redox-active molecules, which are feasible for modifying the electrode surface, possess the ability to act as electron acceptors or donors for microorganisms, effectively bridging the electron flow between microbial cells and the anode surface. The binding strength of such redox mediators to electrode materials is a key determinant for fully harnessing their advantages in BESs (Li and Cheng, 2019; Martinez and Alvarez, 2018).

Moreover, functional group modification of the anode surface alters its physicochemical properties, thereby affecting initial bacterial adhesion and metabolic activity, promoting subsequent biofilm colonization and development through an increased number of adsorption sites, and ultimately enhancing the overall BES performance in terms of start-up time, COD removal, and current density (Li and Cheng, 2019; Ratheesh *et al.*, 2024). Collectively, these insights support more sustainable and productive biofilm formation on functionalized electrodes and underscore their potential for future applications.

4.1.2. Effect of surface roughness on the efficiency of BES

A second approach to enhance electron transfer in BES is to improve electrode surface roughness. In this thesis, the influence of surface roughness on the current generation was evaluated by comparing electrodes with varying surface roughness with riboflavin pre-treatment. The medium-roughness electrode produced a current density of 32.13 µA cm^{-2} on day 7. Notably, the rough electrode, which was used for functionalization experiments discussed above, exhibited a substantial enhancement in performance, yielding a current density of 125.92 µA cm^{-2} (see section 3.1.2, Figure 24), approximately four times higher than that of the medium-roughness electrode. Further, using rough electrodes led to substantially higher mean current densities (55.22 µA cm^{-2}) than medium electrodes (10.56 µA cm^{-2}), with a 5.2-fold improvement in performance (Figure 25). These indicate that the rough electrode surface improved the generated current, and this enhancement in current was ascribed to the increased surface area available for biofilm formation.

The rough electrode surface corresponds to the accentuation of peaks and valleys on the electrode, resulting in the enhancement of accessible surface area and improving initial colonization of EAB (Erben *et al.*, 2021b; Heydorn *et al.*, 2020; Pons *et al.*, 2011). The presence of these surface cavities promotes biofilm development by generating low-shear microenvironments and reducing hydrodynamic forces (Champigneux *et al.*, 2019; Li and Cheng, 2019). According to Moß *et al.* (2019), the improvement in biofilm start-up is primarily attributed to the axial flow component generated by the electrode microstructures, which reduces shear stress on electrode surfaces and thereby enhances irreversible cell attachment and biofilm maturation. Further, increasing the microbe-electrode interaction also leads to enriched mass transfer (Kudier *et al.*, 2022). Optimal surface topographies are expected to be those that enhance mass transfer while simultaneously limiting local acidification within the micro-structured regions (Kulchartvijit *et al.*, 2022; Li and Cheng, 2019). For example, Pons *et al.* (2011) demonstrated that an increase in the surface roughness (Ra) from 2.0 µm to 4.0 µm led to a 1.6-fold enhancement in the measured current. Further, an average roughness of about 4.0 µm is preferable, because increasing Ra beyond this value does not significantly enhance performance. Even though surface roughness helps reduce the loss of biofilm from the surface, mass transfer limitations are taken into consideration in highly rough surfaces.

Conversely, the electrode with a smooth surface generated almost no measurable current in this study (Figure 24). Unlike a rough surface electrode, a smooth electrode surface is unfavorable for stable biofilm establishment because such surfaces hinder robust bacterial attachment and colonization, leading to weak and easily disrupted cell adhesion (Champigneux *et al.*, 2019; Moß *et al.*, 2019). Consequently, completely smooth electrodes ultimately suppresses biofilm development and thereby diminish overall electron transfer and BES performance (Martinez and Alvarez, 2018; Salim *et al.*, 2025).

As aforementioned, electrode surface modifications, including functional groups and micro-structures, promote robust microbial adhesion and biofilm development, significantly shortening start-up times in BES. These modifications are beneficial for long-start-up bacteria by accelerating initial attachment and biofilm establishment. Commercial deployment of bioelectrochemical technologies requires high current densities, making improved EET essential. Ultimately, these strategies minimize electron transfer distances for strains in early biofilm stages, fostering faster current output (Champigneux *et al.*, 2019; Zheng *et al.*, 2020). Although the strategies outlined above have been shown to enhance EET, substantial performance gains in BESs will require their combined implementation. Together, these strategies enhance system performance by enabling efficient carbon removal from wastewater.

Additionally, conventional wastewater treatment processes are limited by high energy use and poor recovery of wastewater's energy content, which together raise costs and environmental burdens. In this context, microliter-scale microfluidic systems provide powerful research tools for the detailed investigation and optimization of complex treatment processes, thereby supporting environmental protection and sustainable wastewater management in applications such as biological phosphate removal from wastewater.

4.2. Phosphate elimination and resource recovery with PAOs in MMBS

Microfluidic platforms enable precise control and systematic variation of operational parameters, thereby allowing detailed analysis of the complex interactions between process conditions and microorganisms. The objective of this study was to comprehensively summarize phosphorus removal efficiencies while elucidating the relationship between external operational conditions and PAO performance, and characterize PAO-GAO interactions under varied conditions. In this regard, key environmental factors, including carbon source, pH, COD:P ratio, and temperature, which govern PAO proliferation, PAO-GAO interactions and

the phosphorus-removal capacity (Haiming *et al.*, 2014), were evaluated using MMBS to identify optimal operating parameters for maximizing PAO activity. This facilitates their effective implementation in engineered wastewater treatment systems to enhance treatment outcomes.

4.2.1. Impact of carbon sources on the efficiency of MMBS

Among the various operational parameters, the type of carbon source is crucial in determining the efficiency and stability of EBPR performance (Xie *et al.*, 2017), as it influences PAO metabolism (Zhang *et al.*, 2025). Acetate and propionate are generally used as carbon and energy sources in biological nutrient removal systems. Despite the well-established suitability of VFAs for EBPR, fermentable substrates such as glycerol, ethanol, glucose and amino acids have been proposed as alternative carbon sources to support the EBPR process, thereby increasing the versatility of these systems (Zhang *et al.*, 2025). In this section, overall system performance and efficiency of PAOs were examined regarding various C-sources systematically.

The use of acetate and propionate, as VFA, led to higher P-release (1.89 µg PO_4-P), whereas glucose resulted in relatively lower P-release (1.24 µg PO_4-P), as reported in a previous study (Qiu *et al.*, 2019). Moreover, feeding with acetate/propionate and glucose exhibited the highest P-uptake rates (4.65 µg PO_4-P and 4.52 µg PO_4-P, respectively) among all tested carbon sources, while the maximal P-removal was achieved with glucose (3.27 µg PO_4-P), followed by acetate/propionate (2.76 µg PO_4-P) (see section 3.2.1, Figure 27a). In MMBS, the addition of acetate/propionate as well as glucose resulted in anoxic P-release by PAOs, accompanied by excess phosphorus uptake during the oxic stage, indicating that they can serve as effective carbon sources for enhancing phosphorus removal performance.

The use of acetate and propionate stimulated phosphate release to a greater extent than glucose. The uptake of substrates under anoxic conditions is an energy-intensive process, and not all organic compounds are suitable for assimilation in this environment. VFA uptake during the anoxic phase requires higher energy input and results in greater phosphorus release compared to glucose (Mulkerrins *et al.*, 2004; Xie *et al.*, 2017). Moreover, the use of acetate or propionate as the sole carbon source often leads to the enrichment of a particular microbial population

capable of anoxic substrate uptake and PHA synthesis (Elahinik *et al.*, 2023). Maintaining acetate and propionate within a moderate concentration range ensures achieving stable and effective system performance (Zhang *et al.*, 2025). However, using glucose was more efficient in terms of phosphate removal. The effectiveness of glucose lies in its rapid uptake and metabolism by the microbial consortium present in EBPR reactors (Jeon *et al.*, 2001). According to Xie *et al.* (2017), using glucose as the carbon source was found to enhance phosphorus removal despite reduced anoxic P-release. Glucose-dominated reactors can be linked with increased glycogen synthesis during the anoxic phase. Glycogen metabolism can lead to lower anoxic phosphorus release, as its degradation provides additional energy, thereby reducing the need for poly-P breakdown.

Among all tested carbon sources, NZ-Amine elicited the greatest P-release during the anoxic phase (2.45 µg PO_4-P). In contrast, the lowest P-removal with 1.44 µg PO_4-P in the effluent was observed due to high P-release and relatively low P-uptake with 3.89 µg PO_4-P, resulting in the least efficient substrate in terms of P-removal among the carbon sources studied (Figure 27a).

Casein hydrolysate promoted anoxic poly-P hydrolysis, leading to the release of ortho-phosphate (Petriglieri *et al.*, 2021). Qiu *et al.* (2019) reported that substantial P-release was observed with using amino acids. On the other hand, as Mulkerrins *et al.* (2004) mentioned, when NZ-Amine was used as a carbon source P-uptake amount was lower than with an acetate and propionate mixture, because these substrates often promote microbial communities that are less efficient in P-uptake compared to VFAs. It may even disrupt metabolic pathways or favor the growth of non-PAO bacteria, causing competition for substrates and reduced EBPR efficiency. Amino acid-rich synthetic wastewaters are generally considered highly detrimental to P-removal performance in EBPR systems. Therefore, the presence of amino acids in influent wastewater can impair EBPR system stability and performance (Mulkerrins *et al.*, 2004).

Besides, glycerol utilization in the system led to reduced P-release with 0.38 µg PO_4-P. In parallel, low P-uptake (2.63 µg PO_4-P) observed corresponds with the limited P-removal (2.25 µg PO_4-P) achieved in the glycerol-feed system. Furthermore, ethanol also insignificantly induced the anoxic P-release (0.97 µg PO_4-P), which is a key step in the EBPR process, adversely affected subsequent P-uptake (2.90 µg PO_4-P) and removal (1.93 µg PO_4-P) like glycerol (Figure 27a). The P-removal was found to be relatively low for both glycerol and ethanol, which are both classified as alcohols.

Qiu *et al.* (2019) and Hu *et al.* (2018) reported that low P-release from biomass was observed for alcohols. Fermenting glycerol, serves as a more energy-rich substrate, can lead to energy surpluses, which may reduce reliance on poly-P hydrolysis and thus potentially decrease phosphate release (Coats *et al.*, 2015; Zhang *et al.*, 2024). Moreover, surplus energy from energy-rich substrate fermentation can favor the growth of GAOs that compete with PAOs but do not contribute to phosphate removal. The use of glycerol led to reduced PHA synthesis, thereby limiting the energy available for subsequent phosphorus uptake and therefore reducing EBPR performance (Zhang *et al.*, 2025). The prevailing explanation for this issue is that there is often insufficient anoxic fermentation time, since two consecutive anoxic processes are necessary: first, the fermentation of glycerol to VFAs, and second, the assimilation of VFAs by PAOs. To mitigate EBPR deterioration caused by pure glycerol, increasing the anoxic HRT or integrating a side-stream reactor for fermenting glycerol to VFAs may be an effective approach to avoid deterioration. According to Zhang *et al.* (2025), in a single-sludge anoxic/oxic SBR, favorable EBPR performance was achieved when glycerol served as the sole carbon source under sufficient anoxic hydraulic retention time (4 hours), yielding a high phosphorus-to-carbon (P/C) molar ratio of 0.22.

Furthermore, ethanol is a relatively low-cost and readily available carbon source compared to acetate, propionate, or other conventional sources such as starch, and thus represents a feasible alternative when a supplementary carbon source is required in wastewater treatment processes (Wei *et al.*, 2014). However, ethanol has been demonstrated as an effective supplementary carbon source capable of sustaining EBPR performance during prolonged reactor operation (Zhang *et al.*, 2025).

Apart from the amounts of P-removal, biofilm volume can also be used as an indicator of overall system efficiency in MMBS. Among the carbon sources tested, glycerol promoted the greatest biofilm development, with an average biovolume of 5.18 $mm^3 cm^{-2}$, followed by ethanol with 3.42 $mm^3 cm^{-2}$. However, NZ-Amine yielded the lowest biovolume, measured at 1.01 $mm^3 cm^{-2}$. Besides, while mixture of acetate and propionate promoted robust PAO-dominated communities and biofilm structures (2.77 $mm^3 cm^{-2}$), glucose utilization showed poorer biofilm development, with volumes of 1.52 $mm^3 cm^{-2}$ (Figure 27b).

Using alcohols as carbon sources enhanced biofilm growth in the system, whereas amino acid utilization may hinder biofilm growth. For instance, Yadav *et al.* (2021) demonstrated that activated sludge fortified with crude glycerol led to enhanced EPS production. Additionally,

glycerol stimulates biofilm formation by enhancing surface attachment (Pan *et al.*, 2024). Ethanol is also considered a readily biodegradable carbon source (Hu *et al.*, 2018) and Zhang *et al.* (2025) reported that microorganisms directly assimilated ethanol. This availability and quick consumption by organisms could be the reason for enhanced biofilm growth. However, Su *et al.* (2022) demonstrated that using amino acids as a carbon source can inhibit both adhesion efficiency and biomass of mixed microorganisms by reducing EPS protein and carbohydrate content, which in turn decreases microbial adhesion and biofilm formation.

Besides, EBPR studies suggest that distinct PAO types or strains may develop, depending on whether acetate or propionate serves as the predominant carbon source, as PAOs metabolize these substrates at different uptake rates. Due to these metabolic differences, the use of a mixture of acetate and propionate led to highly enriched, PAO-dominated cultures compared with systems fed a single substrate, thereby promoting stable PAO dominance over GAOs and the development of a resilient biofilm structure (Gonzalez-Gil and Holliger, 2011; Shen and Zhou, 2016). However, according to Xie *et al.* (2017), glucose-fed systems demonstrated a decline in main microbial diversity, which may lead to poor biofilm formation; nevertheless, P-removal performance remained strong.

The choice of carbon source strongly affects the phosphate removal capacity of biofilm-based EBPR systems. Due to the observed negative correlation between biovolume and phosphate removal capacity in PCA (see section 3.2.4., Figure 33), which is likely attributable to restricted substrate diffusion, glycerol and ethanol demonstrated low biofilm-based P-removal capacities (0.14 µg PO_4-P mm^{-3} and 0.18 µg PO_4-P mm^{-3}, respectively) among the carbon sources tested (Figure 27c). In thick biofilms, the highest PAO activity was observed predominantly in the peripheral layers, where substrate and oxygen availability are greatest (Sandeep *et al.*, 2023). This zonation can also give a competitive advantage to non-PAO populations in deeper layers, further diminishing overall phosphorus removal efficiency within the system. Once glycerol and ethanol were employed as carbon sources, *Zoogloea* as GAO exhibited higher abundance relative to *Dechloromonas as PAO* in the MMBS. Controversy, thin biofilms cultivated with glucose and acetate/propionate exhibited superior P-removal capacity (0.75 µg PO_4-P mm^{-3} and 0.32 µg PO_4-P mm^{-3}, respectively) compared to thicker biofilms cultivated with glycerol and ethanol (Figure 27b). Consequently, thick biofilms have a lower P-removal capacity compared to well-managed, thinner biofilms, where substrate and oxygen penetration are more uniform, supporting higher PAO activity throughout the biofilm.

This suggests that reduced biofilm thickness ensures greater metabolic activity and a more uniform distribution of phosphorus content within the biomass. Maintaining a thinner biofilm minimizes diffusion limitations and restricts the proliferation of non-PAO populations, which in turn enhances the P-removal capacity of the biofilm. However, excessively thin biofilms may compromise PAO competitiveness, as faster-growing non-PAO organisms can dominate the microbial community under these conditions. In this thesis, the biofilm with the lowest thickness, cultivated with NZ-Amine, demonstrated a lower abundance of PAOs compared to biofilms cultivated with glucose and acetate/propionate (Figure 27b), highlighting the importance of optimizing biofilm thickness to balance PAO enrichment and biofilm functionality (Falkentoft, 2000; Sandeep *et al.*, 2023). Therefore, glucose and acetate/propionate provide the highest phosphate removal per unit biofilm volume, whereas glycerol and ethanol reduce this metric through both metabolic inefficiency and community shifts.

4.2.2. Impact of carbon sources on the PAO-GAO abundance

Optimal EBPR performance is associated with the dominance of PAOs in the microbial community and the efficient use of available carbon sources. The type of carbon source selectively enriches specific PAO populations among the various putative PAOs that have been identified (Zhang *et al.*, 2025). In this study, the relative abundances of potential PAOs and GAOs were evaluated across different carbon sources at the end of cultivation in the MMBS compared to the initial inoculum.

Accumulibacter is a key organism and the most common PAO in wastewater treatment systems. However, even though the relative abundance of *Accumulibacter* under the ethanol-feed reactor was only 1.10%, it remained scarcely enriched across the tested carbon sources (Figure 29). Alcohol dehydrogenase (ADH), which catalyzes the conversion of ethanol to acetaldehyde, is present in all *Accumulibacter* genomes (Skennerton *et al.*, 2015). Besides, *Accumulibacter* taxa belonging to clade IIF are proposed to further oxidize ethanol to acetate to support EBPR, as this clade possesses acetaldehyde dehydrogenase (ALDH), an enzyme that likely catalyzes the final step of ethanol degradation from acetaldehyde to acetate (Skennerton *et al.*, 2015; Zhang *et al.*, 2025). Ethanol to acetate degradation via enzymes can be the reason for a slight preference for ethanol in *Accumulibacter* in MMBS.

The low abundance of *Accumulibacter* may be attributed to its limited metabolic capacity. In full-scale, often biofilm-dominated EBPR systems, PAOs such as *Tetrasphaera* and *Dechloromonas* typically have higher abundance than *Accumulibacter*. These organisms exhibit broader metabolic capabilities, including the utilization of sugars, amino acids, and fermentation products, enabling them to outcompete *Accumulibacter* in biofilm environments with diverse and variable substrates (Stokholm-Bjerregaard *et al.*, 2017). Further, unlike *Accumulibacter*, *Dechloromonas* use nitrate (NO_3^-) rather than O_2 as an electron acceptor for P-uptake following P-release and PHAs storage, and NO_3^- finally reduced to N_2 (W. Zhao *et al.*, 2022). *Dechloromonas* has the ability to respire with NO_3^- and/or nitrite (NO_2^-), whereas *Accumulibacter* uses O_2 and/or NO_2^- (Petriglieri *et al.*, 2021). Therefore, *Accumulibacter* lacks the capacity to reduce NO_3^-, and its P-uptake relies on NO_2^- produced by *Dechloromonas* (W. Zhao *et al.*, 2022). Thus, *Accumulibacter* is poorly adapted to denitrifying phosphorus removal systems, leading to its progressive decline or eventual elimination. In contrast, *Dechloromonas,* as a DPAO, has emerged as the predominant PAO in such systems (Zhang *et al.*, 2025; W. Zhao *et al.*, 2022).

In contrast to *Accumulibacter*, *Dechloromonas* dominated the MMBS under varying operational conditions and was a key player in P-removal regardless of the carbon source, as also reported by Sandeep *et al.* (2025). *Dechloromonas* (currently designated as *Azonexus*; however, this study adopts the commonly used former designation *Dechloromonas*) from the family *Rhodocyclaceae* attained the highest relative abundance when acetate/propionate was supplied (25.24%), with a marginally lower abundance observed under ethanol treatment (24.09%). However, the abundance of *Dechloromonas* showed the lowest ratio of 1.05% when NZ-Amine was used (Figure 29). This indicates that *Dechloromonas* became more abundant in the system when acetate/propionate and ethanol were supplied, whereas the enrichment of *Dechloromonas* was not significantly affected by the presence of amino acids.

Even though acetate is widely recognized as an effective external carbon source in EBPR systems (Hu *et al.*, 2018), a mixture of acetate and propionate (3:1) with a pH of 7.5 was found to support the metabolism of PAO over GAO (W. Zhao *et al.*, 2022). Izadi *et al.* (2020) also supported these conditions that a carbon source ratio of 75% acetate to 25% propionate, when maintained at optimal temperature and pH conditions, inhibits the growth of GAOs and promotes the proliferation of PAOs. Additionally, Zhang *et al.* (2025) reported that *Dechloromonas* was detected in the acetate and propionate system. Further, ethanol serves as

a preferred organic substrate for heterotrophic microorganisms and effectively promotes their growth (Iannacone *et al.*, 2021). According to Zhang *et al.* (2025), the inclusion of ethanol as an external carbon source promoted the enrichment and metabolic functionality of active PAO populations, contributing to improved phosphorus removal efficiency in EBPR systems. Unlike VFAs and ethanol, it is clear that amino acids do not play a significant role in the enrichment of *Dechloromonas*. For example, according to Rey Martínez (2019), *Dechloromonas* accounted for 1.7% of the total bacteria when glutamate was used as the amino acid, which supports the findings.

In addition to *Dechloromonas*, *Zoogloea*, a putative GAO, was also highly abundant in the MMBS. In both substrate conditions (i.e., ethanol and acetate/propionate), a co-enrichment of *Dechloromonas and Zoogloea* was detected, and Spearman-based co-occurrence networks revealed a positive association between them (see section 3.2.4., Figure 34). Ethanol utilization notably favored the proliferation of *Zoogloea*, leading to a relative abundance of 30.19%, compared to 22.82% in the acetate/propionate condition. *Zoogloea* also increased with amino acid feeding, but stayed at a moderate level with 11.37% (Figure 29). These findings implied that the presence of ethanol, acetate/propionate and amino acids promoted the growth and enrichment of *Zoogloea* within the system.

According to Eghombi *et al.* (2022), ethanol supplementation to the anoxic zone stimulated biomass growth and led to high levels of protein- and carbohydrate-rich EPS secretion. EPS production resulting from the enhanced biovolume upon ethanol addition can strengthen the structural integrity of the biofilms, which is a hallmark of *Zoogloea*-dominated biofilms. Further, the presence of *Zoogloea* increased in environments rich in VFAs, particularly when propionate is available, due to its ability to rapidly utilize these substrates and produce EPS, promoting denser and more robust formation (Gonzalez-Gil and Holliger, 2011). Although the use of amino acids promoted the abundance of *Zoogloea*, the effect is less pronounced than that of ethanol or VFAs. Similarly, in the study of Rey Martínez (2019), glutamate, an amino acid, was used as a carbon source in an EBPR reactor. In that system, *Zoogloea* reached a relative abundance of 8.58%, which was notable but not dominant within the microbial community, aligning with the findings.

While *Zoogloea* has been reported to store PHAs under oxic conditions and to accumulate P in volutin granules, there is currently no conclusive evidence that it exhibits classical PAO metabolism and is instead often described as a competitor for VFAs (Sandeep *et al.*, 2025). In

line with this, *Zoogloea* abundance may be attributed to the specific reactor cultivation conditions and design that favor its enrichment among GAOs. In this thesis, a PDMS-based microfluidic meandering cultivation reactor with a working volume of 159.17 µL was used, thereby increasing the available surface area for biomass growth. The meandering microchannels enhance the surface area-to-volume (SA:V) ratio, achieving ~5,900 m^{-1} (area in m^2 per volume in m^3) in the reactor. This high ratio facilitates efficient attachment, substrate uptake, microbial interactions, and treatment (Waqas *et al.*, 2023). Further, the use of biocompatible, oxygen-permeable PDMS-based microfluidic reactors establishes a controlled microscale environment that is favorable for biofilm development.

Moreover, microorganisms secrete substantial quantities of proteins and polysaccharides (F. Wang *et al.*, 2024). The attached microorganisms on the surface become embedded in EPS, which constitute the structure of the biofilm (Blanco-Cabra *et al.*, 2021). Besides, fluid shear forces present in flow-through systems contribute to the stimulation of biofilm development by improving the synthesis of EPS and enhancing the availability of nutrients required for microbial proliferation (Zheng *et al.*, 2021). The increase of these extracellular polymers and nutrient-rich environment establishes favorable conditions for the development of *Zoogloea* (Wang *et al.*, 2024), resulting in selective growth on carrier material. *Zoogloea* is also recognized for its ability to involve the production of EPS, which plays a critical role in biofilm development and formation (Seguel Suazo *et al.*, 2024; Yuan *et al.*, 2025), leading to denser and more resilient biofilms due to its pronounced EPS production capabilities.

With regard to a co-enrichment of *Dechloromonas and Zoogloea*, PCA supported a positive correlation between them in the dataset (Figure 33), which may indicate a potential association within the microbial community. However, these statistical associations do not demonstrate direct interactions or mutualism but instead suggest that their occurrences or functional roles may overlap under certain operational conditions. First of all, the co-occurrence of *Zoogloea* and *Dechloromonas* may be supported by their shared capacity for EPS production. An *et al.* (2016) demonstrated that both genera possess gene clusters involved in EPS biosynthesis, which underpins their selective enrichment and promotes biofilm development as well as structural resilience within wastewater treatment systems. Fujii *et al.* (2024) likewise reported the identification of homologous gene clusters in *Zoogloea* MAGs associated with EPS biosynthesis, export and floc formation. Further, *Zoogloea* forms homogeneous biofilms that provide a structural matrix supporting the development and spatial organization of other

microorganisms, including nitrifiers, PAOs, and GAOs. This biofilm architecture facilitates the co-existence and integration of these functional microbial groups by forming microcolonies within engineered wastewater treatment systems (Blanco-Cabra *et al.*, 2021; Montoya *et al.*, 2008; Weissbrodt *et al.*, 2013). Consequently, the co-occurrence of these taxa not only enhances biofilm structural integrity but also improves functional performance in advanced biological treatment systems.

The second explanation for *Zoogloea* and *Dechloromonas* co-occurrence can also rely on oxic denitrification. In the MMBS, the ammonium (form of NH_4Cl) was supplied via the nutrient medium. Nitrifiers can oxidize ammonium to nitrate during the oxic phase, as it is a suitable environment for them because there is no organic carbon. *Nitrosomonas* (ammonia-oxidizing bacteria) and *Nitrospira* (nitrite-oxidizing bacteria) were detected as nitrifiers in the system. In MMBS, ammonia oxidation ($NH_4^+ \rightarrow NO_2^-$) by *Nitrosomonas* followed by nitrite oxidation ($NO_2^- \rightarrow NO_3^-$) by *Nitrospira* showed a complete nitrification (Mehrani *et al.*, 2020). *Zoogloea* and *Dechloromonas* can facilitate heterotrophic nitrification and oxic denitrification (HNAD) (Deng *et al.*, 2020). Oxic denitrifiers perform co-respiration of oxygen and nitrate (Huang *et al.*, 2015), thereby enabling denitrification to proceed in the presence of oxygen. Moreover, PHA was converted from organic matter, and it could be used as a carbon and energy source in the oxic phase for denitrification (Gnida *et al.*, 2020; Kapagiannidis *et al.*, 2013; Yin *et al.*, 2018). The ability of *Dechloromonas* and *Zoogloea* to facilitate HNAD suggests their potential coexistence in MMBS, thereby promoting the integration of phosphate uptake and nitrate reduction processes in the oxic phase through simultaneous denitrification and dephosphatation processes. This synergy can ultimately result in the absence of detectable N-fractions in the treated effluent.

Phosphorus removal performance can be unstable due to insufficient influent VFAs, competition between nitrogen and phosphorus removal processes for available carbon sources, and the complex nature of wastewater characteristics in WWTPs. Furthermore, conventional biological phosphorus removal necessitates substantial aeration energy input, as oxygen functions as an electron acceptor (W. Zhao *et al.*, 2022). As stated above, the HNAD mechanism has the potential to reduce the requirement for carbon source and aeration energy consumption during the oxic phosphorus uptake phase. The improved removal of N and P suggests a substantial potential for implementation in full-scale WWTPs (Zhang et al., 2025, 2024). DPAOs are capable of reducing the required carbon source by 50%, lowering oxygen

consumption by 30% during the P- and N-removal process, and decreasing sludge production compared to conventional processes (Tian *et al.*, 2013; W. Zhao *et al.*, 2022).

In addition to PAOs that enhance system performance, GAOs also emerge and adapt in response to prevailing environmental conditions. In this study, the use of acetate and propionate as carbon sources resulted in *Propionivibrio* reaching a relative abundance of 0.66% in the community. In contrast, *Micropruina* decreased to its lowest level, with a relative abundance of 0.07% under acetate- and propionate-fed conditions (Figure 29). While the supplementation of acetate and propionate promotes the enrichment of certain GAO species, it may simultaneously cause a decline in others. The observed abundance of these species in the system can be linked to their distinct metabolic capabilities.

For instance, the majority of *Propionivibrio* isolates are characterized as anoxic to aero-tolerant and predominantly exhibit a fermentative metabolic pathway, generating propionate and acetate as characteristic metabolic end products. Conversely, *Propionivibrio militaris* displays a strictly respiratory metabolism, capable of utilizing different substrates such as acetate and propionate (Albertsen *et al.*, 2016). Moreover, according to McIlroy *et al.* (2018), microautoradiography–fluorescence in situ hybridization (MAR-FISH) analyses conducted on activated sludge from two wastewater treatment plants revealed that *Micropruina* assimilated a wide spectrum of tested substrates, such as glucose, fructose, galactose, amino acids, pyruvate, glycerol, and butyrate, under both oxic and anoxic conditions. In contrast, N-acetylglucosamine (NAG), ethanol, acetate, propionate, and oleate were not assimilated as substrates.

Further, under glucose supplementation, *Micropruina* and *Tessaracoccus* as GAOs exhibited relative abundances of 2.14% and 2.21%, respectively. Additionally, *Competibacter* (0.47%) and *Contendobacter* (0.30%) were detected, with members of the *Competibacteraceae* family shown to assimilate glucose under both oxic and anoxic conditions according to McIlroy *et al.*(2014). However, the relative abundance of *Zoogloea* was the lowest (2.46%) when using glucose compared to other carbon sources. Despite the low abundances of *Dechloromonas* (3.52%) and *Accumulibacter* (0.46%) as PAOs, glucose supplementation led to the highest P-removal.

Moreover, the dominance of glycerol-fermenting genera, such as *Tessaracoccus* and *Micropruina*, along with *Accumulibacter* was observed, with their relative abundances of

0.29%, 0.35%, and 0.62% (Figure 29), respectively. The interaction between glucose-fermenting organisms and *Dechloromonas,* as well as glycerol-fermenting organisms and *Accumulibacter* highlights the significance of substrate cascades and microbial syntropy in enhancing phosphorus removal performance. In addition to glucose, glycerol use in EBPR may enhance the metabolic interactions between fermentative bacteria and PAOs, suggesting that EBPR`s suitability for treating high-sugar wastewaters containing glucose or glycerol.

When substrates such as acetate or propionate serve as carbon sources, enrichment typically results in a highly specialized monoculture capable of anoxic substrate uptake and PHA synthesis. In contrast, the use of non-VFA substrates like glucose or glycerol promotes the development of a microbial consortium engaging in a sequential biotransformation cascade. In this cascade, fermentative organisms convert the original substrates into intermediate fermentation products, which are subsequently utilized and stored by PAO or GAO-like organisms for energy and growth. This metabolic cooperation underscores the complexity of substrate utilization pathways in EBPR systems (Elahinik *et al.*, 2023; Izadi *et al.*, 2020; Mulkerrins *et al.*, 2004).

Additionally, lower diversity doesn't necessarily mean poor performance; some glucose-fed systems achieve effective P-removal despite reduced diversity, though they may be less resilient to environmental fluctuations (Xie *et al.*, 2017). Elahinik *et al.* (2023) reported that when glucose was used as a sole carbon source, the long-term stable performance of the reactor and P-removal was achieved by cooperation among lactic acid producers (*Micropruina*) and PAOs. Further, according to Zhang *et al.* (2025), an increase in the relative abundances of both PAOs and fermentative bacteria was observed with higher glycerol dosages.

Unlike GAOs, the prevailing consensus has been that PAOs are unable to anoxically consume fermentable substrates such as glucose directly. Instead, glucose first undergoes fermentation to form VFAs, which are then used by PAOs to facilitate subsequent phosphate uptake (W. Zhao *et al.*, 2022; Ziliani *et al.*, 2023). For example, Zengin *et al.* (2010) suggested that glucose can indirectly serve as a carbon source for EBPR via its fermentation to lactate, which is subsequently utilized by PAOs for PHA synthesis under anoxic conditions, thereby requiring the coexistence of fermentative bacteria capable of converting glucose into lactate. However, some studies have shown that under specific conditions, glucose can serve directly as a carbon and energy source for EBPR (Chuang *et al.*, 2011; Zhang *et al.*, 2025). For instance, Zhang (2025) and Ziliani (2023) proposed that *Accumulibacter*, a key PAO in wastewater treatment,

can anoxically assimilate glucose, primarily converting it into glycogen using energy (ATP) generated by the hydrolysis of stored poly-P. Additionally, a portion of the glucose can be stored as PHA. Thus, the decision between storing glucose as glycogen or as PHA depends on the balance between ATP consumption for making glycogen and ATP production from storing PHA under anoxic glucose-fed conditions.

In a nutshell, the availability of readily biodegradable organic carbon is crucial for supplying the energy required to sustain EBPR (Hu *et al.*, 2018). Although external carbon addition is commonly recommended to enhance EBPR stability under VFA-limited conditions, this approach is economically and environmentally unsustainable, and the high cost of industrial VFAs underscores the need for exploring more cost-effective alternative carbon sources (Xie *et al.*, 2017; Zhang *et al.*, 2025). Identifying the carbon source that most strongly promotes phosphorus removal and PAO enrichment is therefore of critical importance.

VFAs, particularly acetate and propionate, generally lead to more stable and effective EBPR performance compared to other organic substrates (Wei *et al.*, 2014). Maintaining a moderate concentration of VFAs is important to favor PAO activity. In contrast, more complex organic compounds, which cannot be directly metabolized by PAOs as sole carbon sources, may result in unstable phosphorus removal performance or even system deterioration. For successful EBPR operation, using these complex substrates (e.g. glucose or glycerol) generally requires extended anoxic fermentation time for their conversion into VFAs or their co-utilization with VFAs (e.g. glucose and acetate) (Zhang *et al.*, 2025). Xie *et al.* (2017) observed that a glucose and acetate mixture (50:50) showed better P-removal performance than acetate alone to a certain degree. According to Zhang *et al.* (2025), the latest study demonstrated that an EBPR system supplied with an acetate/glucose (1:1) mixture and dominated by approximately 65% *Accumulibacter* is capable of efficiently utilizing glucose as the sole carbon source. These indicate that glucose may serve as a potential temporary supplementary carbon source to enhance EBPR performance with additional VFAs.

Last but not least, the microbial community structure of the seed sludge was highly complex, although most microbes were present in low abundance (Xie *et al.*, 2017). After the enrichment period, *Dechloromonas* and *Zoogloea* are abundant in the system. Notably, *Dechloromonas* is capable of metabolizing all substrates used in this study, despite differences in composition, with *Zoogloea* and other GAOs, thereby facilitating synergistic phosphorus removal. Furthermore, the hydrolysis and fermentation of complex substrates into VFAs has been

proposed as an alternative strategy to maximize the utilization of these compounds present in real wastewater (Zhang *et al.*, 2025). This flexibility is important in dynamic environments and with complex organic-carbon mixtures, as found in full-scale WWTPs.

4.2.3. Impact of pH, COD:P ratio and temperature on the efficiency of MMBS and PAO-GAO abundance

In recent years, studies on EBPR have been conducted in both lab-scale and full-scale settings, primarily examining the effects of operational factors. These parameters, such as pH, COD-to-P ratio, and temperature, strongly influence microorganism enrichment in the EBPR system and, consequently, phosphorus removal. Selecting external conditions for stable EBPR requires consideration of microbial community metabolism, system performance, as well as the economic and practical feasibility of operation (Izadi *et al.*, 2020; Shen and Zhou, 2016). In particular, a holistic evaluation of these factors is necessary to ensure robust and sustainable wastewater treatment.

4.2.3.1. Impact of pH on the efficiency of MMBS and PAO-GAO abundance

In EBPR systems, pH is a key factor influencing the proliferation of PAOs and the efficiency of phosphorus removal. The rates of phosphorus release and uptake were affected by pH values within the range of 6.5 to 8.0. In this thesis, an increased pH from 6.5 to 7.5 promoted P-release by PAOs from 1.80 µg PO_4-P to 1.89 µg PO_4-P. However, at pH 8.0, P-release decreased to 1.13 µg PO_4-P. This aligns with findings by Zhang *et al.* (2007). Moreover, the results showed that the P-uptake was lower at pH 7.5 with 4.65 µg PO_4-P. The limited biofilm growth observed at pH 7.5 may be a contributing factor for this outcome. Further, the amounts of P-uptake at pH 6.5 and 8.0 were comparable (6.53 µg PO_4-P and 6.00 µg PO_4-P, respectively) (see section 3.2.2, Figure 30a).

In this study, the behavior of P-release during the anoxic phase remained relatively consistent. The substrate uptake, PHA production, and glycogen consumption were independent of the external pH changes between 6.0 and 8.0 under anoxic conditions (Nguyen et al., 2023; Wang et al., 2013), which may account for the consistency of P-release across the different pH

conditions. The minor changes observed in P-release can be ascribed to the energy required for substrate uptake. For instance, according to Chen and Gu (2006), an increase in pH from 6.5 to 7.5 was attributed to the increased energy requirement for VFA uptake, which causes more poly-P degradation (to generate more ATP) and results in more phosphorus release by PAOs in the anoxic phase (Zhang *et al.*, 2007). However, at pH 8.0, phosphorus release decreased, likely because VFA uptake under anoxic conditions becomes less energetically favorable at elevated pH levels, as higher pH increases ATP requirements (Randall, 2012). In contrast to P-release in the anoxic phase, P-uptake during the subsequent phase exhibited variability in pH, as PHA degradation, phosphate uptake rates and biomass growth by PAOs were sensitive to changes in pH levels at the oxic stage (Filipe *et al.*, 2001; Liu *et al.*, 2007).

Previous studies have shown that the phosphorus removal, calculated as the difference between P-uptake and P-release, increases as the pH rises from 6.0 to 8.0 (Liu *et al.*, 2007; Nguyen *et al.*, 2023). However, the pH experiments conducted in the MMBS revealed that changes in P-removal appear to be related to biofilm thickness. In MMBS, thicker biofilms (75.5 µm and 65.8 µm) enhanced the P-removal amount (4.87 µg PO_4-P and 4.73 µg PO_4-P), particularly at pH 8.0 and 6.5, respectively. In contrast, thinner biofilms (27.7 µm) limited the P-removal (2.76 µg PO_4-P) at pH 7.5 (Figure 30), where *Zoogloea* reached its maximum abundance (Figure 31). Although metabolically active EBPR biofilms typically support higher P-removal due to increased PAO biomass and activity, a thickness of below 400 µm is generally recommended to prevent mass transfer limitations (Sandeep *et al.*, 2025). Further, according to Sandeep *et al.* (2023), a thickness below 30 µm indicates that the biofilm is dominated by non-PAO, which can be the reason for the enrichment of *Zoogloea* in the system at pH 7.5.

However, when the biofilm becomes thinner, an apparent optimum in P-release and uptake capacity was observed at 7.5. Additionally, pH 7.5 exhibited the highest P-removal capacity of 0.32 µg PO_4-P mm^{-3}, an observation aligned with the finding of Zhang *et al.* (2007), likely attributable to its comparatively reduced biovolume. In contrast, at pH 8.0, the P-removal capacity declined to 0.21 µg PO_4-P mm^{-3} (Figure 30c). This trend is consistent with reports that phosphorus removal generally increases with pH up to a certain point, beyond which further increases in pH can lead to a decline in removal efficiency (Liu *et al.*, 2007). Li *et al.* (2018) suggested that elevated pH levels may trigger non-productive P-release that does not contribute to organic substrate assimilation, thereby impairing PHB synthesis. This chain of effects ultimately exerts a detrimental influence on the overall removal process in EBPR

systems. The other reason for the lowest P-removal capacity observed at pH 8.0 may be that it reflected the negative correlation between biofilm volume and P-removal capacity.

Further, biofilm volume observed at pH 6.5 (6.58 $mm^3\ cm^{-2}$) was lower compared to that at pH 8.0 (7.57 $mm^3\ cm^{-2}$) (Figure 30b), indicating that alkaline conditions are more favorable for cellular growth relative to acidic conditions (Chen and Gu, 2006). Even at pH levels of 6.5 and 8.0, biofilm growth was promoted; at pH 7.5, the lowest biovolume of 2.77 $mm^3\ cm^{-2}$ was observed. The limited biofilm growth at pH 7.5 may be due to the inherent washout effect of the flow-through system. This effect can cause biomass to detach and be removed, despite the pH conditions being otherwise favorable.

When considering the abundance of PAOs in the MMBS, the relative abundance of *Dechloromonas* in the total community increased markedly, reaching 27.28% and 25.24% at pH 6.5 and 7.5, respectively (Figure 31). These results confirm an increase in the abundance of *Dechloromonas*, which was the main polyphosphate-accumulating organism at pH ≤ 7.5, as reported previously (Horn *et al.*, 2005; Kang *et al.*, 2019). Further, the similarity in the abundance could be attributed to intracellular pH regulation in the steady state. According to Liu *et al.* (2007), in weak acidic or alkaline conditions, the EBPR system's pH tended to approach neutrality by the end of the anoxic phase, indicating an ability to self-regulate around pH 7.0. This pH adjustment appears linked to microbial intracellular buffering, as intracellular pH in most bacteria is maintained within a narrow neutral range and only shifts when extracellular pH deviates beyond this range.

The other PAO*, Accumulibacter,* was slightly enriched at pH 6.5 and 8.0, with relative abundances of 1.13% and 1.03%, respectively (Figure 31). Compared with suspended activated sludge systems, the relatively low abundance of *Accumulibacter* observed in some biofilm-based EBPR systems may be linked to differences in EPS production strategies and substrate availability. Recent work indicates that *Accumulibacter* exhibits a limited capacity for synthesizing extracellular enzymes, suggesting that its ecological strategy relies primarily on the utilization of soluble and readily biodegradable compounds (Kondrotaite *et al.*, 2025). *Accumulibacter* may therefore be less competitive within biofilms than populations that more efficiently produce EPS and extracellular enzymes supporting biofilm formation and stability, such as *Dechloromonas* and *Zoogloea* in MMBS.

Unlike *Accumulibacter*, at pH 7.5, *Zoogloea* exhibited greater dominance, with its relative abundance increasing to 22.82% (Figure 31). According to Unz (2015), the optimal pH for *Zoogloea* is between 7.0 and 7.5, which proves that neutral pH conditions favor its proliferation. Lastly, according to Zhang *et al.* (2024), PAO abundance and activity decrease markedly at pH values below 6.0 and above 8.0. Besides, the results of this study indicate that pH≤7.5 enhanced system performance, although the examined pH range did not exert a pronounced effect overall.

4.2.3.2. Impact of COD:P ratio on the efficiency of MMBS and PAO-GAO abundance

Influent COD:P loading variations are important because they have been associated with EBPR performance, process stability, and the relative abundances of PAOs and GAOs within the system (Majed and Gu, 2020). The competition between PAOs and the other bacteria is also affected by the ratio of COD to P (Chuang *et al.*, 2011). In the COD:P experiments, the influent COD:P ratios (10, 40 and 80) were varied by keeping the influent COD concentration constant (100 mg L^{-1}) and changing the influent P concentration (10, 2.5, and 1.25 mg L^{-1}).

Increased influent phosphate concentration (10 mg PO_4-P L^{-1}) and low COD:P ratio (10) enhanced phosphate release (5.23 µg PO_4-P) of the active biomass, which corresponded to an improved phosphate removal of 5.67 µg PO_4-P by promoting the activity and metabolism of PAOs by enhancing poly-P cycling. This selective advantage supports the development of biofilms, resulting in an enriched biomass of 8.99 mm^3 cm^{-2}; however, due to the high biofilm volume, P-removal capacity decreased (0.22 µg PO_4-P mm^{-3}) (Figure 30). Further, using a COD to P ratio of 10 indicated support for the abundance of *Dechloromonas* (22.48%) over *Zoogloea* (13.26%) in the community (Figure 31), which aligns with the expectation for phosphate-accumulating organisms due to the improved P-content in the active biomass.

An increase in influent phosphate concentration resulted in an enrichment of poly-P within the biomass. As the intracellular phosphorus content increased, the conversion of poly-P enhanced both phosphate release and the associated energy generation, consequently stimulating a higher substrate uptake rate. The accumulation of poly-P in biomass was also accompanied by a reduction in glycogen content, indicating a metabolic shift from glycogen-dominated to poly-P-dominated metabolism. Accordingly, a gradual shift from a GAO metabolism to a PAO metabolism occurred with increasing influent phosphate concentration and elevated

intracellular poly-P content (Welles, 2015). This metabolic shift from glycogen- to poly-P-dependent energy generation underlines how PAOs optimize phosphorus cycling under high P load with low COD:P conditions. This threshold, in the range of 8 to 10, ensures that PAOs are not carbon-limited during the anoxic phase, facilitating their accumulation of storage polymers for subsequent phosphate uptake (Gu *et al.*, 2008). Furthermore, lower COD:P ratios between 10 and 20 mg COD per mg P correspond to cultures in which PAOs predominate (Majed and Gu, 2019; Oehmen *et al.*, 2007), as evidenced by the high abundance of *Dechloromonas* in the system. However, the efficiency of EBPR processes is not necessarily directly proportional to the relative abundance of PAOs alone (Majed and Gu, 2020).

Further, using a COD:P ratio of 40 (2.5 mg PO_4-P L^{-1}) resulted in a higher phosphate storage, with a P-uptake capacity of 0.54 µg PO_4-P per volume of biomass in the oxic phase, compared to ratios of 10 (0.42 µg PO_4-P mm^{-3}) and 80 (0.03 µg PO_4-P mm^3). In parallel, among the tested COD:P ratios, a ratio of 40 achieved an improved phosphate removal capacity of 0.32 µg PO_4- P mm^{-3}, associated with a lower biovolume (2.77 mm^3 cm^{-2}) compared to other COD:P conditions (Figure 30). Once the influent contains an adequate concentration of VFAs, lower COD:P ratios, ranging from 10 to 20 mg COD to mg P, are more favorable for the proliferation of PAOs (Izadi *et al.*, 2020; Oehmen *et al.*, 2007). However, an influent COD to P ratio above 15–20 is recommended to achieve effluent phosphorus concentrations <1 mg L^{-1} and ensure more stable performance (Gu *et al.*, 2008).

Moreover, phosphate concentrations of 2.5 mg L^{-1} (COD:P ratio of 40) and 10 mg L^{-1} (COD:P ratio of 10) promoted the growth of *Dechloromonas,* with relative abundances of 25.24% and 22.48%, respectively. This suggests that *Dechloromonas* could benefit from an optimal COD:P ratio range between 10 and 40 for improved system performance. Besides, once the influent COD:P ratio increased from 10 to 40, an enrichment of *Zoogloea* was observed from 13.26% to 22.82% (Figure 31), which was expected, as elevated COD:P ratios are typically associated with GAOs proliferation (Majed and Gu, 2019; Oehmen *et al.*, 2007). Despite the increasing abundance of GAOs, Gu *et al.* (2008) hypothesized that an EBPR system with coexisting PAOs and GAOs can maintain stable performance if conditions favor PAOs to preferentially uptake sufficient carbon for complete phosphorus removal, leaving excess carbon for GAOs.

It is generally agreed that efficient EBPR, achieving effluent P concentrations below 1.0 mg L^{-1}, necessitates an influent COD:P ratio greater than 20:1 entering the anoxic zone of

the system. Conversely, elevated influent COD:P ratios over 50 mg COD per mg P are typically associated with communities dominated by GAOs (Majed and Gu, 2019; Oehmen *et al.*, 2007) due to the limited P availability (Chuang *et al.*, 2011; Erdal *et al.*, 2008), and EBPR alone is insufficient to meet the targeted effluent P levels (Mulkerrins *et al.*, 2004). Low phosphate concentrations may diminish the metabolic activity of PAOs as well as that of other microbial populations. However, Nurmiyanto *et al.* (2017) showed that PAOs enrichment was achieved even at an extremely low phosphate concentration (0.05 mg L^{-1}). The explanation of this phenomenon may be due to a metabolic shift. A decline in the poly-P content within the biomass limits the energy generation derived from poly-P consumption. This necessitates compensation through energy production via glycogen conversion, leading to a metabolic shift from polyphosphate metabolism to glycogen metabolism within the system (Majed and Gu, 2020; Welles, 2015). This indicated that PAOs can adopt GAO-like metabolic pathways (i.e. using the glycolysis pathway to produce required energy for substrate uptake) under conditions lacking poly-P and are capable of proliferating even in phosphate-limited systems (Majed and Gu, 2020).

In this thesis, lower phosphate loading at 1.25 mg PO_4-P L^{-1} (COD:P ratio of 80) caused negligible P-removal (0.04 µg PO_4-P). Although P-removal was markedly low, biovolume (6.84 mm^3 cm^{-2}) remained comparatively high, suggesting that the COD:P ratio does not exert a direct influence on biofilm growth in the absence of nutrient limitation (Figure 30b). Moreover, the relative abundances of *Dechloromonas* and *Zoogloea* decreased to 14.13% and 12.01%, respectively, compared to their abundances under other COD:P conditions (10 and 40 mg COD per mg P, in Figure 31). Although PAO enrichment was achieved even at lower P-loading, consistent with the findings of Nurmiyanto *et al.* (2017), the decrease in their abundance indicates that facilities with higher influent COD:P ratios may be more susceptible to process upsets due to the relatively increased abundance of GAOs in the microbial community.

Poly-P degradation enables cells to yield 1 mol of ATP per P-mol of poly-P, whereas glycogen metabolism provides 0.5 mol of ATP per C-mol of glycogen (Welles, 2015). Due to the lowered ATP amount, a metabolic shift toward glycogen utilization may suppress the development of PAO, resulting in reduced carbon use efficiency and poor P-removal by PAOs, as well as increased GAO activities (Gu *et al.*, 2008; Majed and Gu, 2020; Mulkerrins *et al.*, 2004). These findings suggest that a high COD:P ratio provides excess carbon, which promotes

the proliferation of GAO and other non-PAO heterotrophic bacteria. This, in turn, increases overall biomass but reduces EBPR efficiency because of the competition with PAOs (Majed and Gu, 2019). Even though P-limitation tends to favor GAOs, it does not necessarily lead to the enrichment of GAO-dominated cultures (Welles, 2015).

In summary, conditions that favor GAOs can lead to their proliferation and outcompetition of PAOs, resulting in a decline in phosphorus removal efficiency. Therefore, to maintain system stability, it is necessary to control the operational parameters that support anoxic VFA uptake and oxic growth of PAOs (Gu *et al.*, 2008). Elevated influent COD:P ratios above 50 mg COD to mg P are typically associated with microbial communities dominated by GAOs, whereas lower ratios between 10 and 20 mg COD to mg P correspond to cultures in which PAOs predominate (Majed and Gu, 2019; Oehmen *et al.*, 2007). However, the presence of both GAOs and PAOs in the system may confer mutual benefits, as GAOs facilitate the conversion of complex carbon compounds into VFAs, thereby enhancing substrate availability for PAOs. Further, sufficient VFA availability in the influent during the anoxic phase is also essential to ensure effective P-release and subsequent P-removal (Chuang *et al.*, 2011; Izadi *et al.*, 2020; Oehmen *et al.*, 2007).

4.2.3.3. Impact of temperature on the efficiency of MMBS and PAO-GAO abundance

Temperature is considered to influence phosphorus removal efficiency by altering both the composition and abundance of the dominant PAOs within the biological process (Tian *et al.*, 2025) as well as the competition between PAOs and GAOs (Zhang *et al.*, 2025). The results obtained for the temperature experiment demonstrated that a decrease in temperature enhanced P-release from 1.88 µg PO_4-P at room temperature to 2.04 µg PO_4-P at 12 ºC. Moreover, P-uptake occurred notably higher at 12 ºC compared to room temperature, with 6.87 µg PO_4-P and 4.65 µg PO_4-P. Enhanced intracellular phosphorus content under low-temperature conditions contributed to the development of a more metabolically active biofilm. Analysis of the temperature effects shows that the average biovolume at 12 °C is slightly higher than that at room temperature, with values of 3.79 $mm^3\,cm^{-2}$ and 2.77 $mm^3\,cm^{-2}$, respectively (Figure 30).

The increase in biovolume observed at low temperature may also be attributed to elevated EPS synthesis. EPS in activated sludge, in addition to microbial cells, store a considerable

proportion of phosphorus, accounting for approximately 27–30% of the total phosphorus content. Temperature notably influences the composition of EPS, particularly by elevating the polysaccharide fraction under low-temperature conditions. This increase in polysaccharide content enhances the adsorption capacity of EPS, thereby facilitating phosphorus accumulation and promoting microbial aggregation within the EPS matrix (Zeng *et al.*, 2019). Moreover, EPS functions as a phosphorus reservoir throughout the anoxic-oxic cycle, with the phosphorus content in EPS at the end of the oxic phase contributing roughly 5-9% to overall phosphorus removal (Zhang *et al.*, 2013). This could explain the enhanced biovolume and elevated phosphorus removal efficiency observed under low temperature conditions. In contrast, with increasing temperature, according to Panswad *et al.* (2003), a larger fraction of the energy generated by PAOs was allocated to cellular maintenance processes, thereby reducing the energy available for reproduction; consequently, this could lead to the washout of PAOs from the system.

In parallel with biofilm volume results, P-removal and P-removal capacity were slightly higher at 12 °C (4.84 µg PO_4-P and 0.43 µg PO_4-P mm^{-3}) compared to room temperature (2.76 µg PO_4-P and 0.32 µg PO_4-P mm^{-3}) (Figure 30). These findings suggest that the decrease in temperature contributed to the enhancement of both P-removal and P-removal capacity. The reduction in P-removal performance operated at warm temperatures may not be the reason for GAO proliferation. Instead, this observation may be associated with the efficient utilization of the glycolytic pathway by PAOs. Although poly-P cleavage represents the primary and preferred energy-generating mechanism of PAOs, these organisms are also capable of producing energy through the glycolytic pathway in the anoxic stage. This may lead to excessive glycogen replenishment and reduced P-uptake in the oxic phase, ultimately diminishing the P-removal efficiency (Erdal *et al.*, 2008).

Furthermore, Tian *et al.* (2025) reported that low temperatures inhibit anoxic glycogen degradation, which serves as the main pathway supporting GAO growth and metabolism. This inhibition limited substrate uptake by GAOs, and all these led to a deficiency in ATP production to meet the cellular energy demands. In contrast, PAOs enhanced their phosphorus metabolism to fulfil the energy demand required for the growth mechanism, via generating energy through poly-P cleavage. This metabolic shift enables PAOs to establish a competitive advantage and sustain effective phosphorus and organic matter removal under low-temperature conditions.

In more detail, PAOs utilize the Embden–Meyerhof–Parnas (EMP) pathway for glycogen degradation, with phosphofructokinase (*pfkA*) serving as a key enzyme for the EMP pathway. The activity of *pfkA* is strongly influenced by temperature, which thereby acts as a regulator in controlling glycolytic pathway utilization (Erdal *et al.*, 2008; Tian *et al.*, 2025). Tian *et al.* (2025) reported a marked reduction in *pfkA* gene expression at 12 ˚C, indicating that low temperature slows glycogen metabolism at the gene-expression level. Erdal *et al.* (2008) also showed that at low temperatures, the metabolism of glycogen was diminished, thereby allocating more energy toward PHA synthesis and phosphorus uptake, which conferred a competitive advantage to microorganisms using poly-P metabolism. Additionally, the enzymes responsible for anoxic P-release and oxic energy generation pathways are *ppx* and *ppk*, respectively. Tian *et al.* (2025) demonstrated that a decrease in temperature to 12 ºC elevated the expression level of *ppx*, thereby enhancing P-release. Besides, the expression level of *ppk* increased markedly at 12 °C, suggesting that low temperature slowed glycogen metabolism while favoring poly-P metabolism. Consequently, poly-P cleavage became the predominant energy source, supporting the energy demand for higher PHB synthesis at low temperatures.

In addition to the effects of enzymes, the tricarboxylic acid (TCA) cycle contributes to glycogen and PHB synthesis by supplying ATP during anoxic P-release and by balancing the excess NADH generated through the EMP pathway, thus maintaining intracellular redox balance (Erdal *et al.*, 2008; Tian *et al.*, 2025). Tian *et al.* (2025) revealed that the expression of the key TCA cycle genes *glt*A (citrate synthase) and *sucA* (oxoglutarate dehydrogenase) increased as the temperature decreased. The TCA cycle is less affected by low temperatures, and more of the energy produced by this process is used for PHB synthesis in order to maintain ATP and NADH balance, while glycogen degradation is suppressed.

Temperature is one of the key factors in the metabolic shift of PAOs. Phosphorus metabolism and ATP supply in PAOs are maintained at low temperature through reduced expression level of the *pfkA* gene, a key enzyme in glycolysis, alongside elevated expression level of the *ppx* and *ppk* genes, which play central roles in poly-P cleavage. Additionally, a modest increase in the TCA cycle helps maintain the redox equilibrium within the metabolic processes.

Further, in the temperature experiment, biofilm sequencing revealed a growth advantage for *Dechloromonas* at room temperature (25.24%) compared with 12 °C (12.92%). Similarly, *Zoogloea* was also more abundant at room temperature (22.82%) than at 12 °C (10.78%) (Figure 31). Even though *Dechloromonas* and *Zoogloea*, representing the dominant

PAO and GAO in the MMBS, exhibited higher abundance at room temperature than at 12 °C, indicating that slightly higher PAO/GAO ratios of 1.11 (room temperature) and 1.20 (12 °C) indicate that a higher PAO-to-GAO abundance ratio was associated with enhanced phosphorus removal performance.

Taken together, these findings demonstrate that investigating low-temperature conditions may be a promising approach to enhance biofilm formation and phosphorus removal efficiency in the system (Tian *et al.*, 2025). However, in an integrated nutrient removal system, low temperatures not only influence P-removal but also hinder nitrification. Moreover, under such conditions, denitrification becomes a limiting step for overall nutrient removal, resulting in higher nitrate concentrations in both the effluent and return sludge. Therefore, the impacts of temperature should be carefully considered for the simultaneous removal of carbon, phosphorus, and nitrogen in WWTPs (Mulkerrins *et al.*, 2004).

4.3. Conclusion and outlook

The improved interaction between the electrode surface and the electroactive biofilm through surface functionalization and increased surface roughness in BES is an important factor influencing current generation. In the first part of the thesis, the co-occurrence of *S. oneidensis* and *G. sulfurreducens* on surface-modified electrodes led to a marked enhancement in current density compared to the naturally formed biofilm matrix. The surface functionalization with redox mediators resulted in a 5.6-fold and 4.7-fold increase in mean current density for riboflavin and AQDS, respectively. Notably, the riboflavin-modified rough electrode demonstrated markedly improved performance, achieving a mean current density more than five times higher than the medium-roughness electrode. However, the electrode with a smooth surface with riboflavin functionalization produced negligible current throughout the experiment, indicating minimal electrochemical activity under the tested conditions.

These results suggest that surface modification strategies can effectively enhance biofilm development and reduce start-up times in BES by promoting initial microbial attachment through increased electrode surface area and reduced electron transfer resistance, while simultaneously accelerating electron transfer and current generation. These alterations offer

substantial advantages for long-start-up-time bacteria such as hydrogenogens, methanogens, and electroactive denitrifying bacteria, as modified anodes expedite initial colonization (Li and Cheng, 2019). In this context, a structure resembling the natural biofilm matrix, which typically develops over a period of days to months, can be introduced in a shorter time. These modifications are straightforward to implement and highly cost-effective, thereby improving current generation and supporting the potential future applications of BES-based biofilm processes at an industrial scale.

Further research could be conducted using transcriptomic analysis of the biofilms to investigate the link between gene expression changes and improved current production. Moreover, alongside co-culture experiments, single-culture experiments with *S. oneidensis* and *G. sulfurreducens* would help determine whether these effects are species-specific or shared.

In this work, the integration of microfluidic technology with BES has demonstrated a powerful framework for elucidating the interplay between biofilm development, extracellular electron transfer, and current generation under dynamic and controllable conditions. Microfluidic BES, capable of real-time monitoring and operation under short retention times, offer opportunities for high-throughput evaluation of how different stimuli influence electrochemical activity (Li *et al.*, 2012). Electroactive microbial communities in these platforms serve as model systems for investigating electron transfer mechanisms and current generation performance, supporting the optimization and sustainability of BESs.

Additionally, further investigations can be carried out to detect electroactive microorganisms with microfluidic BES. One obstacle to discovering novel electroactive microorganisms is the limited availability of reliable methods to determine whether a given species exhibits electrochemical activity. The developed microfluidic platform can be used to detect electroactive species in almost any combination of materials. A comprehensive understanding of how biofilms contribute to electron transfer will not only inform the development of new strategies to enhance BES performance but will also support improvements in wastewater treatment efficiency (Angelaalincy *et al.*, 2018).

In the second part of the thesis, a systematic analysis of key process parameters was performed using MMBS to examine their impact on PAO diversity and abundance, PAO-GAO interactions, phosphorus removal, and overall EBPR performance. To this end, a biofilm-

based PAOs enrichment, based on the principle of the activated sludge system, was successfully achieved under alternating cycles of anoxic feeding and oxic starvation. Additionally, real-time and non-invasive biofilm development was monitored via OCT under flow conditions, which was one of the main targets of scaling down the system to 150 µL.

The presence of key organisms associated with wastewater treatment was confirmed, and variations in microbial diversity and abundance under different operational parameters were analyzed. Whole native DNA sequencing enabled an accurate assessment of the relevance of specific microorganisms to avoid amplification bias. Metagenomic analysis of the enriched biofilm revealed that the *Rhodocyclaceae* family, in particular, became prevalent across all systems over time. Moreover, the presence of *Dechloromonas* (PAO) and *Zoogloea* (GAO) was notably dominant, and they were positively correlated, as indicated by multivariate and network analyses. This study confirms that PAOs and GAOs can be mutually supportive and that PAO-GAO competition is of minor importance compared to the influence of process conditions.

Within the scope of the thesis, the effects of different carbon sources, pH, COD:P ratio, and temperature on the system were evaluated. Among these parameters, the type of carbon source exerted a more pronounced effect on system dynamics than the COD:P ratio, pH, or temperature. In the MMBS, the use of glucose and acetate/propionate resulted in maximal phosphorus removal, whereas system performance was limited when ethanol, glycerol, or amino acids were used. Furthermore, a low COD:P ratio of 10 enhanced the phosphorus removal and biofilm formation. Although system capacity peaked at pH 7.5, which supported the increasing relative abundance of *Dechloromonas* and *Zoogloea*, no significant difference in overall performance was observed among the tested pH levels. Moreover, a low temperature of 12 °C had no negative impact on performance. Optimizing these operational parameters could improve phosphorus removal efficiency, thereby reducing the carbon source requirement and energy consumption. Moreover, in addition to phosphorus removal, the removal of carbon and nitrogen must also be considered to ensure overall system efficiency, compliance with regulatory standards, and mitigation of environmental impacts associated with wastewater discharge.

Further research could be conducted using pure culture experiments with specified organisms instead of complex activated sludge communities in MMBS. Pure cultures enable researchers to directly associate observed metabolic activities, such as substrate uptake, storage polymer

formation (e.g., poly-P, PHA, glycogen), and electron acceptor utilization, with a single organism, without interference from other community members. This approach provides clarity and specificity, offering detailed insights at the organism level that are often obscured by the complex interactions and competition within activated sludge communities. Additionally, with the aid of the cultivation platform, if selected parameters are suitable for PAO enrichment, it could be possible to cultivate challenging niches under alternating cycling conditions over extended periods, without loss of functionality. For instance, samples obtained from the cultivation channels could be used to inoculate additional microfluidic reactors. Applying controlled gradients could promote the formation of individual niches and facilitate the isolation of desired organisms in pure culture through repeated sampling (Klein, 2018).

Finally, the microfluidic cultivation platform has enabled rigorous and systematic investigation of the influence of variable process conditions in a highly parallel manner, thereby facilitating a comprehensive understanding and efficient optimization of full-scale wastewater treatment systems. Optimizing the operational conditions of WWTPs can significantly enhance their capability for carbon and phosphorus removal, as well as energy and phosphorus recovery, ultimately contributing to sustainable water management practices and the circular economy.

5. References

Abouhagger, A., Andriukonis, E., Grigorianaite, G., da Silva, R.R., Kasperaviciute, K., Stirke, A., MA Melo, W.C., 2025. Fabrication and Application of a Microfluidic Chip for Biofilm Cultivation and Analysis under Controlled Flow. ACS Omega 10, 37994–38001. https://doi.org/10.1021/acsomega.5c04643

Albertsen, M., McIlroy, S.J., Stokholm-Bjerregaard, M., Karst, S.M., Nielsen, P.H., 2016. "Candidatus Propionivibrio aalborgensis": A novel glycogen accumulating organism abundant in full-scale enhanced biological phosphorus removal plants. Front. Microbiol. 7, 1–17. https://doi.org/10.3389/fmicb.2016.01033

An, W., Guo, F., Song, Y., Gao, N., Bai, S., Dai, J., Wei, H., Zhang, L., Yu, D., Xia, M., Yu, Y., Qi, M., Tian, C., Chen, H., Wu, Z., Zhang, T., Qiu, D., 2016. Comparative genomics analyses on EPS biosynthesis genes required for floc formation of Zoogloea resiniphila and other activated sludge bacteria. Water Res. 102, 494–504. https://doi.org/10.1016/j.watres.2016.06.058

Andrés, M.P.S., Baños-Cabrera, M., Gutiérrez-Fernández, L., Díez-Pascual, A.M., Vera-López, S., 2021. Fluorescence study of riboflavin interactions with graphene dispersed in bioactive tannic acid. Int. J. Mol. Sci. 22. https://doi.org/10.3390/ijms22105270

Angelaalincy, M.J., Navanietha Krishnaraj, R., Shakambari, G., Ashokkumar, B., Kathiresan, S., Varalakshmi, P., 2018. Biofilm Engineering Approaches for Improving the Performance of Microbial Fuel Cells and Bioelectrochemical Systems. Front. Energy Res. 6, 1–12. https://doi.org/10.3389/fenrg.2018.00063

Arinda, T., Philipp, L.A., Rehnlund, D., Edel, M., Chodorski, J., Stöckl, M., Holtmann, D., Ulber, R., Gescher, J., Sturm-Richter, K., 2019. Addition of riboflavin-coupled magnetic beads increases current production in bioelectrochemical systems via the increased formation of anode-biofilms. Front. Microbiol. 10, 1–8. https://doi.org/10.3389/fmicb.2019.00126

Arle, J., Bartel, H., Baumgarten, C., Bertram, A., Blondzik, K., Brandt, S., Brauer, F., Claussen, U., Damian, H.P., Dieter, D., Galander, C., Ginzky, H., Grimm, S., Helmecke, M., Hofmeier, K., Hofmeier, M., Hülsmann, W., Kirschbaum, B., Knobloch, T., Koppe, K., Koschorr, J., Wolter, R., 2018. Water Resource Management in Germany: Fundamentals, pressures, measures. Dessau-Roßlau.

Arle, J., Frederike Balzer, Baumgarten, C., Bilharz, M., Bünger, B., Dauert, U., Dewitz, A., Drosihn, D., Eckermann, F., Ehlers, K., Frerk, M., Gellrich, A., Geupel, M., Gniffke, P., Go, M., Wolter, R., Editors:, 2017. Data on the Environment 2017, German Environment Agency.

Banerjee, A., Sarkar, S., Govil, T., González-Faune, P., Cabrera-Barjas, G., Bandopadhyay, R., Salem, D.R., Sani, R.K., 2021. Extremophilic Exopolysaccharides: Biotechnologies and Wastewater Remediation. Front. Microbiol. 12. https://doi.org/10.3389/fmicb.2021.721365

Barr, J.J., Dutilh, B.E., Skennerton, C.T., Fukushima, T., Hastie, M.L., Gorman, J.J., Tyson, G.W., Bond, P.L., 2016. Metagenomic and metaproteomic analyses of Accumulibacter phosphatis-enriched floccular and granular biofilm. Environ. Microbiol. 18, 273–287. https://doi.org/10.1111/1462-2920.13019

Blanco-Cabra, N., López-Martínez, M.J., Arévalo-Jaimes, B.V., Martin-Gómez, M.T., Samitier, J., Torrents, E., 2021. A new BiofilmChip device for testing biofilm formation and antibiotic susceptibility. npj Biofilms Microbiomes 7. https://doi.org/10.1038/s41522-021-00236-1

Brutinel, E.D., Gralnick, J.A., 2012. Shuttling happens : soluble flavin mediators of extracellular electron transfer in Shewanella 41–48. https://doi.org/10.1007/s00253-011-3653-0

Caccavo, F., Lonergan, D.J., Lovley, D.R., Davis, M., Stolz, J.F., Mcinerneyl, M.J., 1994. Geobacter sulfurreducens sp. nov., a Hydrogen- and Acetate- Oxidizing Dissimilatory Metal-Reducing Microorganism. Appl. Environ. Microbiol. 60, 3752–3759. https://doi.org/DOI: 10.1128/aem.60.10.3752-3759.1994

Carmona, A., 2012. Investigation of electron transfer mechanisms in electrochemically active microbial biofilms. Technischen Universität Carolo-Wilhelmina. https://doi.org/10.13140/RG.2.1.2528.7841

Champigneux, P., Renault-Sentenac, C., Bourrier, D., Rossi, C., Delia, M.L., Bergel, A., 2019. Effect of surface roughness, porosity and roughened micro-pillar structures on the early formation of microbial anodes. Bioelectrochemistry 128, 17–29. https://doi.org/10.1016/j.bioelechem.2019.03.002

Chen, J., Tang, X., Wu, X., Li, B., Lin, X., Li, P., Chen, H., Huang, F., Deng, X., Xie, X., Wei, C., Zou, Y., Qiu, G., 2024. Relating the carbon sources to denitrifying community in full-scale wastewater treatment plants. Chemosphere 361, 142329. https://doi.org/10.1016/j.chemosphere.2024.142329

Chen, L., Chen, H., Hu, Z., Tian, Y., Wang, C., Xie, P., Deng, X., Zhang, Y., Tang, X., Lin, X., Li, B., Wei, C., Qiu, G., 2022. Carbon uptake bioenergetics of PAOs and GAOs in full-scale enhanced biological phosphorus removal systems. Water Res. 216, 118258. https://doi.org/10.1016/j.watres.2022.118258

Chen, S., Ding, Y., 2023. A bibliography study of Shewanella oneidensis biofilm. FEMS Microbiol. Ecol. 99, 1–10. https://doi.org/10.1093/femsec/fiad124

Chen, Y., Gu, G., 2006. Effect of changes of pH on the anaerobic/aerobic transformations of biological phosphorus removal in wastewater fed with a mixture of propionic and acetic acids. J. Chem. Technol. Biotechnol. 81, 1021–1028. https://doi.org/10.1002/jctb.1516

Chuang, S.H., Chang, W.C., Huang, Y.H., Tseng, C.C., Tai, C.C., 2011. Effects of different carbon supplements on phosphorus removal in low C/P ratio industrial wastewater. Bioresour. Technol. 102, 5461–5465. https://doi.org/10.1016/j.biortech.2010.11.118

Coats, E.R., Dobroth, Z.T., Brinkman, C.K., 2015. EBPR Using Crude Glycerol: Assessing

Process Resiliency and Exploring Metabolic Anomalies. Water Environ. Res. 87, 68–79. https://doi.org/10.2175/106143014x14062131179113

Daims, H., 2009. Use of fluorescence in situ hybridization and the daime image analysis program for the cultivation-independent quantification of microorganisms in environmental and medical samples. Cold Spring Harb. Protoc. 4, 1–8. https://doi.org/10.1101/pdb.prot5253

Daims, H., Lücker, S., Wagner, M., 2006. Daime, a Novel Image Analysis Program for Microbial Ecology and Biofilm Research. Environ. Microbiol. 8, 200–213. https://doi.org/10.1111/j.1462-2920.2005.00880.x

Deng, M., Dai, Z., Senbati, Y., Li, L., Song, K., He, X., 2020. Aerobic Denitrification Microbial Community and Function in Zero-Discharge Recirculating Aquaculture System Using a Single Biofloc-Based Suspended Growth Reactor: Influence of the Carbon-to-Nitrogen Ratio. Front. Microbiol. 11, 1–11. https://doi.org/10.3389/fmicb.2020.01760

Dockx, L., Caluwé, M., De Vleeschauwer, F., Dobbeleers, T., Dries, J., 2021. Impact of the substrate composition on enhanced biological phosphorus removal during formation of aerobic granular sludge. Bioresour. Technol. 337. https://doi.org/10.1016/j.biortech.2021.125482

Dueholm, M.K.D., Nierychlo, M., Andersen, K.S., Rudkjøbing, V., Knutsson, S., Arriaga, S., Bakke, R., Boon, N., Bux, F., Christensson, M., Chua, A.S.M., Curtis, T.P., Cytryn, E., Erijman, L., Etchebehere, C., Fatta-Kassinos, D., Frigon, D., Garcia-Chaves, M.C., Gu, A.Z., Horn, H., Jenkins, D., Kreuzinger, N., Kumari, S., Lanham, A., Law, Y., Leiknes, T.O., Morgenroth, E., Muszyński, A., Petrovski, S., Pijuan, M., Pillai, S.B., Reis, M.A.M., Rong, Q., Rossetti, S., Seviour, R., Tooker, N., Vainio, P., van Loosdrecht, M., Vikraman, R., Wanner, J., Weissbrodt, D., Wen, X., Zhang, T., Nielsen, Per H., Albertsen, M., Nielsen, Per Halkjær, 2022. MiDAS 4: A global catalogue of full-length 16S rRNA gene sequences and taxonomy for studies of bacterial communities in wastewater treatment plants. Nat. Commun. 13, 1–15. https://doi.org/10.1038/s41467-022-29438-7

Edel, M., Sturm, G., Sturm-Richter, K., Wagner, M., Ducassou, J.N., Couté, Y., Horn, H., Gescher, J., 2021. Extracellular riboflavin induces anaerobic biofilm formation in Shewanella oneidensis. Biotechnol. Biofuels 14, 1–14. https://doi.org/10.1186/s13068-021-01981-3

Eghombi, E., Kim, H., Choi, Y.H., Baek, M.H., Nadagouda, M.N., Park, P.K., Chae, S., 2022. Efficient Phosphorus Recovery from Municipal Wastewater Using Enhanced Biological Phosphorus Removal in an Anaerobic/Anoxic/Aerobic Membrane Bioreactor and Magnesium-Based Pellets. Membranes (Basel). 12, 1–15. https://doi.org/10.3390/membranes12020210

Elahinik, A., de Clercq, F., Pabst, M., Xevgenos, D., van Loosdrecht, M.C.M., Pronk, M., 2024. Effects of salinity on glycerol conversion and biological phosphorus removal by aerobic granular sludge. Water Res. 257, 121737. https://doi.org/10.1016/j.watres.2024.121737

Elahinik, A., Haarsma, M., Abbas, B., Pabst, M., Xevgenos, D., van Loosdrecht, M.C.M., Pronk, M., 2022. Glycerol conversion by aerobic granular sludge. Water Res. 227, 119340. https://doi.org/10.1016/j.watres.2022.119340

Elahinik, A., Li, L., Pabst, M., Abbas, B., Xevgenos, D., van Loosdrecht, M.C.M., Pronk, M., 2023. Aerobic granular sludge phosphate removal using glucose. Water Res. 247, 120776. https://doi.org/10.1016/j.watres.2023.120776

Engel, C., Schattenberg, F., Dohnt, K., Schröder, U., Müller, S., Krull, R., 2019. Long-Term Behavior of Defined Mixed Cultures of Geobacter sulfurreducens and Shewanella oneidensis in Bioelectrochemical Systems. Front. Bioeng. Biotechnol. 7, 1–12. https://doi.org/10.3389/fbioe.2019.00060

Erben, J., Pinder, Z.A., Lüdtke, M.S., Kerzenmacher, S., 2021a. Local Acidification Limits the Current Production and Biofilm Formation of Shewanella oneidensis MR-1 with Electrospun Anodes. Front. Microbiol. 12, 1–10. https://doi.org/10.3389/fmicb.2021.660474

Erben, J., Wang, X., Kerzenmacher, S., 2021b. High Current Production of Shewanella Oneidensis with Electrospun Carbon Nanofiber Anodes is Directly Linked to Biofilm Formation**. ChemElectroChem 8, 1836–1846. https://doi.org/10.1002/celc.202100192

Erdal, U.G., Erdal, Z.K., Daigger, G.T., Randall, C.W., 2008. Is it PAO-GAO competition or metabolic shift in EBPR system? Evidence from an experimental study. Water Sci. Technol. 58, 1329–1334. https://doi.org/10.2166/wst.2008.734

Falkentoft, C.M., 2000. Simultaneous removal of nitrate and phosphorus in a biofilm reactor: The aspect of diffusion. Technical University of Denmark.

Feng, C., Li, F., Liu, H., Lang, X., Fan, S., 2010a. A dual-chamber microbial fuel cell with conductive film-modified anode and cathode and its application for the neutral electro-Fenton process. Electrochim. Acta 55, 2048–2054. https://doi.org/10.1016/j.electacta.2009.11.033

Feng, C., Ma, L., Li, F., Mai, H., Lang, X., Fan, S., 2010b. A polypyrrole/anthraquinone-2,6-disulphonic disodium salt (PPy/AQDS)-modified anode to improve performance of microbial fuel cells. Biosens. Bioelectron. 25, 1516–1520. https://doi.org/10.1016/j.bios.2009.10.009

Fernández-Ávila Cobo, M., Rezaei, B., Keller, S.S., Zhang, Y., 2025. Exploring the impact of surface properties, porosity and lattice size on bacterial energy harvesting with 3D pyrolytic carbon electrodes. J. Power Sources 643. https://doi.org/10.1016/j.jpowsour.2025.237018

Filipe, C.D.M., Daigger, G.T., Grady, C.P.L., 2001. Effects of pH on the Rates of Aerobic Metabolism of Phosphate-Accumulating and Glycogen-Accumulating Organisms. Water Environ. Res. 73, 213–222. https://doi.org/10.2175/106143001x139191

Fujii, N., Kuroda, K., Narihiro, T., Aoi, Y., Ozaki, N., Ohashi, A., Kindaichi, T., 2024. Unique episymbiotic relationship between Candidatus Patescibacteria and Zoogloea in activated

sludge flocs at a municipal wastewater treatment plant. Environ. Microbiol. Rep. 16. https://doi.org/10.1111/1758-2229.70007

Gao, C., Yang, F., Tian, Z., Sun, D., Liu, W., Peng, Y., 2025. Pathways of inhibition of filamentous sludge bulking by slowly biodegradable organic compounds. J. Environ. Sci. (China) 150, 104–115. https://doi.org/10.1016/j.jes.2024.03.021

Gemünde, A., Lai, B., Pause, L., Krömer, J., Holtmann, D., 2022. Redox Mediators in Microbial Electrochemical Systems. ChemElectroChem 9. https://doi.org/10.1002/celc.202200216

Ghimire, U., Sarpong, G., Gude, V.G., 2021. Transitioning Wastewater Treatment Plants toward Circular Economy and Energy Sustainability. https://doi.org/10.1021/acsomega.0c05827

Gnida, A., Zubrowska-Sudoł, M., Sytek-Szmeichel, K., Podedworna, J., Surmacz-Górska, J., Marciocha, D., 2020. Effect of anaerobic phases length on denitrifying dephosphatation biocenosis - A case study of IFAS-MBSBBR. BMC Microbiol. 20, 1–12. https://doi.org/10.1186/s12866-020-01896-3

Gonzalez-Gil, G., Holliger, C., 2011. Dynamics of microbial community structure of and enhanced biological phosphorus removal by aerobic granules cultivated on propionate or acetate. Appl. Environ. Microbiol. 77, 8041–8051. https://doi.org/10.1128/AEM.05738-11

Gu, A.Z., Saunders, A., Neethling, J.B., Stensel, H.D., Blackall, L.L., 2008. Functionally Relevant Microorganisms to Enhanced Biological Phosphorus Removal Performance at Full-Scale Wastewater Treatment Plants in the United States. Water Environ. Res. 80, 688–698. https://doi.org/10.2175/106143008x276741

Haiming, Z., Xiwu, L., Abualhail, S., Jing, S., Qian, G., 2014. Enrichment of PAO and DPAO responsible for phosphorus removal at low temperature. Environ. Prot. Eng. 40, 67–83. https://doi.org/10.5277/epe140106

Hansen, S.H., Kabbeck, T., Radtke, C.P., Krause, S., Krolitzki, E., Peschke, T., Gasmi, J., Rabe, K.S., Wagner, M., Horn, H., Hubbuch, J., Gescher, J., Niemeyer, C.M., 2019. Machine-assisted cultivation and analysis of biofilms. Sci. Rep. 9, 1–10. https://doi.org/10.1038/s41598-019-45414-6

Heydorn, R.L., Engel, C., Krull, R., Dohnt, K., 2020. Strategies for the Targeted Improvement of Anodic Electron Transfer in Microbial Fuel Cells. ChemBioEng Rev. 7, 4–17. https://doi.org/10.1002/cben.201900023

Horn, M.A., Ihssen, J., Matthies, C., Schramm, A., Acker, G., Drake, H.L., 2005. Dechloromonas denitrificans sp. nov., Flavobacterium denitrificans sp. nov., Paenibacillus anaericanus sp. nov. and Paenibacillus terrae strain MH72, N2O-producing bacteria isolated from the gut of the earthworm Aporrectodea caliginosa. Int. J. Syst. Evol. Microbiol. 55, 1255–1265. https://doi.org/10.1099/ijs.0.63484-0

Hu, X., Sobotka, D., Czerwionka, K., Zhou, Q., Xie, L., Makinia, J., 2018. Effects of different

external carbon sources and electron acceptors on interactions between denitrification and phosphorus removal in biological nutrient removal processes. J. Zhejiang Univ. Sci. B 19, 305–316. https://doi.org/10.1631/jzus.B1700064

Huang, L., Tang, J., Chen, M., Liu, X., Zhou, S., 2018. Two Modes of Riboflavin-Mediated Extracellular Electron Transfer in Geobacter uraniireducens. Front. Microbiol. 9, 1–8. https://doi.org/10.3389/fmicb.2018.02886

Huang, T.L., Zhou, S.L., Zhang, H.H., Bai, S.Y., He, X.X., Yang, X., 2015. Nitrogen removal characteristics of a newly isolated indigenous aerobic denitrifier from oligotrophic drinking water reservoir, Zoogloea sp. N299. Int. J. Mol. Sci. 16, 10038–10060. https://doi.org/10.3390/ijms160510038

Huber, M., Athanasiadis, K., Helmreich, B., 2020. Phosphorus removal potential at sewage treatment plants in Bavaria – a case study. Environ. Challenges 1, 100008. https://doi.org/10.1016/j.envc.2020.100008

Iannacone, F., Di Capua, F., Granata, F., Gargano, R., Esposito, G., 2021. Shortcut nitrification-denitrification and biological phosphorus removal in acetate- and ethanol-fed moving bed biofilm reactors under microaerobic/aerobic conditions. Bioresour. Technol. 330, 124958. https://doi.org/10.1016/j.biortech.2021.124958

Inoue, K., Leang, C., Franks, A.E., Woodard, T.L., Nevin, K.P., Lovley, D.R., 2011. Specific localization of the c-type cytochrome OmcZ at the anode surface in current-producing biofilms of Geobacter sulfurreducens. Environ. Microbiol. Rep. 3, 211–217. https://doi.org/10.1111/j.1758-2229.2010.00210.x

Izadi, Parnian, Izadi, Parin, Eldyasti, A., 2020. Design, operation and technology configurations for enhanced biological phosphorus removal (EBPR) process: a review. Rev Env. Sci Biotechnol 19, 561–593. https://doi.org/10.1007/s11157-020-09538-w

Jeon, C.O., Lee, D.S., Lee, M.W., Park, J.M., 2001. Enhanced Biological Phosphorus Removal in an Anaerobic–Aerobic Sequencing Batch Reactor: Effect of pH. Water Environ. Res. 73, 301–306. https://doi.org/10.2175/106143001x139407

Kang, A.J., Munz, G., Yuan, Q., 2019. Influence of pH control on material characteristics, bacterial community composition and BNR performance of mature aerobic granules. Process Saf. Environ. Prot. 124, 158–166. https://doi.org/10.1016/j.psep.2019.02.014

Kapagiannidis, A.G., Zafiriadis, I., Aivasidis, A., 2013. Comparison between aerobic and anoxic metabolism of denitrifying-EBPR sludge: Effect of biomass poly-hydroxyalkanoates content. N. Biotechnol. 30, 227–237. https://doi.org/10.1016/j.nbt.2012.05.022

Kim, J., Steinegger, M., 2024. Metabuli: sensitive and specific metagenomic classification via joint analysis of amino acid and DNA. Nat. Methods 21, 971–973. https://doi.org/10.1038/s41592-024-02273-y

Kim, S., Chairattanawat, C., Kim, E., Lee, D., Hwang, S., 2025. Changes in bacterial diversity of full-scale anaerobic digesters treating secondary sludge. Bioresour. Technol. 418,

131894. https://doi.org/10.1016/j.biortech.2024.131894

Klein, E., 2018. Darstellung von Biofilmen der Abwasserreinigung in mikrofluidischen Systemen. Karlsruher Institut für Technologie, Karlsruhe, Germany.

Klein, E., Heintz, H., Wurst, R., Schuldt, S., Hähl, H., Jacobs, K., Gescher, J., 2024a. Comparative analysis of the influence of BpfA and BpfG on biofilm development and current density in Shewanella oneidensis under oxic, fumarate- and anode-respiring conditions. Sci. Rep. 14, 1–12. https://doi.org/10.1038/s41598-024-73474-w

Klein, E., Weiler, J., Wagner, M., Čelikić, M., Niemeyer, C.M., Horn, H., Gescher, J., 2022. Enrichment of phosphate-accumulating organisms (PAOs) in a microfluidic model biofilm system by mimicking a typical aerobic granular sludge feast/famine regime. Appl. Microbiol. Biotechnol. 106, 1313–1324. https://doi.org/10.1007/s00253-022-11759-8

Klein, E., Wurst, R., Rehnlund, D., Gescher, J., 2024b. Elucidating the development of cooperative anode-biofilm-structures. Biofilm 7. https://doi.org/https://doi.org/10.1016/j.bioflm.2024.100193

Klein, E.M., Heintz, H., Wurst, R., Lapp, C.J., Edel, M., Hähl, H., Jacobs, K., Gescher, J., 2025. Tailored enzyme expression modifies Shewanella oneidensis biofilms and increases current density. N. Biotechnol. 89, 1–10. https://doi.org/10.1016/j.nbt.2025.05.006

Klein, E.M., Knoll, M.T., Gescher, J., 2023. Microbe-Anode Interactions: Comparing the impact of genetic and material engineering approaches to improve the performance of microbial electrochemical systems (MES). Microb. Biotechnol. 1179–1202. https://doi.org/10.1111/1751-7915.14236

Knoll, M.T., 2023. Sprayable biofilm – Agarose hydrogels as 3D matrix for enhanced productivity in bioelectrochemical systems. Technischen Universität Hamburg, Hamburg, Germany. https://doi.org/10.1016/j.bioflm.2022.100077

Knoll, M.T., Fuderer, E., Gescher, J., 2022. Biofilm Sprayable biofilm – Agarose hydrogels as 3D matrix for enhanced productivity in bioelectrochemical systems. Biofilm 4, 100077. https://doi.org/10.1016/j.bioflm.2022.100077

Kolmogorov, M., Bickhart, D.M., Behsaz, B., Gurevich, A., Rayko, M., Shin, S.B., Kuhn, K., Yuan, J., Polevikov, E., Smith, T.P.L., Pevzner, P.A., 2020. metaFlye: scalable long-read metagenome assembly using repeat graphs. Nat. Methods 17, 1103–1110. https://doi.org/10.1038/s41592-020-00971-x

Kondrotaite, Z., Petersen, J., Singleton, C., Peces, M., Petriglieri, F., Jensen, T.B.N., Sereika, M., Daugberg, A.O.H., Wagner, M., Dueholm, K.D., Nielsen, P.H., 2025. Ecophysiology and niche differentiation of three genera of polyphosphate-accumulating bacteria in a full-scale wastewater treatment plant. Am. Soc. Microbiol. 10. https://doi.org/https://doi.org/10.1128/msystems.00322-25

Kotal, A., Jana, K., Roy, S., Satpathy, J.K., Kar, R.K., 2024. Induced surface process of graphene variants' dispersion with biocompatible riboflavin. Colloids Surfaces A Physicochem. Eng. Asp. 702, 135029. https://doi.org/10.1016/j.colsurfa.2024.135029

Kudier, W.N., Atta, S.Z., Majdi, H.S., Hasan, B.O., 2022. Effect of Electrode Surface Enhancement on the Performance of Microbial Fuel Cell Under Flow Conditions. Egypt. J. Chem. 65, 781–789. https://doi.org/10.21608/EJCHEM.2022.121700.5454

Kulchartvijit, T., Chianrabutra, C., Sukontasing, S., Chianrabutra, S., 2022. The Effects of Surface Roughness of the Stainless-Steel Anode on Electricity Enhancement of Microbial Fuel Cell. Trends Sci. 19. https://doi.org/10.48048/tis.2022.3680

Kutuzova, S., Piera, P., Nor Nielsen, K., Olsen, N.S., Riber, L., Gobbi, A., Forero-Junco, L.M., Dougherty, P.E., Westergaard, J.C., Christensen, S., Hansen, L.H., Nielsen, M., Nissen, J.N., Rasmussen, S., 2024. Binning meets taxonomy: TaxVAMB improves metagenome binning using bi-modal variational autoencoder. https://doi.org/10.1101/2024.10.25.620172

Lakshminarasimman, N., McKnight, M.M., Neufeld, J.D., Parker, W., 2025. Characterizing biofilm thickness, density, and microbial community composition in a full-scale hybrid membrane aerated biofilm reactor. Bioresour. Technol. 423. https://doi.org/10.1016/j.biortech.2025.132207

Li, C., Cheng, S., 2019. Functional group surface modifications for enhancing the formation and performance of exoelectrogenic biofilms on the anode of a bioelectrochemical system. Crit. Rev. Biotechnol. 39, 1015–1030. https://doi.org/10.1080/07388551.2019.1662367

Li, H., 2016. Minimap and miniasm: fast mapping and de novo assembly for noisy long sequences. Bioinformatics 32, 2103–2110. https://doi.org/10.1093/bioinformatics/btw152

Li, H., Zhong, Y., Huang, H., Tan, Z., Sun, Y., Liu, H., 2020. Simultaneous nitrogen and phosphorus removal by interactions between phosphate accumulating organisms (PAOs) and denitrifying phosphate accumulating organisms (DPAOs) in a sequencing batch reactor. Sci. Total Environ. 744, 140852. https://doi.org/10.1016/j.scitotenv.2020.140852

Li, T., Li, C. ying, Liang, H. lin, Li, X. xue, Yang, X. li, Li, H., Song, H. liang, 2024. Enhancement of stress resistance of electroactive biofilms against hypersaline shock via exogenous electron mediator addition. Chem. Eng. J. 499. https://doi.org/10.1016/j.cej.2024.155905

Li, W., Zhang, H. yan, Sun, H. zhi, Zeng, F., Gao, Y. nan, Zhu, L., 2018. Influence of pH on short-cut denitrifying phosphorus removal. Water Sci. Eng. 11, 17–22. https://doi.org/10.1016/j.wse.2018.03.006

Li, Z., Venkataraman, A., Rosenbaum, M.A., Angenent, L.T., 2012. A laminar-flow microfluidic device for quantitative analysis of microbial electrochemical activity. ChemSusChem 5, 1119–1123. https://doi.org/10.1002/cssc.201100736

Liu, Y., Chen, Y., Zhou, Q., 2007. Effect of initial pH control on enhanced biological phosphorus removal from wastewater containing acetic and propionic acids. Chemosphere 66, 123–129. https://doi.org/10.1016/j.chemosphere.2006.05.004

Liu, Z., Zhang, D., Yang, R., Wang, Jingwen, Duan, Y., Gao, M., Wang, Jiaxuan, Zhang, A., Liu, Y., Li, Z., 2024. Changes and stage disparity of aerobic sludge granulation with

increasing organic load rate under low organotrophic conditions. J. Clean. Prod. 450, 141937. https://doi.org/10.1016/j.jclepro.2024.141937

Logan, B.E., Rossi, R., Ragab, A., Saikaly, P.E., 2019. Electroactive microorganisms in bioelectrochemical systems. Nat. Rev. Microbiol. 17, 307–319. https://doi.org/10.1038/s41579-019-0173-x

Loosdrecht, M.C.M., Nielsen, P.H., Lopez-Vazquez, C.M., Brdjanovic, D., 2016. Experimental Methods in Wastewater Treatment, 1st ed. IWA Publishing, UK.

Majed, N., Gu, A.Z., 2020. Phenotypic dynamics in polyphosphate and glycogen accumulating organisms in response to varying influent C/P ratios in EBPR systems. Sci. Total Environ. 743, 140603. https://doi.org/10.1016/j.scitotenv.2020.140603

Majed, N., Gu, A.Z., 2019. Impact of influent carbon to phosphorus ratio on performance and phenotypic dynamics in Enhanced Biological Phosphorus Removal (EBPR) system - Insights into carbon distribution, intracellular polymer stoichiometry and pathways shifts. bioRxiv. https://doi.org/https://doi.org/10.1101/671081

Malinauskas, A., 2008. Electrochemical study of ribofavin adsorbed on a graphite electrode. Chemija 19, 1–3.

Manz, W., Amann, R., Ludwig, W., Wagner, M., Schleifer, K.H., 1992. Phylogenetic Oligodeoxynucleotide Probes for the Major Subclasses of Proteobacteria: Problems and Solutions. Syst. Appl. Microbiol. 15, 593–600. https://doi.org/10.1016/S0723-2020(11)80121-9

Martinez, C.M., Alvarez, L.H., 2018. Application of redox mediators in bioelectrochemical systems. Biotechnol. Adv. 36, 1412–1423. https://doi.org/10.1016/j.biotechadv.2018.05.005

McIlroy, S.J., Albertsen, M., Andresen, E.K., Saunders, A.M., Kristiansen, R., Stokholm-Bjerregaard, M., Nielsen, K.L., Nielsen, P.H., 2014. 'Candidatus Competibacter'-lineage genomes retrieved from metagenomes reveal functional metabolic diversity. ISME J. 8, 613–624. https://doi.org/10.1038/ismej.2013.162

McIlroy, S.J., Onetto, C.A., McIlroy, B., Herbst, F.A., Dueholm, M.S., Kirkegaard, R.H., Fernando, E., Karst, S.M., Nierychlo, M., Kristensen, J.M., Eales, K.L., Grbin, P.R., Wimmer, R., Nielsen, P.H., 2018. Genomic and in Situ Analyses reveal the Micropruina spp. as Abundant fermentative glycogen accumulating organisms in enhanced biological phosphorus removal systems. Front. Microbiol. 9, 1–12. https://doi.org/10.3389/fmicb.2018.01004

McIlroy, S.J., Saunders, A.M., Albertsen, M., Nierychlo, M., McIlroy, B., Hansen, A.A., Karst, S.M., Nielsen, J.L., Nielsen, P.H., 2015. MiDAS: The field guide to the microbes of activated sludge. Database 2015, 1–8. https://doi.org/10.1093/database/bav062

Mcilroy, S.J., Starnawska, A., Starnawski, P., Saunders, A.M., Nierychlo, M., Nielsen, P.H., Nielsen, J.L., 2016. Identification of active denitrifiers in full-scale nutrient removal wastewater treatment systems. Environ. Microbiol. 18, 50–64.

https://doi.org/10.1111/1462-2920.12614

Mehrani, M., Sobotka, D., Kowal, P., Ciesielski, S., 2020. The occurrence and role of Nitrospira in nitrogen removal systems 303. https://doi.org/10.1016/j.biortech.2020.122936

Mier, A.A., Olvera-Vargas, H., Mejía-López, M., Longoria, A., Verea, L., Sebastian, P.J., Arias, D.M., 2021. A review of recent advances in electrode materials for emerging bioelectrochemical systems: From biofilm-bearing anodes to specialized cathodes. Chemosphere 283. https://doi.org/10.1016/j.chemosphere.2021.131138

Montoya, T., Borrás, L., Aguado, D., Ferrer, J., Seco, A., 2008. Detection and prevention of enhanced biological phosphorus removal deterioration caused by Zoogloea overabundance. Environ. Technol. 29, 35–42. https://doi.org/10.1080/09593330802008560

Moß, C., Patil, S.A., Schröder, U., 2019. Scratching the surface-how decisive are microscopic surface structures on growth and performance of electrochemically active bacteria? Front. Energy Res. 7, 1–10. https://doi.org/10.3389/fenrg.2019.00018

Mulkerrins, D., Dobson, A.D.W., Colleran, E., 2004. Parameters affecting biological phosphate removal from wastewaters. Environ. Int. 30, 249–259. https://doi.org/10.1016/S0160-4120(03)00177-6

Nguyen, P.Y., Marques, R., Wang, H., Reis, M.A.M., Carvalho, G., Oehmen, A., 2023. The impact of pH on the anaerobic and aerobic metabolism of Tetrasphaera-enriched polyphosphate accumulating organisms. Water Res. X 19, 100177. https://doi.org/10.1016/j.wroa.2023.100177

Nielsen, P.H., McIlroy, S.J., Albertsen, M., Nierychlo, M., 2019. Re-evaluating the microbiology of the enhanced biological phosphorus removal process. Curr. Opin. Biotechnol. 57, 111–118. https://doi.org/10.1016/j.copbio.2019.03.008

Nittami, T., Oi, H., Matsumoto, K., Seviour, R.J., 2011. Influence of temperature, pH and dissolved oxygen concentration on enhanced biological phosphorus removal under strictly aerobic conditions. N. Biotechnol. 29, 2–8. https://doi.org/10.1016/j.nbt.2011.06.012

Nurmiyanto, A., Kodera, H., Kindaichi, T., Ozaki, N., Aoi, Y., Ohashi, A., 2017. Dominant Candidatus accumulibacter phosphatis enriched in response to phosphate concentrations in EBPR process. Microbes Environ. 32, 260–267. https://doi.org/10.1264/jsme2.ME17020

Oehmen, A., Lemos, P.C., Carvalho, G., Yuan, Z., Keller, J., Blackall, L.L., Reis, M.A.M., 2007. Advances in enhanced biological phosphorus removal: From micro to macro scale. Water Res. 41, 2271–2300. https://doi.org/10.1016/j.watres.2007.02.030

Pan, S., Underhill, S.A.M., Hamm, C.W., Stover, M.A., Butler, D.R., Shults, C.A., Manjarrez, J.R., Cabeen, M.T., 2024. Glycerol metabolism impacts biofilm phenotypes and virulence in Pseudomonas aeruginosa via the Entner-Doudoroff pathway. mSphere 9, 1–20. https://doi.org/10.1128/msphere.00786-23

Panswad, T., Doungchai, A., Anotai, J., 2003. Temperature effect on microbial community of enhanced biological phosphorus removal system. Water Res. 37, 409–415. https://doi.org/10.1016/S0043-1354(02)00286-5

Parks, D.H., Chuvochina, M., Rinke, C., Mussig, A.J., Chaumeil, P.-A., Hugenholtz, P., 2022. GTDB: an ongoing census of bacterial and archaeal diversity through a phylogenetically consistent, rank normalized and complete genome-based taxonomy. Nucleic Acids Res. 50, D785–D794. https://doi.org/10.1093/nar/gkab776

Perchikov, R., Cheliukanov, M., Plekhanova, Y., Tarasov, S., Kharkova, A., Butusov, D., Arlyapov, V., Nakamura, H., Reshetilov, A., 2024. Microbial Biofilms: Features of Formation and Potential for Use in Bioelectrochemical Devices. Biosensors 14. https://doi.org/10.3390/bios14060302

Petriglieri, F., Singleton, C., Peces, M., Petersen, J.F., Nierychlo, M., Nielsen, P.H., 2021. "Candidatus Dechloromonas phosphoritropha" and "Ca. D. phosphorivorans", novel polyphosphate accumulating organisms abundant in wastewater treatment systems. ISME J. 15, 3605–3614. https://doi.org/10.1038/s41396-021-01029-2

Pincam, T., Liu, Y.Q., Booth, A., Wang, Y., Lan, G., Zeng, P., 2024. A comprehensive comparison of microbial communities between aerobic granular sludge and flocculent sludge for nutrient removal in full-scale wastewater treatment plants. Chemosphere 362, 142644. https://doi.org/10.1016/j.chemosphere.2024.142644

Pinck, S., Ostormujof, L.M., Teychené, S., Erable, B., 2020. Microfluidic microbial bioelectrochemical systems: An integrated investigation platform for a more fundamental understanding of electroactive bacterial biofilms. Microorganisms 8, 1–22. https://doi.org/10.3390/microorganisms8111841

Pons, L., Délia, M.L., Bergel, A., 2011. Effect of surface roughness, biofilm coverage and biofilm structure on the electrochemical efficiency of microbial cathodes. Bioresour. Technol. 102, 2678–2683. https://doi.org/10.1016/j.biortech.2010.10.138

Qiu, G., Zuniga-Montanez, R., Law, Y., Thi, S.S., Nguyen, T.Q.N., Eganathan, K., Liu, X., Nielsen, P.H., Williams, R.B.H., Wuertz, S., 2019. Polyphosphate-accumulating organisms in full-scale tropical wastewater treatment plants use diverse carbon sources. Water Res. 149, 496–510. https://doi.org/10.1016/j.watres.2018.11.011

Randall, A.A., 2012. Contrast of Volatile Fatty Acid Driven and Inorganic Acid or Base Driven Phosphorus Release and Uptake in Enhanced Biological Phosphorus Removal. Water Environ. Res. 84, 305–312. https://doi.org/10.2175/106143012x13373550426715

Răsădean, D.M., Machida, T., Sada, K., Pudney, C.R., Pantoș, G.D., 2021. Flavin mimetics: Synthesis and photophysical properties. Tetrahedron 82. https://doi.org/10.1016/j.tet.2021.131925

Ratheesh, A., Sreelekshmy, B.R., Namitha, S., Sasidharan, S., Nair, K.S., George, S., Shibli, S.M.A., 2024. Regulation of extracellular electron transfer by sustained existence of Fe^{2+}/Fe^{3+} redox couples on iron oxide-functionalized woody biochar anode surfaces in bioelectrochemical systems. Surfaces and Interfaces 54, 105114.

https://doi.org/10.1016/j.surfin.2024.105114

Ren, Y., Wang, C., Chen, Z., Allan, E., Mei, H.C. Van Der, Busscher, H.J., 2018. Emergent heterogeneous microenvironments in biofilms : substratum surface heterogeneity and bacterial adhesion force-sensing 259–272. https://doi.org/10.1093/femsre/fuy001

Rey Martínez, N., 2019. Advances in enhanced biological phosphorus removal: amino acids as carbon source and envisaging its integration in high-rate systems. Universitat Autònoma de Barcelona (UAB).

Rong, Y., Zhang, Y., Sun, Y., Liu, Z., 2024. Mechanism of Nitrogen Removal Enhancement in Low Carbon/Nitrogen Municipal Sewage by AAO Process with Activated Sludge-Biofilm Composite System. Polish J. Environ. Stud. 33, 2281–2290. https://doi.org/10.15244/pjoes/174839

Saini, S., Tewari, S., Dwivedi, J., Sharma, V., 2023. Biofilm-mediated wastewater treatment: a comprehensive review. Mater. Adv. 4, 1415–1443. https://doi.org/10.1039/d2ma00945e

Salama, Y., Chennaoui, M., Sylla, A., Mountadar, M., Rihani, M., Assobhei, O., 2016. Characterization, structure, and function of extracellular polymeric substances (EPS) of microbial biofilm in biological wastewater treatment systems: a review. Desalin. Water Treat. 57, 16220–16237. https://doi.org/10.1080/19443994.2015.1077739

Salim, H., Al Farraji, A., Khadim, H.J., 2025. A Review on Microbial Fuel Cell-Photobioreactor (MFC-PBR) Systems: Wastewater Treatment, Bioenergy Recovery, and CO2 Sequestration. Int. J. Des. Nat. Ecodynamics 20, 537–546. https://doi.org/10.18280/ijdne.200309

Sandeep, R., Madsen, J.S., Marzocchi, U., Vergeynst, L., 2025. Synergizing carbon and phosphorus recovery from wastewater: Integrating biofilm-based phosphorus removal in high-rate activated sludge. Water Res. 280, 123546. https://doi.org/10.1016/j.watres.2025.123546

Sandeep, R., Muscolino, J.F., Macêdo, W.V., Piculell, M., Christensson, M., Poulsen, J.S., Nielsen, J.L., Vergeynst, L., 2023. Effect of biofilm thickness on the activity and community composition of phosphorus accumulating bacteria in a moving bed biofilm reactor. Water Res. 245, 1–10. https://doi.org/10.1016/j.watres.2023.120599

Sang, Y., Jiang, Q., Guan, F., Wang, N., Etim, I.I.N., Fan, K., Duan, J., 2025. WS2/WO3 modified carbon anode as efficient electrocatalysts for enhancing electricity generation and pollution removal. Front. Microbiol. 16, 1–13. https://doi.org/10.3389/fmicb.2025.1589441

Sangamnere, R., Misra, T., Bherwani, H., Kapley, A., Kumar, R., 2023. A critical review of conventional and emerging wastewater treatment technologies. Sustain. Water Resour. Manag. 9, 1–26. https://doi.org/10.1007/s40899-023-00829-y

Sauer, K., Stoodley, P., Goeres, D.M., Hall-Stoodley, L., Burmølle, M., Stewart, P.S., Bjarnsholt, T., 2022. The biofilm life cycle: expanding the conceptual model of biofilm formation. Nat. Rev. Microbiol. 20, 608–620. https://doi.org/10.1038/s41579-022-00767-

0

Seguel Suazo, K., Dobbeleers, T., Dries, J., 2024. Bacterial community and filamentous population of industrial wastewater treatment plants in Belgium. Appl. Microbiol. Biotechnol. 108, 1–16. https://doi.org/10.1007/s00253-023-12822-8

Shen, N., Zhou, Y., 2016. Enhanced biological phosphorus removal with different carbon sources. Appl. Microbiol. Biotechnol. 100, 4735–4745. https://doi.org/10.1007/s00253-016-7518-4

Shen, Y., Monroy, G.L., Derlon, N., Janjaroen, D., Huang, C., Morgenroth, E., Boppart, S.A., Ashbolt, N.J., Liu, W.-T., Nguyen, T.H., 2015. Role of Biofilm Roughness and Hydrodynamic Conditions in Legionella pneumophila Adhesion to and Detachment from Simulated Drinking Water Biofilms. Env. Sci Technol. 49, 4274–4282. https://doi.org/10.1021/es505842v.Role

Shi, K., Shiu, K.K., 2004. Adsorption of some quinone derivatives at electrochemically activated glassy carbon electrodes. J. Electroanal. Chem. 574, 63–70. https://doi.org/10.1016/j.jelechem.2004.07.027

Sichler, T.C., Adam, C., Montag, D., Barjenbruch, M., 2022. Future nutrient recovery from sewage sludge regarding three different scenarios - German case study. J. Clean. Prod. 333, 130130. https://doi.org/10.1016/j.jclepro.2021.130130

Singleton, C.M., Petriglieri, F., Kristensen, J.M., Kirkegaard, R.H., Michaelsen, T.Y., Andersen, M.H., Kondrotaite, Z., Karst, S.M., Dueholm, M.S., Nielsen, P.H., Albertsen, M., 2021. Connecting structure to function with the recovery of over 1000 high-quality metagenome-assembled genomes from activated sludge using long-read sequencing. Nat. Commun. 12, 2009. https://doi.org/10.1038/s41467-021-22203-2

Skennerton, C.T., Barr, J.J., Slater, F.R., Bond, P.L., Tyson, G.W., 2015. Expanding our view of genomic diversity in Candidatus Accumulibacter clades. Environ. Microbiol. 17, 1574–1585. https://doi.org/10.1111/1462-2920.12582

Stokholm-Bjerregaard, M., McIlroy, S.J., Nierychlo, M., Karst, S.M., Albertsen, M., Nielsen, P.H., 2017. A critical assessment of the microorganisms proposed to be important to enhanced biological phosphorus removal in full-scale wastewater treatment systems. Front. Microbiol. 8, 1–18. https://doi.org/10.3389/fmicb.2017.00718

Su, X., Cheng, X., Wang, Y., Luo, J., 2022. Effect of different D-amino acids on biofilm formation of mixed microorganisms. Water Sci. Technol. 85, 116–124. https://doi.org/10.2166/wst.2021.623

Ta, T.C., Kanda, V., McDermott, M.T., 1999. Voltammetric and scanning force microscopic investigation of anthraquinone films spontaneously adsorbed on ordered graphite. J. Phys. Chem. B 103, 1295–1302. https://doi.org/10.1021/jp983724u

Tarayre, C., Nguyen, H., Brognaux, A., Delepierre, A., Clercq, L. De, Charlier, R., Michels, E., Meers, E., Delvigne, F., 2016. Characterisation of Phosphate Accumulating Organisms and Techniques for Polyphosphate Detection : A Review.

https://doi.org/10.3390/s16060797

Tian, W. De, Lopez-Vazquez, C.M., Li, W.G., Brdjanovic, D., van Loosdrecht, M.C.M., 2013. Occurrence of PAOI in a low temperature EBPR system. Chemosphere 92, 1314–1320. https://doi.org/10.1016/j.chemosphere.2013.05.009

Tian, X., Yin, X., Ji, X., Li, H., Duan, H., Zhang, K., Bian, D., 2025. The metabolic strategy of phosphorus-accumulating organisms in response to low temperature in micro pressure swirl reactor. J. Environ. Chem. Eng. 13, 115036. https://doi.org/10.1016/j.jece.2024.115036

Unz, R.F., 2015. Zoogloea. Bergey's Man. Syst. Archaea Bact. 1–13. https://doi.org/10.1002/9781118960608.gbm01005

Vassilev, I., Dessì, P., Puig, S., Kokko, M., 2022. Cathodic biofilms – A prerequisite for microbial electrosynthesis. Bioresour. Technol. 348. https://doi.org/10.1016/j.biortech.2022.126788

Venkateswaran, K., Dollhopf, M.E., Lies, D.P., Saffarini, D.A., Gregor, B.J.M., White, D.C., Ni, M., Ri, D.B., Stackebrandp, E., Nealsonl, K.H., Shewanella, K., 1999. Polyphasic taxonomy of the genus Shewanella and description of Shewanella oneidensis sp. now. Int. J. Syst. Bacteriol. 705–724. https://doi.org/10.1099/00207713-49-2-705

Wagner, M., Horn, H., 2017. Optical coherence tomography in biofilm research: A comprehensive review. Biotechnol. Bioeng. 114, 1386–1402. https://doi.org/10.1002/bit.26283

Wagner, M., Taherzadeh, D., Haisch, C., Horn, H., 2010. Investigation of the mesoscale structure and volumetric features of biofilms using optical coherence tomography. Biotechnol. Bioeng. 107, 844–853. https://doi.org/10.1002/bit.22864

Wang, D., Zheng, W., Liao, D., Li, X., Yang, Q., Zeng, G., 2013. Effect of initial pH control on biological phosphorus removal induced by the aerobic/extended-idle regime. Chemosphere 90, 2279–2287. https://doi.org/10.1016/j.chemosphere.2012.10.086

Wang, F., Cui, Q., Liu, Wenai, Jiang, W., Ai, S., Liu, Wanqi, Bian, D., 2024. Synergistic denitrification mechanism of domesticated aerobic denitrifying bacteria in low-temperature municipal wastewater treatment. npj Clean Water 7, 1–10. https://doi.org/10.1038/s41545-024-00299-5

Wang, S., Zhi, L., Shan, W., Lu, H., Xu, Q., Li, J., 2020. Correlation of extracellular polymeric substances and microbial community structure in denitrification biofilm exposed to adverse conditions. Microb. Biotechnol. 13, 1889–1903. https://doi.org/10.1111/1751-7915.13633

Wang, X., Zhang, J., Li, L., Zhu, Y., Zhang, Y., Ni, M., Ding, Y., Huang, Y., Pan, Y., 2024. Formation mechanism of high biofilm phosphorus storage capacity and its effect on phosphorus uptake-release and carbon source consumption. Bioresour. Technol. 412. https://doi.org/10.1016/j.biortech.2024.131363

Waqas, S., Harun, N.Y., Sambudi, N.S., Abioye, K.J., Zeeshan, M.H., Ali, A., Abdulrahman,

A., Alkhattabi, L., Alsaadi, A.S., 2023. Effect of Operating Parameters on the Performance of Integrated Fixed-Film Activated Sludge for Wastewater Treatment. Membranes (Basel). 13, 1–22. https://doi.org/10.3390/membranes13080704

Wei, J., Huang, X., Wang, H., Wang, F., Liu, X., Yan, Y., Qu, Y., 2023. Insight into biofilm formation of wastewater treatment processes: Nitrogen removal performance and biological mechanisms. Sci. Total Environ. 903, 166550. https://doi.org/10.1016/j.scitotenv.2023.166550

Wei, J., Imai, T., Higuchi, T., Arfaritaa, N., Yamamoto, K., Sekine, M., Kanno, A., 2014. Effect of different carbon sources on the biological phosphorus removal by a sequencing batch reactor using pressurized pure oxygen. Biotechnol. Biotechnol. Equip. 28, 471–477. https://doi.org/10.1080/13102818.2014.924200

Weiler, J., 2020. Weiterführende Entwicklung eines Kultivierungssystems für Biofilme anhand von zwei angewandten Projekten. Karlsruher Institut für Technologie, Karlsruhe, Germany.

Weiler, J., Edel, M., Gescher, J., 2024. Biofilms for Production of Chemicals and Energy. Annu. Rev. Chem. Biomol. Eng. 15, 361–387. https://doi.org/https://doi.org/10.1146/annurev-chembioeng- 100522-110939

Weissbrodt, D.G., Neu, T.R., Kuhlicke, U., Rappaz, Y., Holliger, C., 2013. Assessment of bacterial and structural dynamics in aerobic granular biofilms. Front. Microbiol. 4, 1–18. https://doi.org/10.3389/fmicb.2013.00175

Welles, L., 2015. Enhanced Biological Phosphorus Removal: Metabolic Insights and Salinity Effects. Delft University of Technology.

Wu, Q., Bishop, P.L., Keener, T.C., 2006. Biological Phosphate Uptake and Release: Effect of pH and Magnesium Ions. Water Environ. Res. 78, 196–201. https://doi.org/10.2175/106143005x89652

Wu, S.H., Sun, J.J., Lin, Z. Bin, Wu, A.H., Zeng, Y.M., Guo, L., Zhang, D.F., Dai, H.M., Chen, G.N., 2007. Adsorptive stripping analysis of riboflavin at electrically heated graphite cylindrical electrodes. Electroanalysis 19, 2251–2257. https://doi.org/10.1002/elan.200703959

Xie, T., Mo, C., Li, X., Zhang, J., An, H., Yang, Q., Wang, D., Zhao, J., Zhong, Y., Zeng, G., 2017. Effects of different ratios of glucose to acetate on phosphorus removal and microbial community of enhanced biological phosphorus removal (EBPR) system. Environ. Sci. Pollut. Res. 24, 4494–4505. https://doi.org/10.1007/s11356-016-7860-1

Yadav, B., Yellapu, S.K., Adjallé, K., Drogui, P., Tyagi, R.D., 2021. Comparative study on production and characterisation of extracellular polymeric substances (EPS) using activated sludge fortified with crude glycerol from different biodiesel companies. Syst. Microbiol. Biomanufacturing 1, 208–222. https://doi.org/10.1007/s43393-020-00017-5

Yi, Y., Zhao, T., Zang, Y., Xie, B., Liu, H., 2021. Different mechanisms for riboflavin to improve the outward and inward extracellular electron transfer of Shewanella loihica.

Electrochem. commun. 124, 106966. https://doi.org/10.1016/j.elecom.2021.106966

Yin, W., Wang, K., Xu, J., Wu, D., Zhao, C., 2018. The performance and associated mechanisms of carbon transformation (PHAs, polyhydroxyalkanoates) and nitrogen removal for landfill leachate treatment in a sequencing batch biofilm reactor (SBBR). RSC Adv. 8, 42329–42336. https://doi.org/10.1039/c8ra07839d

You, J., Ye, L., Zhang, S., Zhao, J., Zhao, Y., He, Y., Chen, J., Kennes, C., Chen, D., 2025. Electrode functional microorganisms in bioelectrochemical systems and its regulation: A review. Biotechnol. Adv. 79, 108521. https://doi.org/10.1016/j.biotechadv.2025.108521

Yuan, J., Deng, X., Xie, X., Chen, L., Wei, C., Feng, C., Qiu, G., 2024. Blind spots of universal primers and specific FISH probes for functional microbe and community characterization in EBPR systems. ISME Commun. 4. https://doi.org/10.1093/ismeco/ycae011

Yuan, Q., Du, Y., Chen, S., Zhao, Y., Han, Y., Jiao, Y., Sun, Y., 2025. Impact of N loading on microbial community structure and nitrogen removal of an activated sludge process with long SRT for municipal wastewater treatment. Water Cycle 6, 28–35. https://doi.org/10.1016/j.watcyc.2024.09.002

Zeng, F., Jin, W., Zhao, Q., 2019. Temperature effect on extracellular polymeric substances (EPS) and phosphorus accumulating organisms (PAOs) for phosphorus release of anaerobic sludge. RSC Adv. 9, 2162–2171. https://doi.org/10.1039/C8RA10048A

Zengin, G.E., Artan, N., Orhon, D., Chua, A.S.M., Satoh, H., Mino, T., 2010. Population dynamics in a sequencing batch reactor fed with glucose and operated for enhanced biological phosphorus removal. Bioresour. Technol. 101, 4000–4005. https://doi.org/10.1016/j.biortech.2010.01.044

Zhang, C., Chen, Y., Liu, Y., 2007. The long-term effect of initial pH control on the enrichment culture of phosphorus- and glycogen-accumulating organisms with a mixture of propionic and acetic acids as carbon sources. Chemosphere 69, 1713–1721. https://doi.org/10.1016/j.chemosphere.2007.06.009

Zhang, C., Guisasola, A., Baeza, J.A., 2025. A critical review on the effect of different carbon sources on EBPR: Revaluation of performance and applications. Chem. Eng. J. 509, 161083. https://doi.org/10.1016/j.cej.2025.161083

Zhang, H.-L., Fang, W., Fang, Y.-P., Sheng, G.-P., Zeng, R.J., Li, W.-W., Yu, H.-Q., 2013. Phosphorus Removal in an Enhanced Biological Phosphorus Removal Process: Roles of Extracellular Polymeric Substances. Environ. Sci. Technol. 86, 85–95. https://doi.org/https://doi.org/10.1021/es403227p

Zhang, H., Li, Q., Han, D., Liu, R., 2024. Clarifying the Role of Phosphorus Management Strategies in Enhancing the Sustainability of Wastewater Treatment Plants. Water (Switzerland) 16. https://doi.org/10.3390/w16111539

Zhang, L., Zhang, Y., Liu, Y., Wang, S., Lee, C.K., Huang, Y., Duan, X., 2024. High power density redox-mediated Shewanella microbial flow fuel cells. Nat. Commun. 1–11. https://doi.org/10.1038/s41467-024-52498-w

Zhang, Y., Qiu, X., Luo, J., Li, H., How, S.W., Wu, D., He, J., Cheng, Z., Gao, Y., Lu, H., 2024. A review of the phosphorus removal of polyphosphate-accumulating organisms in natural and engineered systems. Sci. Total Environ. 912. https://doi.org/10.1016/j.scitotenv.2023.169103

Zhao, J., Li, F., Kong, S., Chen, T., Song, H., Wang, Z., 2023. Elongated Riboflavin-Producing Shewanella oneidensis in a Hybrid Biofilm Boosts Extracellular Electron Transfer. Adv. Sci. 10, 1–11. https://doi.org/10.1002/advs.202206622

Zhao, Q., Lv, H., Cui, Z., Zhao, M., Cui, B., Zhou, D., 2022. Riboflavin Enhances the Synergy of Electroactive Bacteria and Fenton Reaction , Improving Chlorophenol Degradation and Fe Circulation. ACS EST Water 2, 1451–1470. https://doi.org/10.1021/acsestwater.2c00208

Zhao, W., Bi, X., Peng, Y., Bai, M., 2022. Research advances of the phosphorus-accumulating organisms of Candidatus Accumulibacter, Dechloromonas and Tetrasphaera: Metabolic mechanisms, applications and influencing factors. Chemosphere 307, 135675. https://doi.org/10.1016/j.chemosphere.2022.135675

Zheng, S., Bawazir, M., Dhall, A., Kim, H.E., He, L., Heo, J., Hwang, G., 2021. Implication of Surface Properties, Bacterial Motility, and Hydrodynamic Conditions on Bacterial Surface Sensing and Their Initial Adhesion. Front. Bioeng. Biotechnol. 9, 1–22. https://doi.org/10.3389/fbioe.2021.643722

Zheng, T., Li, J., Ji, Y., Zhang, W., Fang, Y., Xin, F., Dong, W., Wei, P., Ma, J., Jiang, M., 2020. Progress and Prospects of Bioelectrochemical Systems: Electron Transfer and Its Applications in the Microbial Metabolism. Front. Bioeng. Biotechnol. 8, 1–10. https://doi.org/10.3389/fbioe.2020.00010

Ziegler, A.S., McIlroy, S.J., Larsen, P., Albertsen, M., Hansen, A.A., Heinen, N., Nielsen, P.H., 2016. Dynamics of the fouling layer microbial community in a membrane bioreactor. PLoS One 11, 1–14. https://doi.org/10.1371/journal.pone.0158811

Ziliani, A., Bovio-Winkler, P., Cabezas, A., Etchebehere, C., Garcia, H.A., López-Vázquez, C.M., Brdjanovic, D., van Loosdrecht, M.C.M., Rubio-Rincón, F.J., 2023. Putative metabolism of Ca. Accumulibacter via the utilization of glucose. Water Res. 229, 119446. https://doi.org/10.1016/j.watres.2022.119446

Zou, L., Wu, X., Huang, Y., Ni, H., Long, Z., 2019. Promoting Shewanella Bidirectional Extracellular Electron Transfer for Bioelectrocatalysis by Electropolymerized Riboflavin Interface on Carbon Electrode. Front. Microbiol. 10, 1–9. https://doi.org/10.3389/fmicb.2018.03293

6. Appendix

6.1. Supplementary Figures

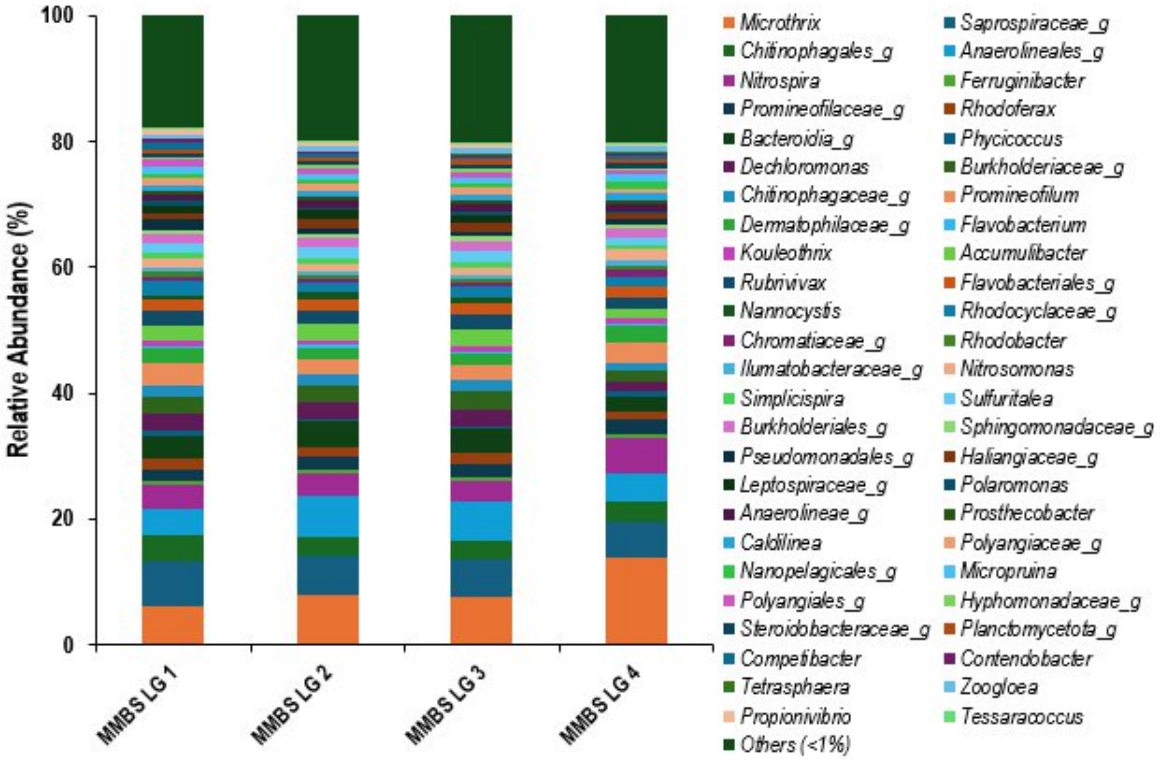

Figure S1. Microbial community composition in activated sludge samples taken from the Langenhagen WWTP (LG1 to LG4) for MMBS inoculation.

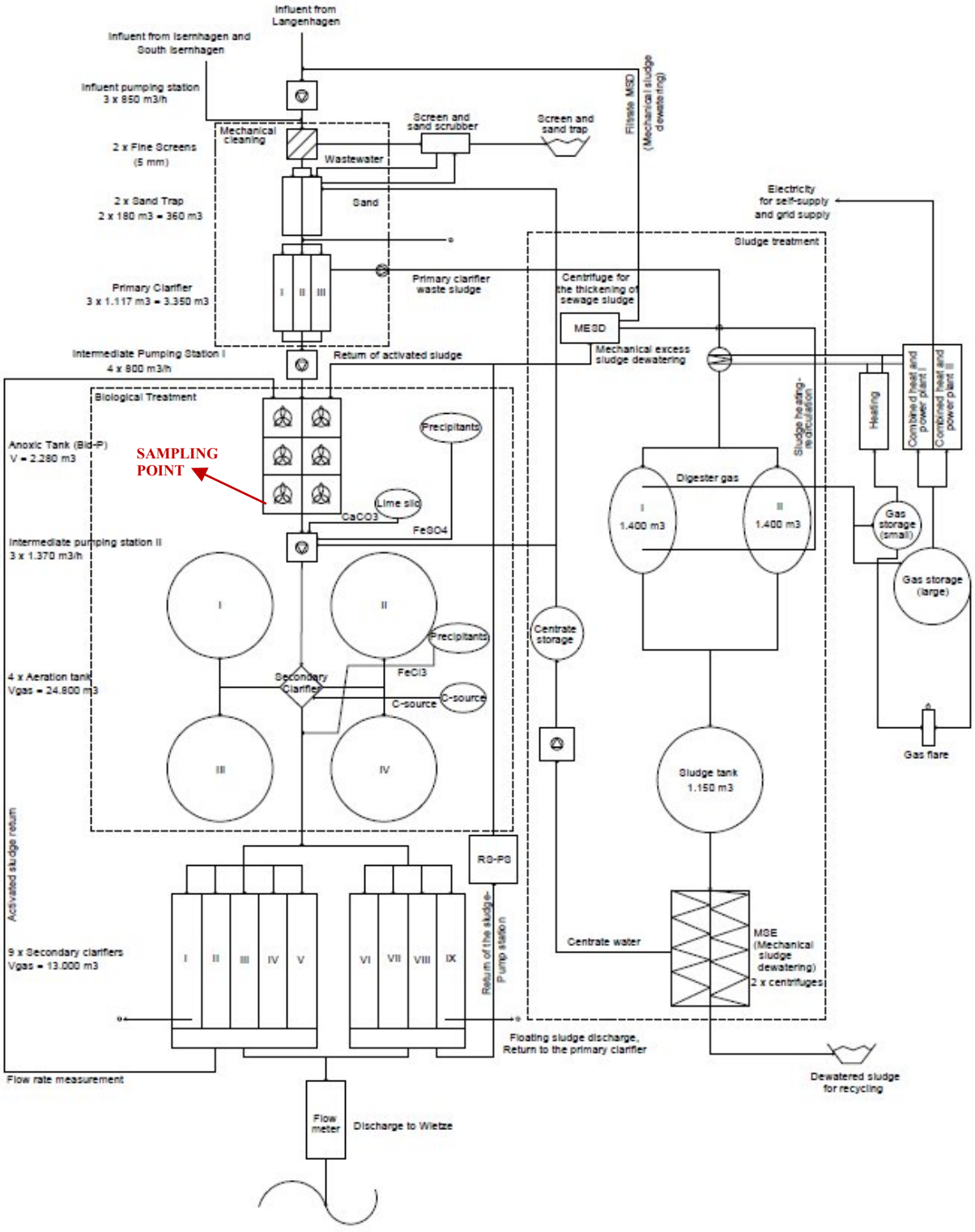

Figure S2. Activated sludge samples were taken from the anoxic (Bio-P) tank of the Langenhagen WWTP for inoculation.

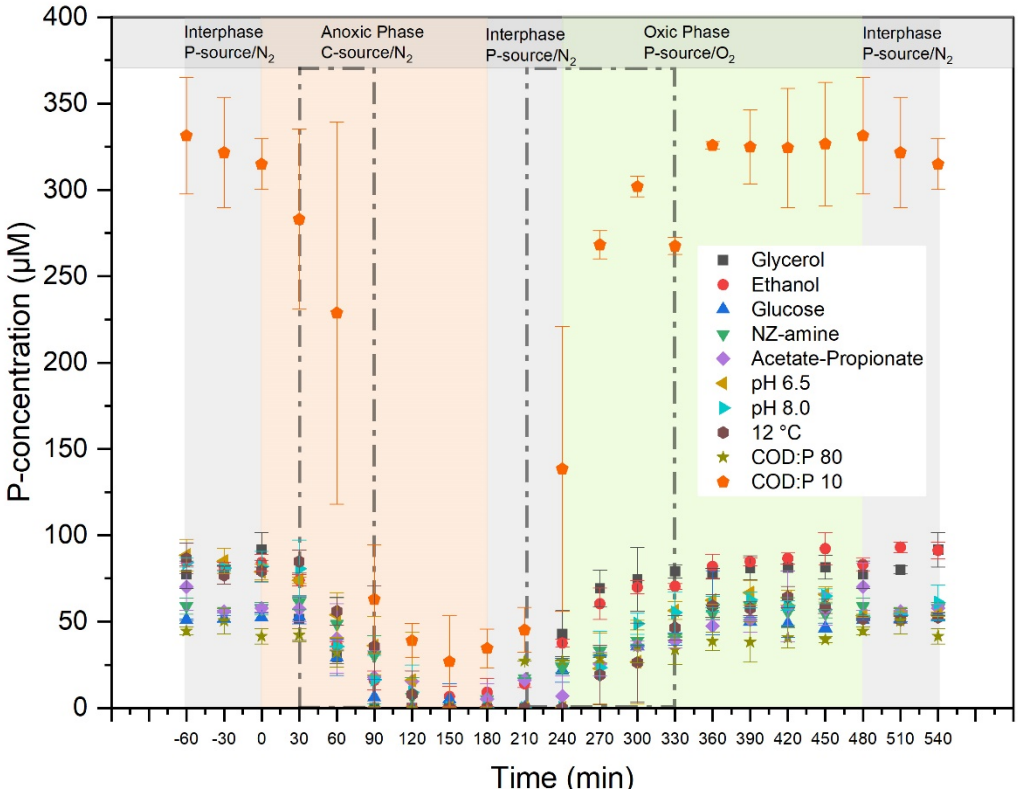

Figure S3. Raw data from IC measurements throughout a complete anoxic and oxic cycle. The intervals from 30 to 90 minutes during the anoxic phase and from 210 to 330 minutes during the oxic phase were selected as active time for estimating phosphate release and uptake amounts. Error bars indicate the standard deviation of individual replicates (n = 3).

6.2. Supplementary Tables

Table S1. Influent and effluent characteristics of the Langenhagen WWTP during the four MMBS sampling campaigns (LG1 to LG4), including pH, phosphate concentrations, temperature, and effluent TOC on the corresponding sampling dates.

Sampling	Sampling Date	Influent		Effluent			
		pH	P (mg L^{-1})	Temp (°C)	pH	P (mg L^{-1})	TOC (mg L^{-1})
MMBS LG1	21.01.24	7.50	5.80	9	7.10	0.15	11.3 (22.01.2024)
MMBS LG2	04.03.24	7.60	6.70	12	6.90	0.36	12.20 (04.03.24)
MMBS LG3	17.04.24	7.90	7.50	13	7.10	0.52	11.6 (15.04.2024)
MMBS LG4	21.05.24	7.50	8.60	18	7.20	0.53	11.5 (20.05.2024)

Table S2: Relative abundance of PAOs and GAOs across different inocula, used in this study, for MMBS.

Sampling	Relative abundance of PAOs (%)			Relative abundance of GAOs (%)					
	Accumulibacter	*Dechloromonas*	*Tetrasphaera*	*Tessaracoccus*	*Competibacter*	*Contendobacer*	*Micropruina*	*Propionivibrio*	*Zoogloea*
MMBS LG1	1.40	1.51	0.35	0.25	0.33	0.45	1.05	0.35	0.78
MMBS LG2	2.71	2.61	0.23	0.37	0.30	0.38	0.87	0.61	0.91
MMBS LG3	2.41	2.59	0.21	0.31	0.34	0.38	0.95	0.61	0.72
MMBS LG4	2.51	2.90	0.18	0.40	0.60	0.10	1.14	0.71	0.60

Table S3: Relative abundance of PAOs and GAOs after enrichment in microfluidic cultivation reactors in MMBS.

Process Condition	Relative abundance of PAOs (%)		Relative abundance of GAOs (%)					
	Accumulibacter	*Dechloromonas*	*Tessaracoccus*	*Competibacter*	*Contendobacer*	*Micropruina*	*Propionivibrio*	*Zoogloea*
Standard (LG1)*	0.78	25.24	0.03	0.27	0.08	0.07	0.66	22.82
Ethanol (LG2)	1.1	24.09	0.11	0.35	0.21	0.14	0.74	30.19
Glycerol (LG4)	0.62	3.29	0.29	0.71	0.5	0.35	0.82	4.96
Glucose (LG1)	0.46	3.52	2.21	0.47	0.3	2.14	0.37	2.46
NZ-Amine (LG1)	0.4	1.05	0.06	0.68	0.14	0.1	0.27	11.37
12°C (LG3)	0.81	12.92	0.13	0.8	0.54	0.15	0.76	10.78
COD:P 10 (LG4)	0.7	22.48	0.03	0.34	0.12	0.1	0.49	13.26
COD:P 80 (LG4)	0.82	14.14	0.09	0.24	0.14	0.11	0.65	12.01
pH 6.5 (LG3)	1.13	27.28	0.05	0.37	0.14	0.07	0.99	14.21
pH 8.0 (LG3)	1.03	16.84	0.06	0.39	0.22	0.05	1.27	10.88

* Standard process conditions in MMBS were conducted with acetate-propionate, pH 7.5, COD:P 40, and room temperature.

Table S4: Relevant stoichiometric P-variables and biofilm volume, including standard deviation from MMBS experiments.

Process Condition		P-release	P-uptake	P-removal	Biofilm volume					P-release capacity	P-uptake capacity	P-removal capacity
					Front	Middle	Back	Average	Sum			
		µg PO_4-P	µg PO_4-P	µg PO_4-P	$mm^3\ cm^{-2}$	$mm^3\ cm^{-2}$	$mm^3\ cm^{-2}$	$mm^3\ cm^{-2}$	$mm^3\ cm^{-2}$	µg PO_4-P mm^{-3}	µg PO_4-P mm^{-3}	µg PO_4-P mm^{-3}
Standard	Acetate-Propionate, pH 7.5, COD:P 40, and room temperature	1.89±0.96	4.65±0.48	2.76±0.58	4.38±1.10	2.27±1.43	1.92±1.38	2.77±1.65	8.57	0.22±0.11	0.54±0.06	0.32±0.07
Carbon source	Glycerol	0.37±0.16	2.63±0.52	2.25±0.36	11.49±4.33	1.57±0.54	0.53±0.36	5.18±5.82	13.59	0.02±0.01	0.17±0.03	0.14±0.02
	Ethanol	0.97±0.21	2.90±0.35	1.93±0.52	4.67±1.77	2.52±1.94	3.20±2.17	3.42±2.1	10.39	0.09±0.02	0.27±0.03	0.18±0.05
	Glucose	1.24±0.61	4.52±0.24	3.27±0.4	3.65±1.81	0.57±0.56	0.45±0.33	1.52±1.82	4.68	0.28±0.14	1.03±0.06	0.75±0.09
	NZ-Amine	2.45±0.63	3.89±0.16	1.44±0.48	2.60±1.56	0.42±0.31	0.20±0.28	1.01±1.38	3.22	0.79±0.21	1.26±0.05	0.47±0.15
pH	6.5	1.8±0.62	6.53±0.75	4.73±0.74	7.81±4.98	6.43±3.16	5.17±1.99	6.58±3.73	19.42	0.09±0.03	0.33±0.04	0.24±0.04
	8.0	1.13±0.04	6.00±0.60	4.87±0.57	10.27±3.93	8.56±2.38	4.29±2.02	7.57±3.78	23.12	0.05±0.00	0.26±0.03	0.21±0.02
COD:P	10	5.23±1.56	10.9±2.43	5.67±2.33	11.9±4.53	7.63±1.84	6.98±1.81	9.00±3.73	26.51	0.2±0.06	0.42±0.09	0.22±0.09
	80	0.69±0.19	0.73±0.35	0.04±0.27	10.05±3.78	5.65±1.56	4.94±2.41	6.84±3.52	20.65	0.03±0.01	0.03±0.02	0.00±0.01
Temp.	12	2.04±0.85	6.88±0.31	4.84±1.05	7.33±1.86	2.87±1.00	1.86±1.14	3.79±2.68	12.06	0.18±0.08	0.61±0.03	0.43±0.09